BNL-96775-2012

A Procedure for Determination of Degradation Acceptance Criteria for Structures and Passive Components in Nuclear Power Plants

A Case Study Using a Condensate Storage Tank

Jinsuo Nie, Joseph Braverman, Charles Hofmayer, BNL
Young-Sun Choun, Daegi Hahm, In-Kil Choi

January 2012

Nuclear Science and Technology Department

Brookhaven National Laboratory

U.S. Department of Energy

DISCLAIMER

BNL-96775-2012

KAERI/TR-4422/2011

Joint Development of
Seismic Capability Evaluation Technology
for Degraded Structures and Components

Annual Report for Year 5 Task

A Procedure for Determination of Degradation Acceptance Criteria for Structures and Passive Components in Nuclear Power Plants - A Case Study using A Condensate Storage Tank

January 2012

Jinsuo Nie, Joseph Braverman, and Charles Hofmayer
Brookhaven National Laboratory
Upton, NY 11973, USA

Young-Sun Choun, Daegi Hahm, and In-Kil Choi
Korea Atomic Energy Research Institute
Daejeon, 305-353, Korea

KAERI Korea Atomic Energy Research Institute

BROOKHAVEN NATIONAL LABORATORY

NOTICE/DISCLAIMER

ABSTRACT

The Korea Atomic Energy Research Institute (KAERI) has been collaborating with Brookhaven National Laboratory since 2007 to develop a realistic seismic risk evaluation system which includes the consideration of aging of structures and components in nuclear power plants (NPPs). This collaboration program aims at providing technical support to a five-year KAERI research project, which includes three specific areas that are essential to seismic probabilistic risk assessment: (1) probabilistic seismic hazard analysis, (2) seismic fragility analysis including the effects of aging, and (3) a plant seismic risk analysis. The understanding and assessment of age-related degradations of structures, systems, and components and their impact on plant safety is the major goal of this KAERI-BNL collaboration. Four annual reports have been published before this report as a result of the collaboration research:

1. *Identification and Assessment of Recent Aging-Related Degradation Occurrences in U.S. Nuclear Power Plants*, BNL Report-81741-2008, KAERI/RR-2931/2008
2. *Identification and Assessment of Material Models for Age-Related Degradation of Structures and Passive Components in Nuclear Power Plants*, BNL Report-82249-2009, KAERI/TR-3757/2009
3. *Fragility Analysis Methodology for Degraded Structures and Passive Components in Nuclear Power Plants – Illustrated Using a Condensate Storage Tank*, BNL Report-93771-2010, KAERI/TR-4068/2010
4. *Seismic Fragility Analysis of a Condensate Storage Tank with Age-Related Degradations*, BNL Report-95030-2011, KAERI/TR-4327/2011

This report describes the research effort performed by BNL and KAERI for the Year 5 scope of work. The goal of this effort is to develop a procedure for determination of degradation acceptance criteria (DAC) for structures and passive components in nuclear power plants. This report covers the identification of an acceptable risk criterion, the development of a general procedure for three-tier DAC, determination of three-tier DAC for a condensate storage tank (CST), and insights on how to apply these DAC in inspection/maintenance planning. The development of DAC for the CST considers five degradation cases: (A) degraded stainless tank shell; (B) degraded anchor bolts; (C) anchorage concrete cracking; (D) a perfect correlation of the degradation scenarios A, B, and C; and (E) a non-perfect correlation of the three degradation scenarios. These degradation cases are the same as those considered in the seismic fragility analyses of the CST with degradations in the Year 3 and Year 4 studies. The effect of degradation on the fragility capacity as well as on the uncertainties was considered in the DAC development. A necessary and very important part of the Year 5 research is the probabilistic safety/risk analyses performed by KAERI to calculate the core damage frequencies (CDFs) for a range of fragility capacities of the CST, which correspond to the undegraded and various degraded conditions of the CST.

This report also includes an extended summary of the seismic fragility analyses of the CST with age-related degradations and three additional seismic fragility analyses to facilitate the development of various DAC and discussions in this report.

TABLE OF CONTENTS

LIST OF TABLES

LIST OF FIGURES

1 INTRODUCTION

1.1 Background

The Korea Atomic Energy Research Institute (KAERI) has been collaborating with Brookhaven National Laboratory since 2007 to develop a realistic seismic risk evaluation system which includes the consideration of aging of structures and components in nuclear power plants (NPPs). This collaboration program aims at providing technical support to a five-year KAERI research project, which includes three specific areas that are essential to seismic probabilistic risk assessment (SPRA): (1) probabilistic seismic hazard analysis, (2) seismic fragility analysis including the effects of aging, and (3) a plant seismic risk analysis. The KAERI-BNL collaboration program is also a five year program, in agreement with KAERI's overall research project.

The five year collaboration program consists of five tasks: (1) identification and characterization of degradation occurrences in US NPPs and important aging characteristics needed for the seismic capability evaluations [Nie et al. 2008], (2) identification and assessment of degradation models for the long-term behavior of dominant materials that are determined to be risk significant to NPPs [Nie et al. 2009], (3) seismic fragility analysis methodology and its application to a condensate storage tank with three degradation scenarios [Nie et al. 2010], (4) additional seismic fragility analysis of the condensate storage tank to consider non-perfect correlations among degradation scenarios [Nie et al. 2011], and (5) development of a procedure for determination of degradation acceptance criteria for structures and passive components (SPCs) in nuclear power plants, which is the topic of this report.

The understanding and assessment of age-related degradations of SPCs and their impact on plant safety is the major goal of this KAERI-BNL collaboration. Previous tasks of this project have covered most of the necessary steps to achieve this overall goal. The Year 1 research task showed that the rate of aging-related degradation in NPPs was not significantly large but increasing as the plants get older [Nie et al. 2008]. In light of the long operating life of typical NPPs (40 to 60 years), this slow but increasing rate of degradation of SPCs indicates a need for determining acceptable levels of degradation for the effectiveness and cost-efficiency of inspection and maintenance.

In contrast to degraded active components, a degraded SPC may not impose an immediate threat to the plant safety during normal operation; however, it can be a dramatic safety threat during low probability high consequence events, such as large earthquakes. The effect of age-related degradations of SPCs on their seismic fragility was investigated in this collaboration program through the integration of the fragility calculation and the degradation effect, which may be expressed in terms of observed degradation levels or time using proper time-dependent degradation models [Nie et al. 2009, 2010, 2011]. The seismic fragility is the conditional probability of failure of an SPC for given levels of seismic demand, often conveniently described in terms of peak ground acceleration (PGA). The effect of degradation of the SPC on its seismic fragility leads to a shift in the fragility curve, which is difficult for use in defining degradation acceptance criteria for the SPC. In addition, the existence of multiple degradation scenarios in one SPC also introduces another level of difficulty into how acceptance criteria can be defined and determined properly.

The Year 5 research task is to develop a procedure for determination of degradation acceptance criteria (DAC) for SPCs in nuclear power plants, based on the potentially increased seismic risk to

the plant due to degradation of the SPCs. Development of DAC for other loadings can be pursued similarly; however, such efforts are beyond the scope of this study.

1.2 Literature Review for DAC Development

The annual reports for the Year 3 and Year 4 scope of work present methods for evaluating the seismic fragility of SPCs with single or multiple age-related degradation cases. Both perfectly correlated and non-perfectly correlated degradation conditions were addressed in the seismic fragility analyses of degraded SPCs. A condensate storage tank (CST) was selected for its safety significance to the plant safety for the purpose of demonstration of the methods for seismic fragility analysis of degraded SPCs. The deterioration in seismic fragility capacities of the CST due to degradation was represented as a function of degradation level or time using age-related degradation models, some of which were identified and documented in the Year 2 annual report. As observed previously, a direct derivation of degradation acceptance criteria based on the family of seismic fragility curves is difficult because of the difficulty in defining an acceptable significance level associated with a given level of shift in the seismic fragility curve.

Since SPCs in an NPP have their intrinsic role in contributing to the plant safety (or risk), as identifiable through probabilistic risk assessment (PRA), a logical way to determine the acceptable level of the degradation is to examine how the degradations in various SPCs affect their intended role in maintaining the plant safety. Because the degradation phenomena always decrease the safety level of the plant (increase of plant risk, in other words), the fundamental philosophy is to ensure such an adverse effect on plant safety is adequately small so that the environment and the public safety and health are adequately protected. Recent studies by Braverman et al. [2001, 2005] are representative of such risk-based methodologies for developing the degradation acceptance criteria, based on the guidelines described in the NRC Regulatory Guide (RG) 1.174 [1998, 2002].

Braverman et al. [2001] studied the role of structural degradation in reinforced concrete components, such as beams and shear walls, on the seismic risk of an NPP and evaluated the acceptance limits for these degraded reinforced concrete components. The reported risk study utilized a well-documented plant logic for the Zion Plant Unit No. 1, a PWR that was widely reviewed in various independent risk studies. The core damage was represented by a simple Boolean expression in this study to assess the risk significance of the structural degradation of the reinforced concrete beams and shear walls [Zion, 1981; Ellingwood and Song, 1996]. It was concluded that aging of structural components that appear as singleton cutsets in the plant logic has a minimal impact on core damage frequency due to seismic events (less than a factor of 2). This impact has been determined to be relatively inconsequential as compared to the large variation (over an order of magnitude) in the CDFs determined in the IPE and IPEEE programs. It was further determined that for the Eastern US, the logarithmic standard deviation, β_C, has only a marginal impact on seismic risk and the impact of structural aging on plant risk can be simply assessed through comparison of seismic hazards evaluated at the undegraded and degraded median capacities. With a postulated degradation that leads to a less than 20% reduction in median plant-level fragility, the increase in CDF was estimated to be at most 40% for the Eastern US and 60% for the Western US. The study concluded that for a typical reduction in fragility capacity by 20% or less, the increase in CDF would generally be 3.9×10^{-6} for plants in the Eastern US and 5.9×10^{-6} for those in the Western US. In light of the NRC RG 1.174, these increases are considered to be “small” (Region II in Figure 4 of RG 1.174, Rev. 2 [2011]), but the cumulative

impact of the aging effects must be tracked. Acceptance criteria for flexural members and shear walls, in terms of loss of steel area or crack width, were developed based on levels of degradation that would not result in a significant plant risk increase, or more specifically that would not result in more than a 20% reduction in the component's capacity using the findings presented above.

In another recent study of degraded buried piping, Braverman et al. [2005] selected 5 representative NPPs (4 PWR and one BWR) from 12 License Renewal Applications, in which buried piping is specifically referenced. Based on the NRC RG 1.174, a ΔCDF of 10^{-6} /reactor year was selected, together with a maximum baseline CDF of 5×10^{-5} /reactor year, as the acceptable risk for the development of the degradation acceptance criteria for buried piping. The corresponding PRA study was based on Standardized Plant Analysis Risk (SPAR) version 3 models, which are full-power, Level-1 models for internal events. Large Early Release Frequency (LERF) was not used for the development due to its unavailability at the time, even though RG 1.174 indicates the need of LERF. Accordingly, buried piping systems that mitigate the events other than Level-1 internal events (e.g., LERF and fire) were excluded from the study. It should be noted that the controlling loading for fragility capacity of the buried piping was determined in the report not to be seismic loading but internal pressure. The system that a subject buried piping belongs to was differentiated into two categories: (1) its failure causes an initiating event, or (2) its failure does not cause an initiating event but it is required to mitigate an initiating event. Degradation acceptance criteria in terms of remaining life (years) were developed for a matrix of assumed constant degradation rates and levels of observed wall loss. Degradation acceptance criteria were further developed in terms of wall loss for a series of pipe diameters.

Both studies summarized above are conducted without identification of specific components and specific plants as well; therefore, a range of representative and risk-significant components must be identified, their systems must be differentiated according to the system's safety function, and representative plant(s) must be selected for the required probabilistic risk analysis. This can introduce additional uncertainties to the DAC so developed, which however were not explicitly investigated. Simple plant logic or limited scope PRA were performed to obtain the degradation induced CDF increase as well as the baseline CDF. Degradation of a component was restricted to single scenario only (i.e., loss of wall thickness or loss of steel area).

1.3 Objectives

The goal of the Year 5 research is to develop a procedure for DAC determination for SPCs in NPPs, as the final step in the seismic risk evaluation of SPCs. The procedure will be developed based on the seismic fragility capacities developed for the condensate storage tank (CST) with various types and levels of degradations. Given the uncertainties associated with seismic loading, the degradation phenomena, their impact on seismic fragility of the subject component, and the effect on the plant safety, it is believed that a probabilistic description of or a probabilistic reasoning for the degradation acceptance criteria is the most appropriate approach in quantifying the acceptable degradation levels.

As described above, U.S. NRC Regulatory Guide (RG) 1.174 has been used in selecting critical levels of CDF and/or LERF increase for the determination of the acceptable levels of degradation. The most recent revision of this guidance (Rev. 2) was utilized in the research summarized in this report.

Since the degradation scenarios and the degradation models used in the seismic fragility analyses of the CST are based on assumed models/data, some of the insights obtained from this study should be viewed as an illustration of the proposed procedure and a literal application of the findings documented in this report is not appropriate.

1.4 Organization of Report

Section 2 introduces a three-tier approach for the development of degradation acceptance criteria, based on guidelines in terms of CDF or LERF as described in RG 1.174, Rev. 2. This three-tier approach allows a flexible application of the DAC based on available degradation information in the inspection/maintenance process.

Section 3 summarizes the fragility analyses of the CST considering various types and levels of degradation, which are in the Year 3 and Year 4 scopes of work. The goal of inclusion of the fragility analysis in this report is to create a coherent document that can be effectively used in developing DAC for the CST and other SPCs. This section also presents three additional seismic fragility analyses of the CST to consider the operational water level in the three basic degradation scenarios.

Section 4 describes the seismic probabilistic risk assessment (PRA), which is also referred to as probabilistic safety assessment (PSA), of a typical NPP to obtain various levels of CDF as a function of fragility capacity, in the context of the three-tier approach for DAC development. The plant information, the system model, the role of the CST in the system model, the scope of PRA, and other relevant information will be presented.

Section 5 describes the application of the three-tier approach to the CST with various degradation scenarios. The focus is on the illustration of the methodology.

Section 6 describes how various DAC obtained in Section 5 can be used for the purpose of inspection/maintenance scheduling.

Section 7 presents a summary of the procedure for DAC development and major findings in its application to the case of the CST.

2 A PROCEDURE FOR THREE-TIER DEGRADATION ACCEPTANCE CRITERIA

2.1 Acceptable Level of Risk Increase Due to Degradation

Age-related degradation of a structure or passive component (SPC) in a nuclear power plant (NPP) can be viewed as a permanent modification to a plant and could be viewed as a change to the licensing basis of the NPP if the degradation level is significant. Unlike the intentional changes to a plant that may or may not increase the plant risk, the degradation phenomena are normally deleterious in nature and increase the plant risk. Therefore, it is important to determine whether a level of degradation in a component is safety-significant and develop strategies for inspection and maintenance. The foremost task in determining the safety significance of a degradation level is to identify a critical risk increase level, which can be specified as the increase in core damage frequency (ΔCDF) or in large early release frequency (ΔLERF).

As introduced in the previous section, previous studies have used U.S. NRC Regulatory Guide (RG) 1.174, "An Approach for Using Probabilistic Risk-Informed Decisions on Plant-Specific Changes to the Licensing Basis," for assessing age-related degradation of SPCs. It should be noted that the use of probabilistic risk assessment techniques in evaluation of a licensing basis change is not mandatory but encouraged as stated in this guide. However, the large uncertainties in the degradation phenomena make such a use a natural choice because a deterministic delineation of the degradation is less reliable. In addition, since the level of degradation in an SPC corresponding to an acceptable level of risk increase is normally significantly below the level that an engineering analysis may indicate a functional limit of the SPC for normal operation condition, the criteria for an acceptable seismic performance of the SPC, in terms of its seismic fragility capacity, may be better characterized by evaluating the degradation effect on the plant risk. In summary, RG 1.174 is suitable for assessing the safety significance of degradation of SPCs in NPPs. Without explicitly stated in the rest of this report, the current Revision 2 of RG 1.174 [2011] is assumed.

Seismic probabilistic risk assessment (SPRA) of NPPs can systematically quantify the seismic risk associated with the NPPs and is the foundation for risk-informed regulation and decision-making. The probabilistic risk assessment (PRA) technology, including SPRA, has been recognized by the nuclear industry and regulatory bodies to be sufficiently established as a tool for risk-informed decision making. PRA has been successfully used to optimize the use of inspection resources and identify the most effective potential backfit strategies for plant safety improvement. RG 1.174 Rev. 2 uses the risk insights determined by a PRA and the NRC's Safety Goal Policy Statement [51 FR 30028, 1986] for decision on proposed changes to plant licensing basis.

RG 1.174 Rev. 2 contains specific statements on what level of risk increase, i.e., ΔCDF and/or ΔLERF, is acceptable due to a change in a plant's licensing basis. In general, the philosophy in this guide is that only small increases in risk are allowed and sufficient defense-in-depth and sufficient margins must be maintained, to account for uncertainties and the fact that safety issues continue to emerge. It should be noted that not all positions stated in RG 1.174 are directly applicable to the assessment of the degradation of SPCs due to the intrinsic differences between the degradation phenomena and manmade changes to the plant. The most important items in RG 1.174 to its application to the development of degradation acceptance criteria (DAC) are *the adequacy of the PRA* and *the allowable risk increases*.

2.1.1 Probabilistic Risk Assessment

As stated in RG 1.174, the PRA should represent the as-built and as-operated plant condition and should have sufficient scope, level of detail, and technical adequacy. The results of the PRA are used to (1) assess the baseline CDF/LERF of the plant and (2) assess the change in CDF/LERF due to the change in the licensing basis (degradation in this report). Section 2.3 of RG 1.174, "Technical Adequacy of Probabilistic Risk Assessment Analysis," provides requirements regarding the scope, level of detail, technical adequacy, and plant representation. *The scope of a PRA* is defined in terms of the causes of initiating events (e.g., internal events, internal floods, seismic events, internal fires, high winds, external flooding) and the plant operating modes (e.g., full power, lower power, shutdown). *The level of detail in a PRA* should be sufficient to characterize the impact of the proposed change (degradation) or should be modified properly otherwise. *The technical adequacy of a PRA* refers to the adequacy of the actual modeling and the reasonableness of the assumptions and approximation [see RG 1.200, 2007 for details]. *The plant representation of a PRA* should reflect the as-built and as-operated plant, and RG 1.200, Rev 1. also provides guidance in this area. This point is actually very important and difficult in practice to achieve for the DAC development, because, ideally, the PRA should reflect the current state of degradation in all SSCs in the PRA model. It has been custom to base the DAC development on the assumption of no significant degradation in SSCs other than the subject SSC.

In spite of these requirement on the PRA, since the DAC should be so defined that an SPC is not allowed to degrade to a level that can cause a substantial increase in the plant risks, the PRA executed for this purpose of DAC development may not need to be highly sophisticated according to RG 1.174.

2.1.2 Acceptable Level of Risk Increases

Figure 2-1 and Figure 2-2 show the RG 1.174 acceptance guidelines for CDF-based and LERF-based risk-metrics, assuming that risk results are estimated through a full-scope (internal and external hazard, at-power, lower power, and shutdown) PRA. RG 1.174 provides two sets of acceptance guidelines for CDF and LERF, respectively, and states both should be used. Guidelines applicable to the DAC development are summarized in the following:

For CDF:

Region III in Figure 2-1: when $\Delta CDF < 10^{-6}$/reactor year, acceptable regardless of whether there is a calculation of the total CDF. However, if there is an indication that the CDF may be considerably higher than 10^{-4}/reactor year, the focus should be on finding ways to decrease rather than increase it.

Region II in Figure 2-1: when $10^{-6} < \Delta CDF < 10^{-5}$/reactor year, acceptable only if the total CDF < 10^{-4} /reactor year.

Region I in Figure 2-1: when $\Delta CDF > 10^{-5}$/reactor year, normally not allowed.

For LERF:

Region III in Figure 2-2: when ΔLERF < 10^{-7}/reactor year, acceptable regardless of whether there is a calculation of the total LERF. However, if there is an indication that the LERF may be considerably higher than 10^{-5}/reactor year, the focus should be on finding ways to decrease rather than increase it.

Region II in Figure 2-2: when 10^{-7} < ΔLERF < 10^{-6}/reactor year, acceptable only if the total LERF < 10^{-5} /reactor year.

Region I in Figure 2-2: when ΔLERF > 10^{-6}/reactor year, normally not allowed.

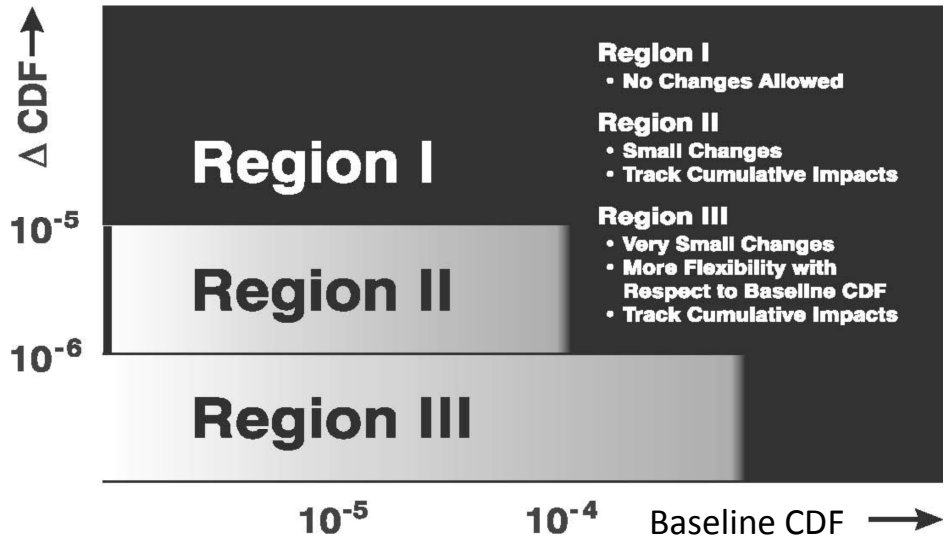

Figure 2-1 Acceptance Guidelines for Core Damage Frequency [RG 1.174, Rev. 2, 2011]

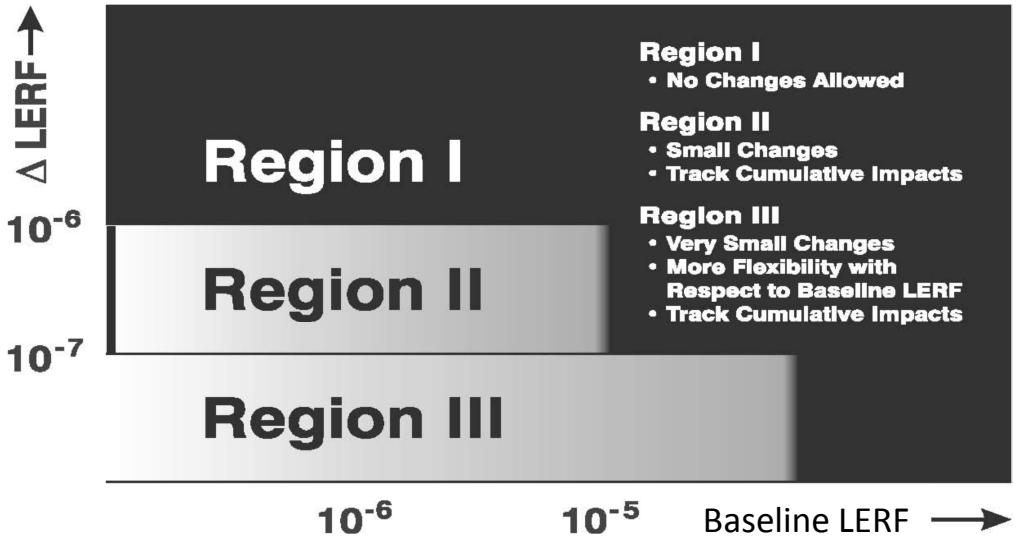

Figure 2-2 Acceptance Guidelines for Large Early Release Frequency [RG 1.174, Rev. 2, 2011]

It should be noted that as stated in RG 1.174, the boundaries between regions are not definitive and the darkness of the shading in Figure 2-1 and Figure 2-2 indicates the level of technical review and management. These guidelines are applicable to at-power, low-power, and shutdown operation conditions. In situations where LERF guidelines are not practical, for example, when the containment function is not maintained during certain shutdown condition, it is allowed to use more stringent baseline CDF (e.g., 10^{-5}/reactor year) to achieve an equivalent risk profile.

RG 1.174 states that the risk acceptance guidelines should not be interpreted to be overly prescriptive and the epistemic uncertainties associated with the PRA calculation preclude a definitive decision purely based on numerical estimates. A comparison of the PRA results and these acceptance guidelines must be based on an understanding of the risk contributors to the PRA results and on the robustness of the assessment of these contributors and the impact of the uncertainties. If the PRA is not full scope, the significance of the out-of-scope items must be addressed in accordance with the margin between the as-calculated values and the acceptance guidelines.

RG 1.174 recognizes that there may not be a Level-2 PRA for some plants. If only a Level-1 PRA is available, one can estimate LERF by allocating a subset of the core damage accidents identified in the Level-1 PRA to a release category [Pratt et al., 2004]. The use of this simplified approach is only allowed when the plant is not close to the CDF and LERF benchmark values.

For the development of DAC for SPCs, it is convenient to assume that risk criteria fell in the regions III (i.e., $\Delta CDF_{cr} = 10^{-6}$/reactor year and $\Delta LERF_{cr} = 10^{-7}$/reactor year) should be considered, as there is no additional requirement on the baseline CDF and LERF. In fact, it is expected that most NPPs would meet the NRC safety goals of CDF = 10^{-4}/reactor year and LERF = 10^{-5} / reactor year, which are discussed in GI-199 [2010] and SECY-97-208 [1997]. If total CDF and total LERF are less than 10^{-4} / reactor year and 10^{-5} / reactor year, respectively for CDF and LERF, risk criteria of $\Delta CDF_{cr} = 10^{-5}$/reactor year and $\Delta LERF_{cr} = 10^{-6}$/reactor year can also be used. However, the quality of the PRA in the calculation of the total CDF and LERF would have to be full-scope; with sufficient level of detail; technically adequate; and representing well the as-built, as-operated, and as-degraded plant. This translates to a significant requirement on the PRA implementation, which may not always be practical. Therefore, $\Delta CDF_{cr} = 10^{-6}$/reactor year and $\Delta LERF_{cr} = 10^{-7}$/reactor year are recommended for use in the development of DAC for SPCs.

2.2 Development of Three-Tier DAC

In this study, only ΔCDF_{cr} will be used for simplicity and the procedure developed based only on ΔCDF_{cr} can be easily generalized to one considering both ΔCDF_{cr} and $\Delta LERF_{cr}$, because the DAC can simply be defined as the smaller of the DAC_{CDF} and DAC_{LERF}. Of course, the calculation of the latter would incur the Level-2 PRA calculation that may not be readily available for any given plant. Hereafter in this report, DAC will be used in place of DAC_{CDF} for simplicity.

Since the fragility analysis and the PRA are performed separately and normally by different group of people, a tight integration of these two types of analyses for the purpose of DAC development is neither efficient nor necessary. As will be shown later, the relationships between the levels of degradations, fragility estimates, and the CDF estimates are often smooth enough up to the ΔCDF_{cr}, so that the fragility analysis and the PRA can be performed

conveniently in two steps avoiding the iterations and the determination of DAC corresponding to the ΔCDF_{cr} can be obtained through proper interpolation. Therefore, the fundamental procedure for the development of the DAC for an SPC can be expressed as,

(1) Develop a range of the fragility values of the subject SPC that various levels of degradation can potentially result in,

(2) Perform PRAs of the plant using these fragility values to obtain a range of corresponding CDFs,

(3) Interpolate the fragility-CDF curve using the $\Delta CDF_{cr} = 10^{-6}$/reactor year to determine a critical fragility capacity F_{cr}.

It should be pointed out that the fragility value can be specified as the median fragility or the high confidence lower probability of failure (HCLPF) capacity, and the associated uncertainties, the latter of which are properly propagated in the PRA to the uncertainty associated with the mean CDF estimate. For step 1, it should be noted that it is not necessary to perform a series of fragility analyses if the fragility range can be developed based on experience and a simple evenly-distributed fragility values within the range can be used. For step 3, there are advanced methods, such as the cubic spline interpolation method, for performing accurate interpolation based on data points that are not so densely populated. However, if the fragility-CDF relationship is found not to be sufficiently smooth, more PRAs should be performed using additional fragility data. Given the uncertainties associated with fragility calculation and PRA, determining an "exact" point by iteration involving multiple fragility analyses and PRAs is not justified.

Based on the F_{cr}, three-tier DAC for an SPC can be defined as: (a) DAC in terms of the fragility capacity, (b) DAC in terms of the level of degradation, and (c) DAC in terms of time, which are hereinafter designated as DAC_F, DAC_D, and DAC_T, respectively. DAC_F is a direct result of step 3 and is the basis for the development of DAC_D and DAC_T.

If there is only one degradation scenario in the subject SPC, such as corrosion in the tank shell of a condensate storage tank, DAC_D can be determined by interpolating the fragility-thickness reduction curve at DAC_F. The fragility-thickness reduction curve can be developed numerically through a series of fragility analyses that covers the F_{cr}. DAC_D is especially useful when a specific level of degradation is observed during an inspection and the inspector wants to assess how the observed level of degradation impacts the seismic CDF. One disadvantage in using DAC_D is that multiple degradation scenarios in an SPC are difficult to be described.

DAC_T can be developed when there are reliable time-dependent degradation models for an SPC, by mapping its DAC_F directly to DAC_T or by converting DAC_D to DAC_T. The former approach is more general because it allows multiple degradation scenarios, as will be seen in Section 5. On the other hand, the latter allows the combination of an observed level of degradation and a time-dependent degradation model to develop the remaining life of an SPC. It should be noted that time-dependent degradation models are rare and difficult to be developed for a particular SPC, as discovered previously in this collaboration program.

2.3 Specific Task Assignments

The procedure described in Section 2.2 was further refined into the following five steps that BNL and KAERI have carried out:

1) (BNL) develop seismic fragilities for SPCs in the undegraded and various levels of degradations (see Section 3 of this report);
2) (KAERI) perform probabilistic safety assessments (PRAs) for a plant using the fragility data from Step 1;
3) (KAERI) tabulate changes in the core damage frequency (ΔCDF) related to various levels of median fragility corresponding to undegraded and degraded conditions;
4) (BNL) based on the acceptance guideline for CDF in the U.S. NRC Regulatory Guide 1.174, determine the appropriate ΔCDF_{cr} and the corresponding threshold level of fragility;
5) (BNL) (5a) using the results from Step 4, quantify the level of degradation which corresponds to a potentially significant effect on seismic safety of the plant, and/or (5b) using the results from Step 4, determine the time for degradation to have a potentially significant effect on seismic safety of the plant.

In summary, BNL focused on the fragility analysis and the development of the DAC for the selected condensate storage tank (CST), and KAERI performed all the PRAs using an existing PRA model to generate the fragility-CDF curves.

Sections 3 through 5 will present a case study for the above procedure, using the condensate storage tank (CST) that was studied for the development of fragility capability considering various degradations in the CST. Section 3 will summarize the previous fragility results, Section 4 will present the results of the PRA, and Section 5 develops the three-tier DAC.

3 SEISMIC FRAGILITY ANALYSIS OF A CONDENSATE STORAGE TANK WITH DEGRADATIONS

This section presents a summary of the seismic fragility analysis of the condensate storage tank with various postulated degradation conditions, which are the topics of the Year 3 and Year 4 annual reports [Nie et al., 2010, 2011]. The intent of this summary is to create a coherent reference that covers the entire process of seismic fragility analysis and the application of the seismic fragility results in the development of seismic degradation acceptance criteria, the latter of which will be focus of this report. More details of the fragility analyses can be found in the Year 3 and Year 4 annual reports.

3.1 Basic Information of the Condensate Storage Tank

The Year 3 and Year 4 research tasks of this collaboration program studied the seismic fragility of a condensate storage tank (CST) with various degradation conditions using the conservative deterministic failure margin (CDFM) method as introduced in Appendix A of NUREG/CR-5270 [Kennedy et al., 1989]. The CST was located in the Ulchin nuclear power plant of Korea, which is located on the east side of Korea on the coast of the Pacific Ocean. The CST is a flat-bottom cylindrical tank filled with water and under atmospheric pressure. Figure 3-1 shows a picture of two CSTs separated by an auxiliary building. The elevation view of the CST shown in Figure 3-2 also shows the key dimensions of the tank, some of which are also summarized in Table 3-1. The CST is heavily anchored to the reinforced concrete foundation through 78 anchor bolts, as shown in Figure 3-3. The anchor bolts have a diameter of 2-1/2" and are A36 steel. The length of the anchor bolts is 3'-6", with an embedment of about 2'-1". The anchor bolts were post-installed in the pre-formed holes in the concrete foundation with non-shrinking grout. In the fragility analysis, soil-structure interaction (SSI) is not considered since the CST is founded on rock.

Figure 3-1 Photo of the Condensate Storage Tanks [Nie et al., 2010, 2011]

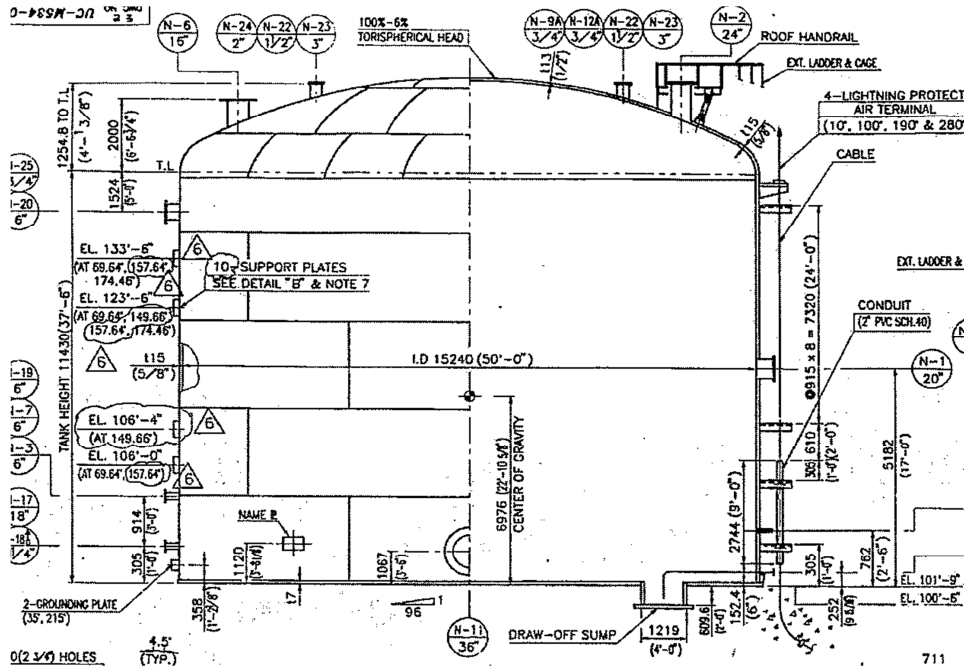

Figure 3-2 Elevation View of the Condensate Storage Tank [Nie et al., 2010, 2011]

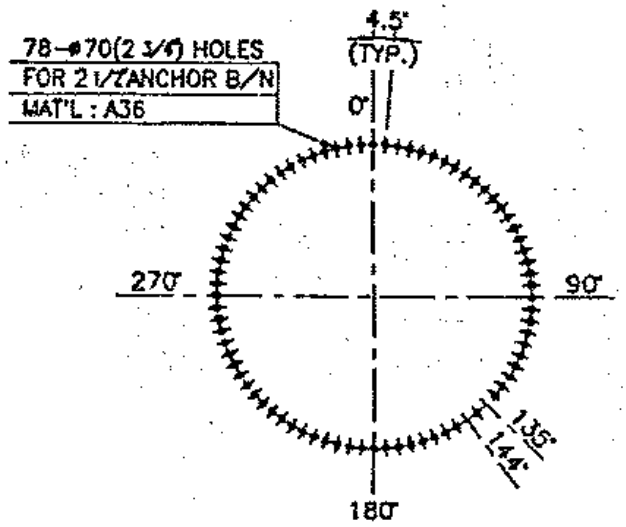

Figure 3-3 Anchor Bolt Orientation [Nie et al., 2010, 2011]

Table 3-1 Key Dimensions of the Condensate Storage Tank [Nie et al., 2010, 2011]

Inner Diameter	50’ (15.24 m)
Tank Height (to water level)	37’-6” (11.43 m)
Shell Thickness	5/8” (15.875 mm)
Torispherical Head Thickness	1/2” (12.7 mm)
Bottom Plate Thickness	1/4” to 5/16” (7 mm)

3.2 Material Degradation Models

The fragility analysis of the CST in Year 3 and Year 4 scope of work considered three basic degradation scenarios: (A) degraded stainless tank shell, (B) degraded anchor bolts, and (C) anchorage concrete cracking. It also considered two combined cases: (D) a perfect correlation of the degradation scenarios A, B, and C; and (E) a non-perfect correlation of the three degradation scenarios. Corresponding to the three basic degradation scenarios A, B, and C, material degradation models were identified/developed to introduce the time factor in describing these postulated age-related degradations.

3.2.1 Material Degradation Model for Stainless Steel Tank Shell

The material degradation model for the stainless steel tank shell used for the seismic fragility analysis of the CST is the mechanochemical model for stress corrosion cracking (SCC), which is

one of the three time-dependent material degradation models for stainless steel that are documented in the Year 2 annual report [Nie et al., 2009]. It can be seen from Figure 3-1 that as there are no signs of significant degradation in the CST shell, the consideration of tank shell degradation in the seismic fragility analysis of the CST was for the purpose of demonstration.

The mechanochemical model [Saito and Kuniya, 2001] was developed to predict the SCC growth in stainless steel components submerged in 288 °C water. This model was judged to be relevant in the NPP environment because austenitic stainless steel (especially type 304) is widely used in light water reactors (LWRs) and in particular used in the subject CST. The structural integrity of the involved components due to inter-granular stress corrosion cracking (IGSCC) is often a concern in NPPs. It should be noted that since the water temperature in the CST is similar to the atmospheric temperature at the site (not 288 °C), effort was taken to identify the proper parameters to alleviate the effect of high temperatures. As a result, the performance of the resultant degradation model appears to be within normal expectation.

This SCC crack growth model for type 304 stainless steel is based on a hypothesis of the slip-formation/dissolution mechanism and is expressed as a function of material conditions, water chemistry, and stress related parameters. This model involves two major mechanisms: 1) slip step formation due to dislocation movement at the crack tip, and 2) anodic dissolution at the bare surface after the slip deformation. The derivation of this model was lengthy, highly theoretical, and cannot be easily summarized in this report. Interested readers are recommended to refer back to the original reference. Fortunately, based on the theoretical development, a relatively simple numerical model was also developed for type 304 stainless steel in 288 °C water, using a minimal number of parameters [Saito and Kuniya, 2001].

This relatively simple model of the SCC crack growth rate (m/s) is represented by the following simple power law of two parameters only,

$$\frac{da}{dt} = 1.1 \times 10^{-7} \left[2.5 \times 10^{10} \exp\left(-\frac{3 - 0.15(K-9)^{1/3}}{0.0774} \right) \right]^n \qquad (3\text{-}1)$$

In which $a(t)$ is the crack size at a time instance t, K is the applied stress intensity factor and $K > 9\ \mathrm{MPa}\sqrt{\mathrm{m}}$, and the numerical constant n can be expressed as,

$$n = -\frac{1}{3}\{\ln[(1 + C_1\ \mathrm{EPR})(C_2\kappa + C_3)(C_4\phi_C + C_5)] + C_6\phi_C + C_7\}, \qquad (3\text{-}2)$$

where EPR is the electrochemical potential kinetic reactivation, κ the bulk water conductivity, and ϕ_C the bulk corrosion potential, C_1-C_7 are numerical constants, which are determined from a database of test data using a wide range of stressing ($11\ \mathrm{MPa}\sqrt{\mathrm{m}} \le K \le 60\ \mathrm{MPa}\sqrt{\mathrm{m}}$), material ($1.4\ \mathrm{C/m^2} \le \mathrm{EPR} \le 13\ \mathrm{C/m^2}$), and water chemistry ($0.1\mu\mathrm{S/cm} \le \kappa \le 1.5\mu\mathrm{S/cm}$, $-280\mathrm{mV} \le \phi_C \le 250\mathrm{mV}$). The values of C_1-C_7 are given as,

$$
\begin{aligned}
C_1 &= 3.57 \times 10^{-2}, \\
C_2 &= 1.49 \times 10^{-8}, \\
C_3 &= 2.23 \times 10^{-8}, \\
C_4 &= 4.57 \times 10^{-3}, \\
C_5 &= \quad 23.12, \\
C_6 &= 2.29 \times 10^{-3}, \\
C_7 &= \quad 11.56.
\end{aligned}
\tag{3-3}
$$

To summarize, the model of the SCC crack growth rate really only has four parameters: *K,* EPR, κ, and ϕ_C. As for application to type 304 stainless steel in 288 °C water, Saito and Kuniya [2001] suggested the following ranges (or typical values) of these four parameters,

$$
\begin{aligned}
K &= 28\ \mathrm{Mpa}\sqrt{\mathrm{m}},\ \text{depends on loading} \\
\kappa &= 0.1 - 1.2\ \mu\mathrm{S/cm} \\
EPR &= 6 - 13\ \mathrm{C/cm^2} \\
\phi_C &= -200 - +250\ \mathrm{mV}.
\end{aligned}
\tag{3-4}
$$

To apply this model to the CST in this study, the effect of the high temperature that biases from the actual temperature of the CST was alleviated by assigning EPR to the lower bound value 6 C/cm^2, κ to 0.4 μS/cm, and ϕ_C to -50 mV. Using these values and Equation 3-2, the exponent *n* in Equation 3-1 was evaluated to 0.87.

The stress intensity factor *K* can be estimated based on the static water pressure, which is 16.3 psi as determined previously [Nie et al., 2010, 2011]. The stress intensity factor is also a function of the crack geometry; therefore *K* is time dependent due to crack growth and can be symbolically represented as $K(a(t))$. Since $K(a(t))$ is not readily available and the purpose of the current study is for demonstration, a simplified approach was used. Assuming a through crack in the vertical direction at the bottom of the tank shell and of a length that is twice of the tank thickness, *K* can be estimated using the following simple formula [Tada et al., 2000]:

$$
\begin{aligned}
\sigma_{hoop} &= \frac{P_{ST} \times R}{t_S} = 7.8\ ksi \\
K &= \sigma_{hoop} \times \sqrt{\pi \delta_S} = 12.018\ MPa\sqrt{m}
\end{aligned}
\tag{3-5}
$$

Based on Equation 3-1, a constant *K* leads to a constant crack growth rate of 0.0075 in/year. A list of crack depths can then be calculated for a period of 80 years, which is the current expectation of the longest operating life of NPPs. Since a few isolated cracks in the tank shell may not affect much the seismic capacity of the tank, it is further assumed that many cracks cluster at a small region at the base of the tank shell and the effect of the crack assembly is similar to loss of material in that location. The fragility analysis of CST with levels of tank shell degradations will follow this assumption.

3.2.2 Material Degradation Model for Anchor Bolts

Unlike the stainless steel tank shell of the CST, the anchor bolts made of A36 are prone to corrosion because of the salty moisture in a location close to the ocean. The protecting stainless steel cover as shown in Figure 3-1 may not be leak-tight. A power model for steel corrosion was chosen from the Year 2 annual report [Nie et al., 2009] to model the degradation of the anchor bolts. This model had been used by Mori [2005] to predict reliability-based service life, indicating its suitability for fragility analysis.

The depth of corrosion in the power model can be represented by,

$$X(t) = Ct^{\alpha} \tag{3-6}$$

in which t is the elapsed time in years, C is the rate parameter, and α is the order of the power model that depends on the nature of the attack. The corrosion rate C is a function of material, ambient moisture, and temperature. Both parameters C and α can be estimated by experiments. Table 3-2 shows the average values for these parameters for various environments, which were determined by Albrecht and Naeemi [1984]. Corresponding to the parameters C and α in this table, the units for the level of attack $X(t)$ and time t are μm and year, respectively.

To be consistent with the coastal environment that the Ulchin NPP is located, the marine environment in Table 3-2 was selected to model the degradation of the anchor bolts using the power model as defined by Equation 3-6, for the fragility analysis of the CST.

Table 3-2 Average Values for Corrosion Parameters C and α [Albrecht and Naeemi, 1984].

Environment	Carbon Steel		Weathering Steel	
	C	α	C	α
Rural	34.0	0.65	33.3	0.50
Urban	80.2	0.59	50.7	0.57
Marine	70.6	0.79	40.2	0.56

Based on the power model and the selected parameters C = 70.6 and α = 0.79, the depth of corrosion of the anchor bolt is shown in Figure 3-4 as a function of the time in years. Albeit the nature of the model is nonlinear, the actual depth of the corrosion for this particular application is close to a linear relation with time.

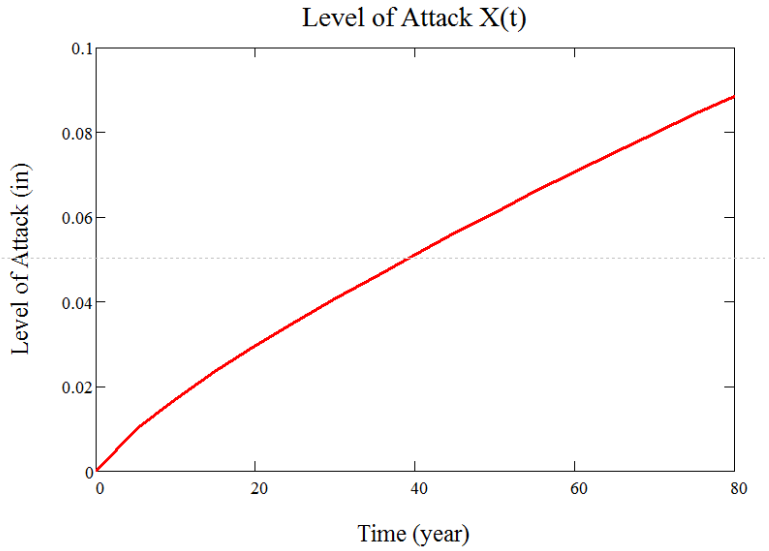

Figure 3-4 The Depth of Corrosion of the Anchor Bolts

3.2.3 Material Degradation Model for Cracked Anchorage Concrete

KAERI identified data regarding the crack width and depth of reinforced concrete that were in four Korean NPPs over a period of about 25 years. Time-dependent models based on regressions of these data were also provided by KAERI, as shown in Figure 3-5 and Figure 3-6. The linear crack width model, as reproduced in the following, was used for the fragility analysis of the CST with cracked anchorage concrete:

$$W(t) = 0.00119\,t + 0.108, \tag{3-7}$$

In which $W(t)$ is the crack width (mm) and time t is in years. Since the impact of this model on the fragility capacity of the CST with cracked anchorage concrete was found to be marginal, a revised version of this model was developed using the same measurements, by disallowing the intercept in the linear regression equation. The original version provided by KAERI is designated as C-1, while the new model is designated as C-2. As shown in Figure 3-7, the new model C-2 can be simply expressed as,

$$W(t) = 0.0078\,t, \tag{3-8}$$

with the same units as in Equation 3-7. It should be pointed out that the measured crack widths have significant variation and the linear regression models do not necessarily represent true underlying relationships. The use of these curves in this study is for the purpose of demonstration; the applicability of these models in practice should be investigated with careful scrutiny.

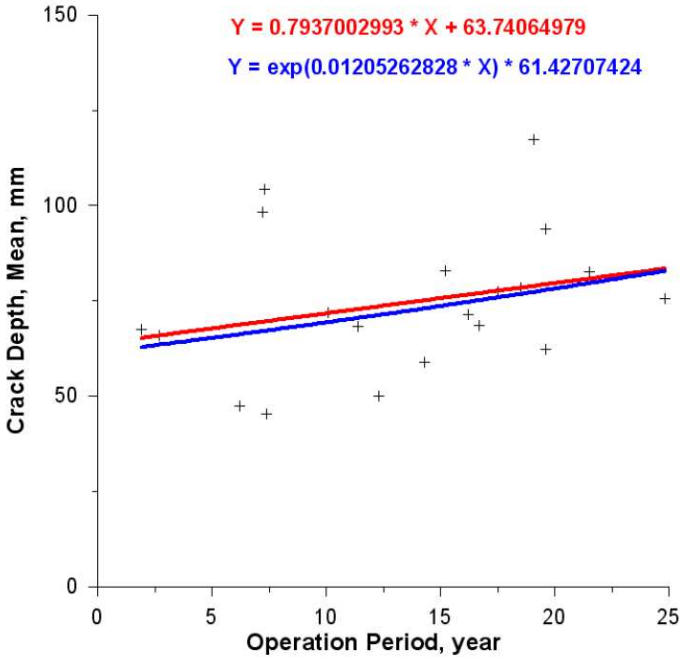

Figure 3-5 Crack Depth Models Based on Measurements in Korean NPPs (Courtesy of KAERI)

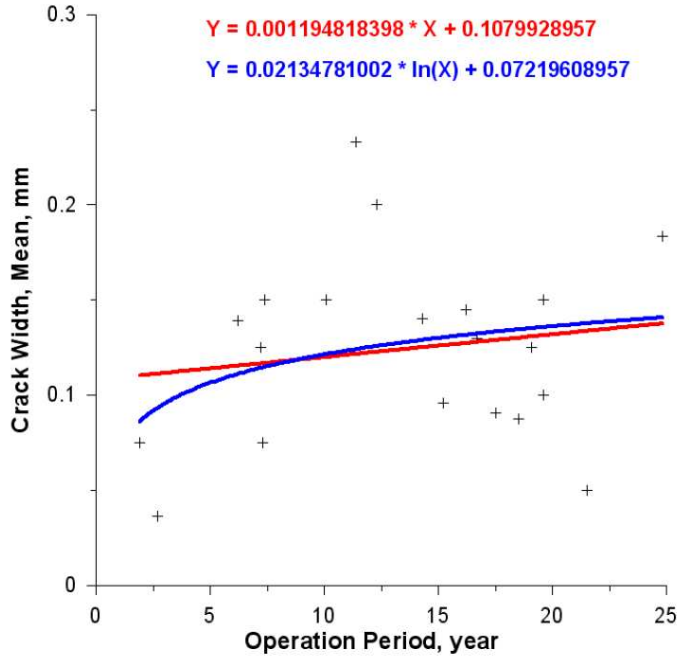

Figure 3-6 Crack Width Models Based on Measurements in Korean NPPs (Courtesy of KAERI)

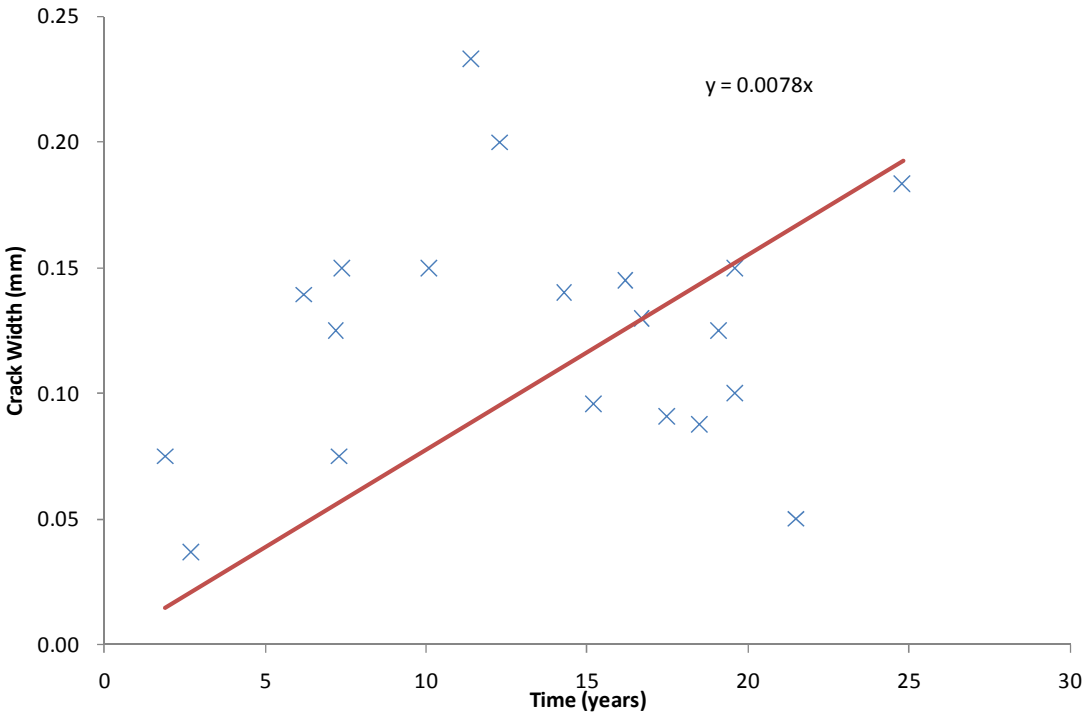

Figure 3-7 New Crack Width Model Based on Measurements in Korean NPPs

The crack width models must be mapped to the anchorage strength for its application to the fragility analysis of the CST with cracked anchorage concrete. Klingner et al. [1998] developed an empirical relation between anchor strength and crack width for grouted anchors:

$$P = k\, h_{eff}^{1.5} \sqrt{f_c'}, \tag{3-9}$$

where k is a constant determined from test that represents the normalized tensile capacity, h_{eff} the effective embedment (in), P observed tensile capacity (lbf), and f_c' is the tested concrete compressive strength. The grouted anchors reported in NUREG/CR-5434 [Klingner et al., 1998] had a diameter of ¾", an embedment of 4", and an effective embedment of 4", which are much smaller than those of the anchor bolts for the subject CST. For the anchorage construction of the subject CST, h_{eff} was estimated to be 23" by subtracting 1" from the total embedment length to account for the nut. The concrete nominal compressive strength for the subject CST was unknown but was assumed to be 4,500 psi according to an experiment by Lee et al. [2001], which appeared to target at a CST very much similar to the subject CST. The measured concrete and grout compressive strength were much higher than 4,500 psi in the test. However, since the use of the nominal compressive strength had already led to a much higher anchor tensile strength, as to be shown later in this section, than the test results reported by Lee et al. [2001], these measured strengths were not utilized.

Grout plug pullout is the most dominant failure mode for the anchor bolts under tensile loads; therefore, the friction between the concrete and the grout is crucial in determining the tensile capacity of the anchor bolts [Lee et al., 2001, Klingner et al., 1998]. As shown in Figure 5.20 of NUREG/CR-5434, the dynamic tensile capacity is higher than the static capacity for uncracked

concrete/grout, while for cracked concrete/grout, the dynamic tensile capacity is lower than the static capacity. Comparing cracked to uncracked conditions, the reduction in dynamic tensile capacity was 73% while the reduction in static tensile capacity was 41%. The data for dynamic load capacity will be utilized for the seismic fragility assessment of the CST. The typical normalized tensile strength k is 57 for uncracked case and 15.5 for cracked case. The artificial crack in the test had a width of 0.3 mm (0.012").

The tensile strength of the anchorage for uncracked case was estimated to be 421.8 kips based on Equation 3-9, which is much higher than the capacity of 200 kips that was reported by Lee et al. [2001]. The reason for this difference may be the substantial difference in the scales of the anchor bolts in the two test studies; smaller scale usually leads to higher strength as commonly observed. Therefore, the test data in NUREG/CR-5434 will be used as factors to scale the test data reported by Lee et al. [2001]. For the subject CST, the tensile capacity of the anchorage for a crack width of 0.3 mm can be estimated as 200 kips × 15.5 / 57 = 54.4 kips. The tensile capacity of the anchorage for a crack width of *w* mm can be estimated based on the following linear interpolation/extrapolation:

$$T = 200 + \frac{w}{0.3}(54.4 - 200) \text{ kips.} \quad (3\text{-}10)$$

In the calculation, T is set to 0 kips as a lower bound value when Equation 3-10 results in an impractical negative tensile strength. Multiple cracks at one anchor bolt location were not considered in NUREG/CR-5434 and were not assumed in this study as well.

The smaller of the tensile strength of the anchorage determined using Equation 3-10 and the anchor bolt tensile capacity becomes the anchor bolt hold-down capacity.

The impact of the cracked concrete is directly on the bolt hold-down capacity but not the tank shell buckling capacity and the fluid pressure capacity; the overturning moment capacity and the sliding capacity are affected as a consequence.

3.3 Seismic Fragility Analyses of CST Using Design Water Level

The mathematical software Mathcad [2007] was chosen to perform the seismic fragility analysis of the CST in this collaboration program because of: (1) its capability in explicitly expressing mathematical equations in a fashion that a common engineer is familiar with, (2) its advanced functions in performing interpolation and root finding without significant programming, (3) its capability in mixing documentation and calculation so that the necessary technical background and explanations can be documented, and (4) its instant numerical calculation and plot rendering when any parameters are varied. The utilization of this tool saved considerable time that would be used in developing a spreadsheet or in-house code, because the clear presentation of equations avoided much unnecessary debugging time.

It should be noted that the design water level was assumed in the Year 3 research, and the operational water level was assumed for the Year 4 research. The use of the operational water level resulted in an increase in the baseline (undegraded case) high confidence low probability of failure (HCLPF) value from 0.426 g to 0.549 g. This subsection presents the fragility analysis using the design water level, and the next subsection presents the fragility analyses using the

operational water level, including three new cases that are not part of the Year 3 and Year 4 scope of work.

3.3.1 Fragility Analysis of CST for Degradation Case A - Degraded Tank Shell

The smaller thickness due to loss of material is assumed to occur at local regions at the base of the tank shell, and therefore only the capacity calculation but not the frequency and the response calculation will be changed. Because of this change of thickness of the tank shell, the upper bound check of the compressive buckling capacity requires the digitalization of the Figure 6 of NASA SP-8007 and implementation of an automatic interpolation to determine the necessary parameters.

The direct impact of the degraded tank shell is on the compressive buckling capacity and the fluid hold down capacity, but obviously not on the bolt hold down capacity. All three major resultant capacities: the overturning moment capacity, sliding capacity, and the fluid pressure capacity are affected. Both the slosh height and the horizontal displacement at the roof level of the auxiliary building become smaller as the seismic margin earthquake (SME) becomes smaller due to degradation. These decreases are because of the decrease in the SME capacity of the CST. Given the same level of input earthquake the slosh height would be unchanged and the horizontal displacement at the roof level of the auxiliary building would increase as the level of degradation increases.

Only mean fragility curves will be presented in this report because it is difficult to present the family of median fragility curves in a plot for more than one degradation level unless utilizing 3D surfaces. Even with 3D surfaces, it will be difficult to interpret the 3D fragility data without an interactive tool because of surface overlapping.

Figure 3-8 shows the mean fragility capacity of the CST with degraded tank shell for a series of years, from 0 up to 60 years, after which the fragility calculation was not mathematically achievable. These mean fragility curves were calculated using unchanged uncertainties, i.e., β_R = 0.2 and β_U = 0.27, the same as utilized for the base case [Nie et al., 2010, 2011]. In reality, since the degradation process is highly random and uncertain, both the epistemic and aleatory uncertainties should vary with time. However, reliable uncertainty data on the degradation model were not available. Provided the uncertainty data are available, the updated uncertainties, as functions of time, can be used to update the mean fragility curves without any technical difficulty. In Figure 3-8, it is obvious that the spacing of the fragility curves suddenly increases significantly after 45 years, when the governing failure mode shifted from the sliding failure to the overturning moment failure.

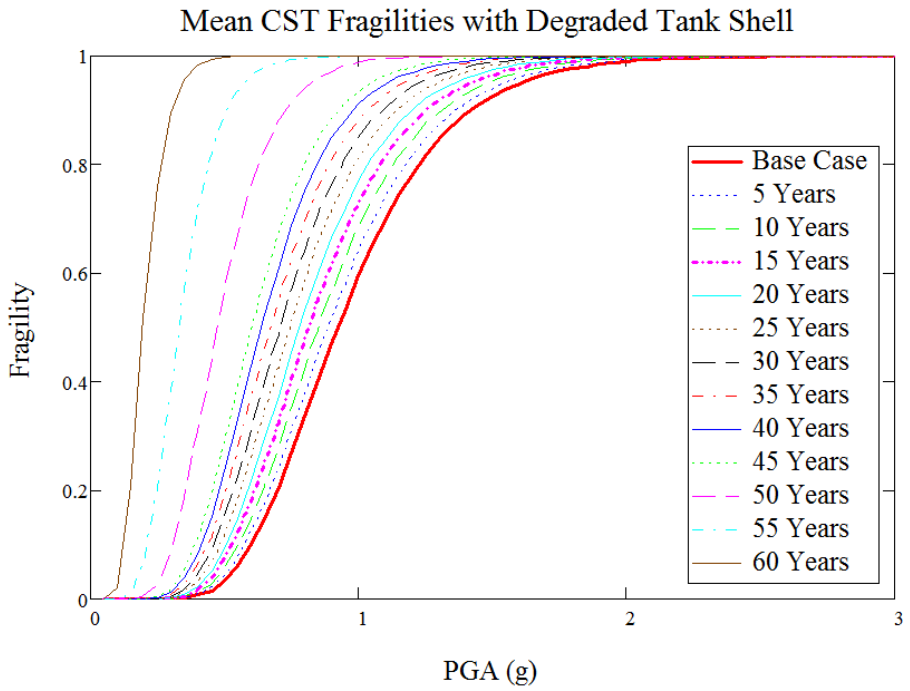

Figure 3-8 Mean Fragility Capacity of the CST with Degraded Tank Shell

It is easier to see the transition of failure mode by the relation of the HCLPF fragilities / the median capacities and time. Figure 3-9 and Figure 3-10 show in solid lines the HCLPF fragilities and the median capacities of the CST as a function of time, respectively. These figures also included the corresponding overturning moment capacities, sliding capacities, and the fluid pressure capacities, in dotted, dashed, and dash-dot lines, respectively. The fragility capacity is taken as the minimum of these three capacities. It is obvious in these figures that the tank shell degradation (wall thinning) has the most significant impact on fluid pressure capacity and the least impact on sliding capacity. The fragility capacity (either HCLPF capacity or the median capacity) is clearly dominated by the sliding mode until slightly after 45 years, and then by the overturning mode. Although the fluid pressure mode does not dominate the fragility capacity up to 60 years, it would be dominant shortly after 60 years had the calculation continued.

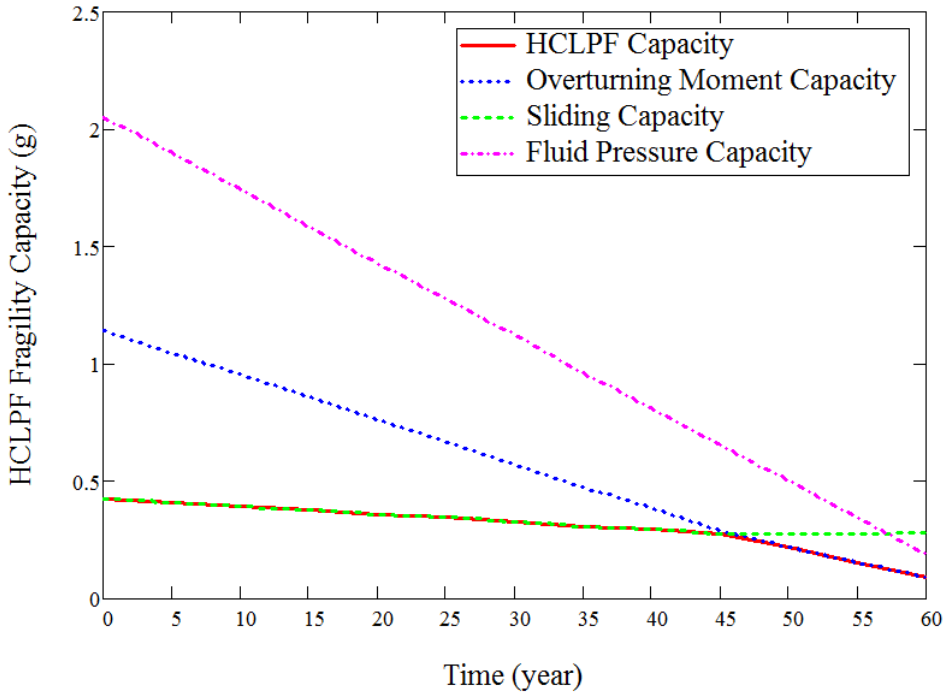

Figure 3-9 HCLPF Capacity of the CST with Degraded Tank Shell

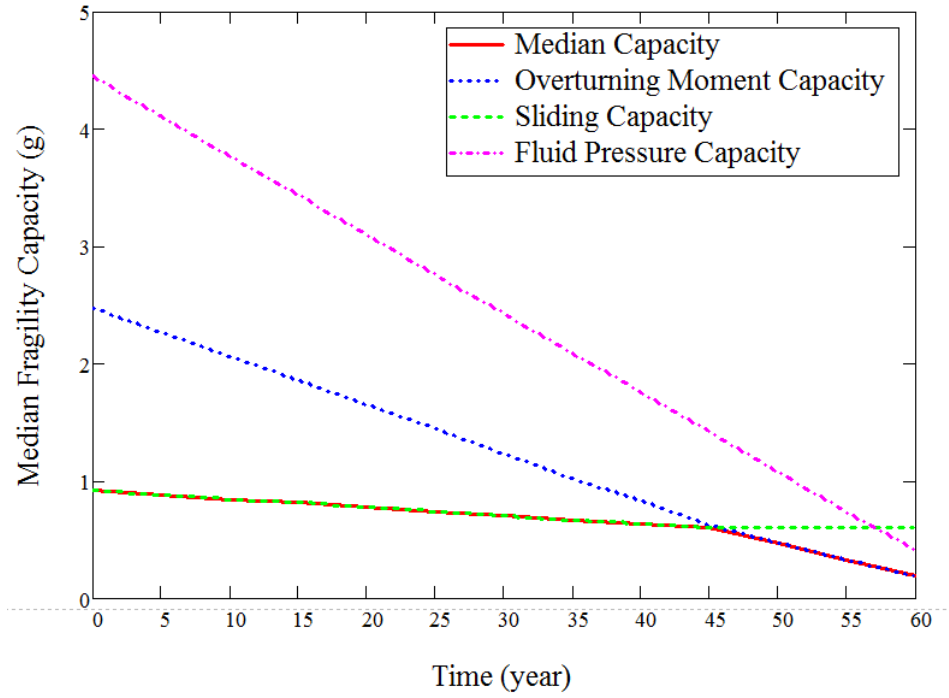

Figure 3-10 Median Capacity of the CST with Degraded Tank Shell

3.3.2 Fragility Analysis of CST for Degradation Case B - Degraded Anchor Bolts

A reduction of bolt diameter was assumed uniformly for all anchor bolts, as expressed by,

$$D_{bolt\_degraded} = D_0 - 2X(t). \tag{3-11}$$

The direct impact of degraded anchor bolts is simply on the bolt hold down capacity, and consequently on the overturning moment capacity and the sliding capacity. The degradation of anchor bolts does not affect the compressive buckling capacity, the fluid hold down capacity, and the fluid pressure capacity. Both the slosh height and the horizontal displacement at the roof level of the auxiliary building become smaller as the SME becomes smaller due to degradation. These decreases are because of the decrease in the SME capacity of the CST. Given the same level of input earthquake the slosh height would be unchanged and the horizontal displacement at the roof level of the auxiliary building would increase as the level of degradation increases.

Figure 3-11 shows the mean fragility capacity of the CST with corroded anchor bolts for a series of years, from 0 up to 80 years. For the same reason as in degradation case A, the effect of the degradation on the uncertainties is not considered. In a practical sense, it is obvious that the mean fragility is virtually unchanged for a period of 80 years. Sliding capacity dominates the HCLPF capacity for the entire period of 80 years. Even with a degradation level of half of the bolt diameter (corresponding to approximately 950 years based on the power model assumed in this study), the HCLPF SME capacity was found to be still as high as 0.34 g, compared to 0.426 g in the base case. With the bolt diameter reduced to half, the overturning moment capacity reduced to about 0.582 g from 1.14 g in the base case (without iteration for convergence to the real overturning moment capacity) and the fluid pressure capacity remains unchanged as expected. The slow reduction in the HCLPF capacity of the CST are believed to be attributed to by the large number of bolts (78 in total).

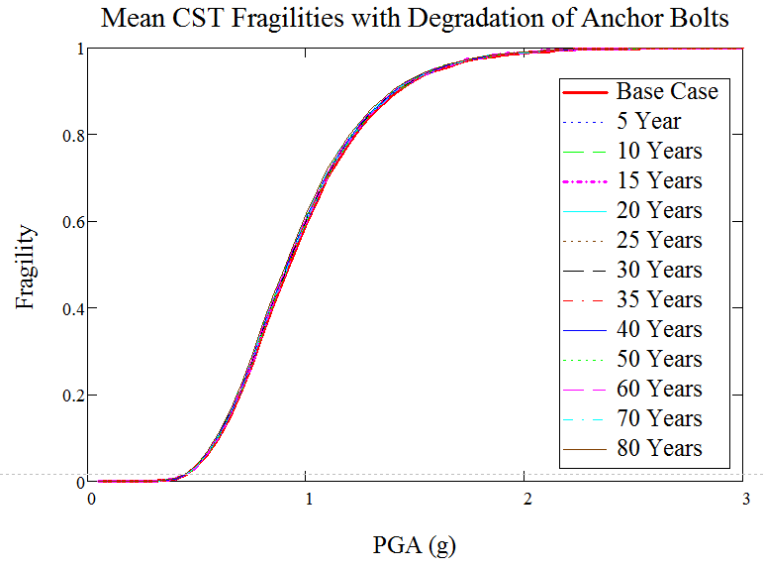

Figure 3-11 Mean Fragility Capacity of the CST with Degraded Anchor Bolts

Figure 3-12 and Figure 3-13 show in solid lines the HCLPF capacity and the median capacity of the CST as a function of time, respectively. These figures also included the corresponding overturning moment capacities, sliding capacities, and the fluid pressure capacities, in dotted, dashed, and dash-dot lines, respectively. The fragility capacity is taken as the minimum of these three capacities. From these figures, it is obvious that the anchor bolt corrosion has no or minimal impact on all three major capacities, with slightly noticeable effect on the overturning moment capacity. It is clear that the sliding capacity dominates.

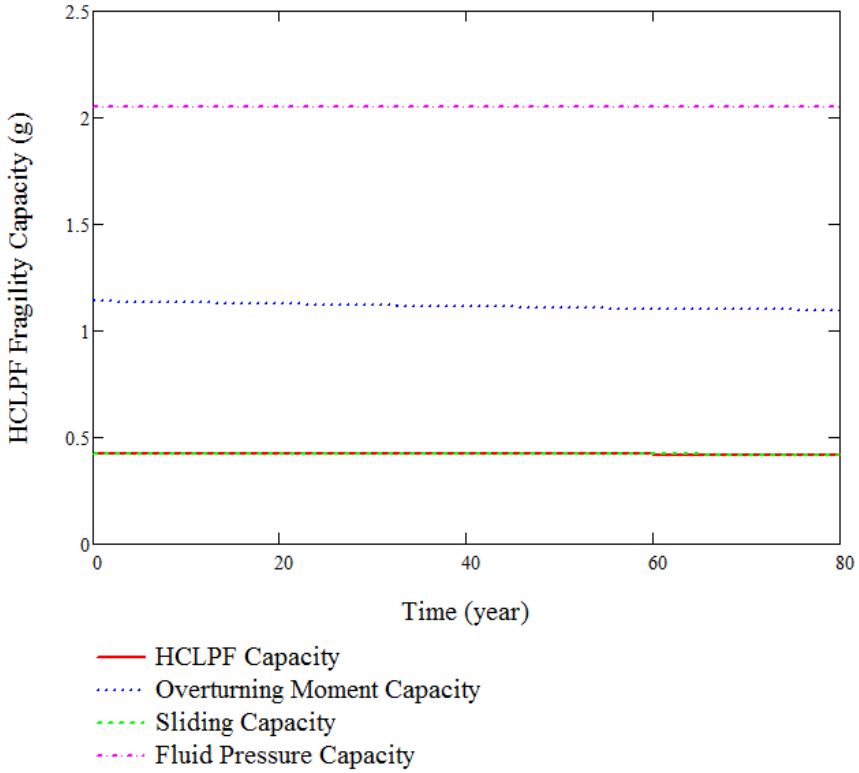

Figure 3-12 HCLPF Capacity of the CST with Degraded Anchor Bolts

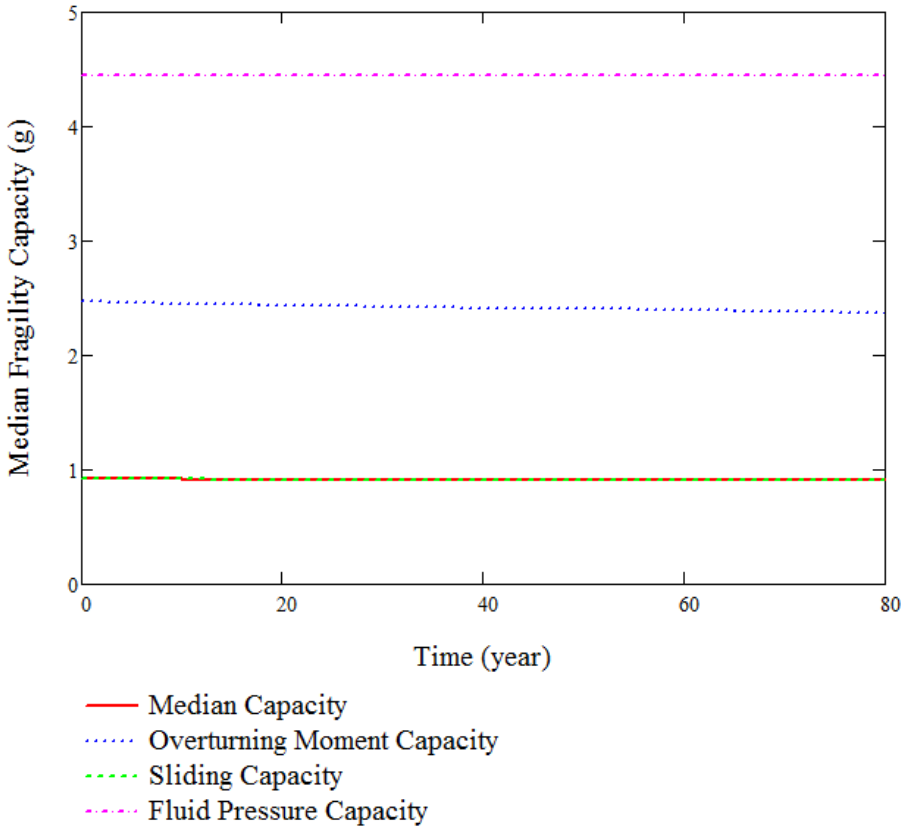

Figure 3-13 Median Capacity of the CST with Degraded Anchor Bolts

3.3.3 Fragility Analysis of CST for Degradation Case C - Anchorage Concrete Cracking

3.3.3.1 Using the C-1 Crack Growth Model

Figure 3-14 shows the mean fragility capacity of the CST with anchorage concrete cracking for a series of years, from 0 up to 80 years. For the same reason as in degradation case A, the effect of the degradation on the uncertainties is not considered. Figure 3-15 and Figure 3-16 shows the HCLPF SME capacity and the median SME capacity, respectively. In a practical sense, it is obvious that all fragility capacities are virtually unchanged for a period of 80 years. The fragility capacity starts to slightly decrease after 60 years and reaches a HCLPF SME capacity of 0.423 g at the end of 80 years, which is almost unchanged from the base case of a 0.426 g HCLPF capacity. Sliding capacity dominates the fragility capacity for the entire period of 80 years. The overturning moment capacity varied similarly to the sliding capacity, while the fluid pressure capacity remained unchanged.

At the end of 80 years, the bolt hold-down capacity reduced to 101.2 kips from 159.4 kips at the base case, representing a 37% reduction. Such a large reduction in the bolt hold-down capacity did not lead to a comparable level of reduction in fragility capacities because of the large number of anchor bolts (78).

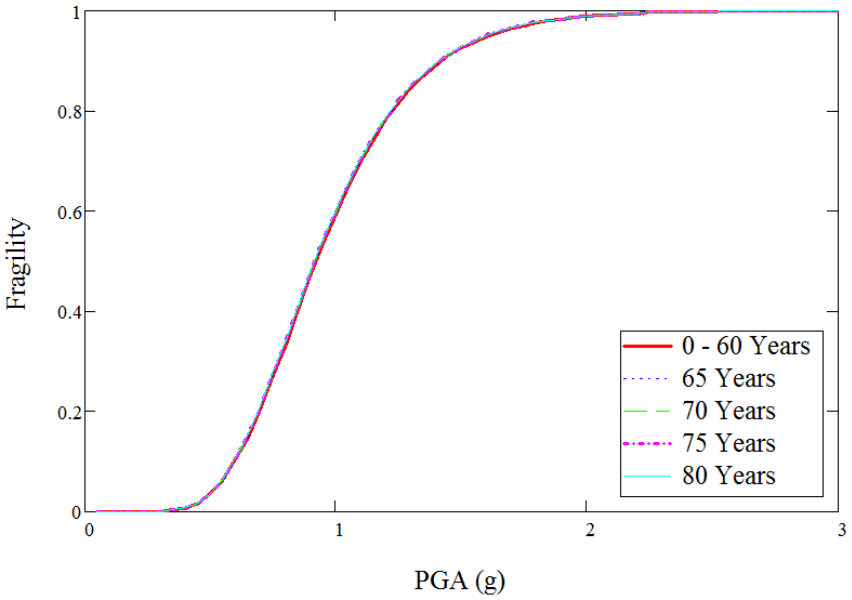

Figure 3-14 Mean Fragility Capacity of the CST with Cracked Anchorage Concrete (C-1)

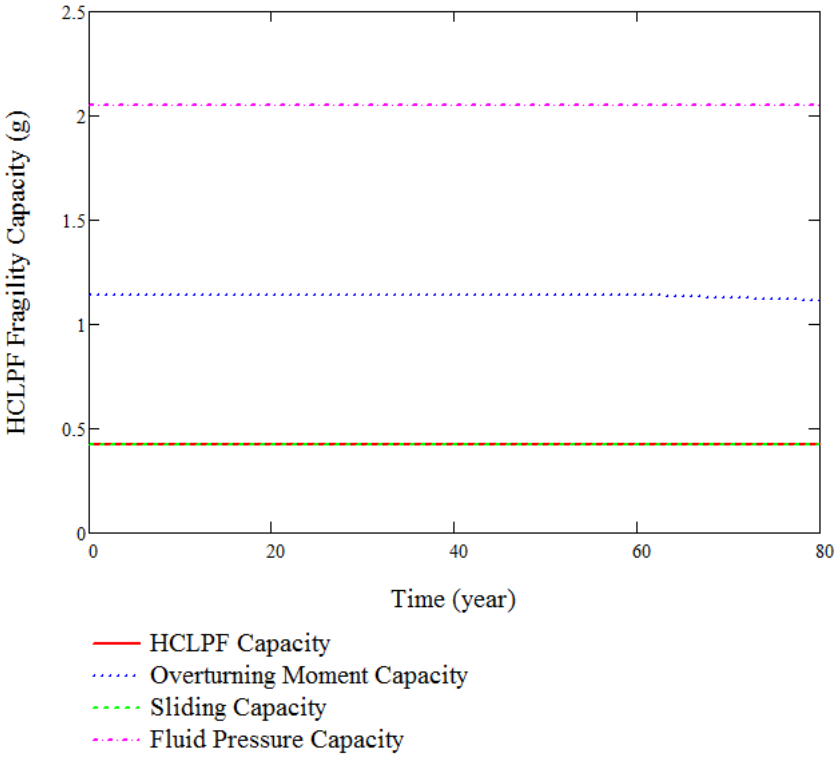

Figure 3-15 HCLPF Capacity of the CST with Cracked Anchorage Concrete (C-1)

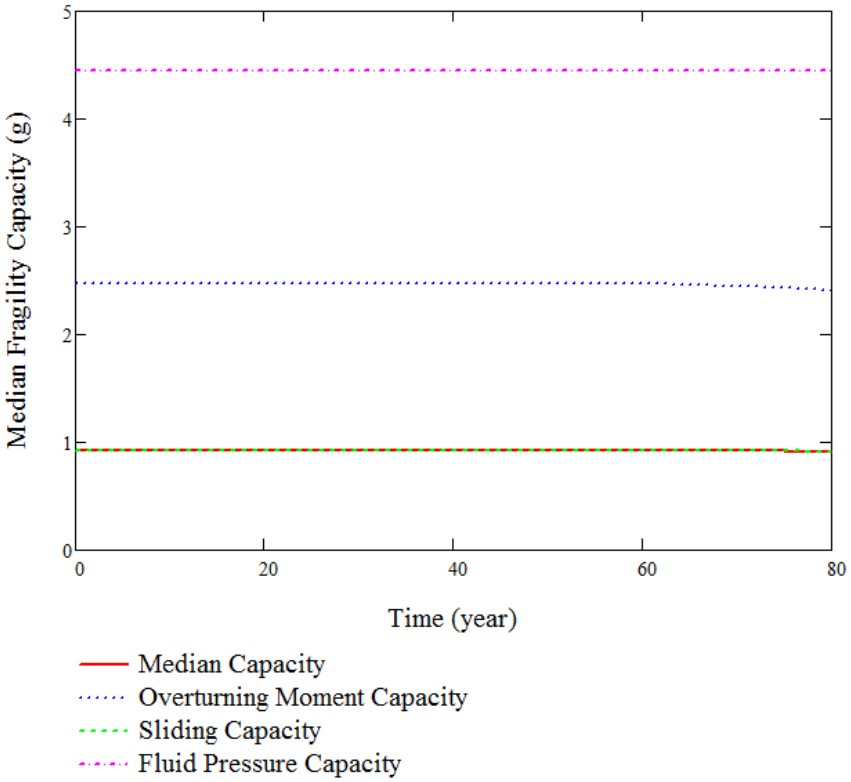

Figure 3-16 Median Capacity of the CST with Cracked Anchorage Concrete (C-1)

3.3.3.2 Using the C-2 Crack Growth Model

Similarly for the crack width model C-2, Figure 3-17 shows the mean fragility capacity of the CST with anchorage concrete cracking for a series of years, from 0 up to 80 years. These mean fragility curves were calculated using constant uncertainties, i.e., $\beta_R = 0.2$ and $\beta_U = 0.27$, and the effect of the degradation on the uncertainties was not considered. As shown in Figure 3-17, the mean fragility does not change in the first 20 years and in the last 25 years, with an increasing rate of deterioration in fragility capacity for the years in between. The governing failure mode changes from the sliding mode to the overturning moment mode at about 50 years.

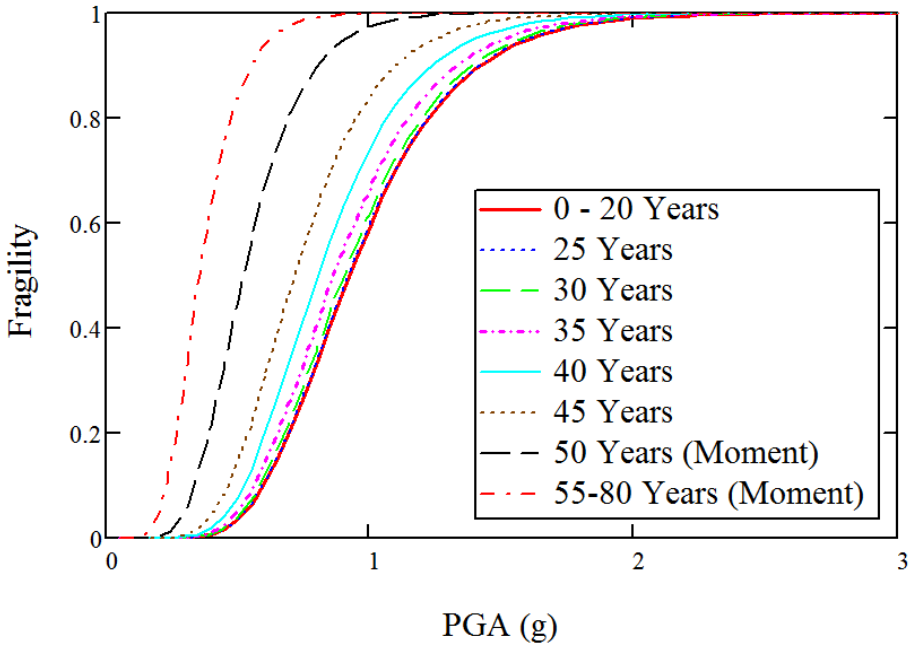

Figure 3-17 Mean Fragility Capacity of the CST with Cracked Anchorage Concrete (C-2)

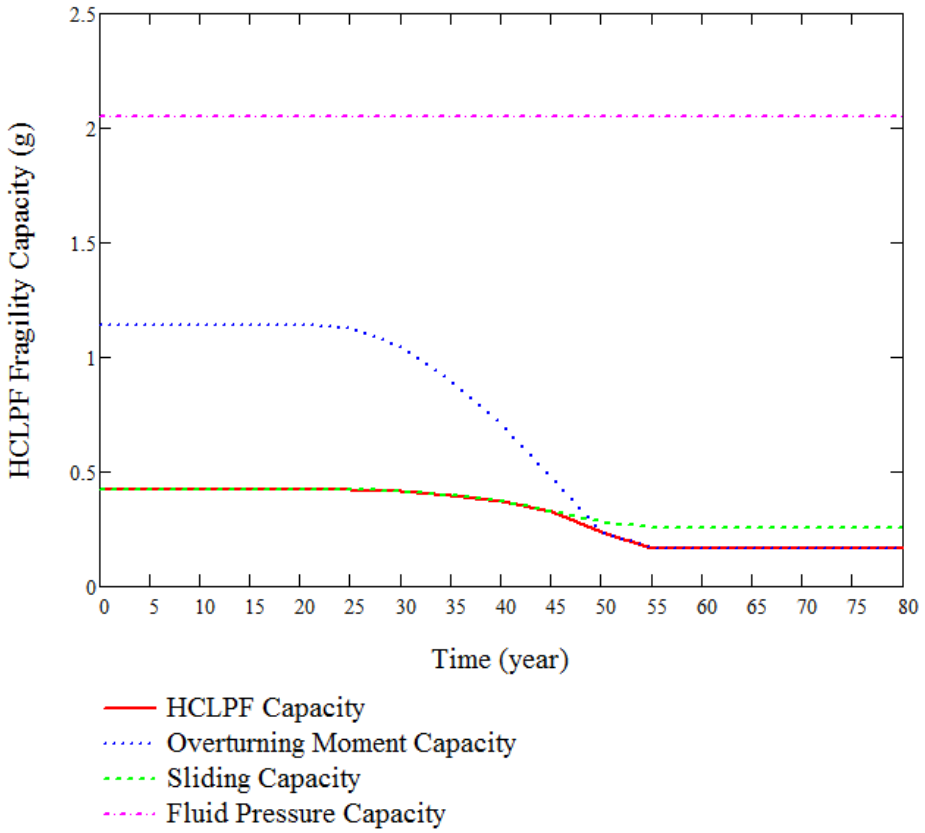

Figure 3-18 HCLPF Capacity of the CST with Cracked Anchorage Concrete (C-2)

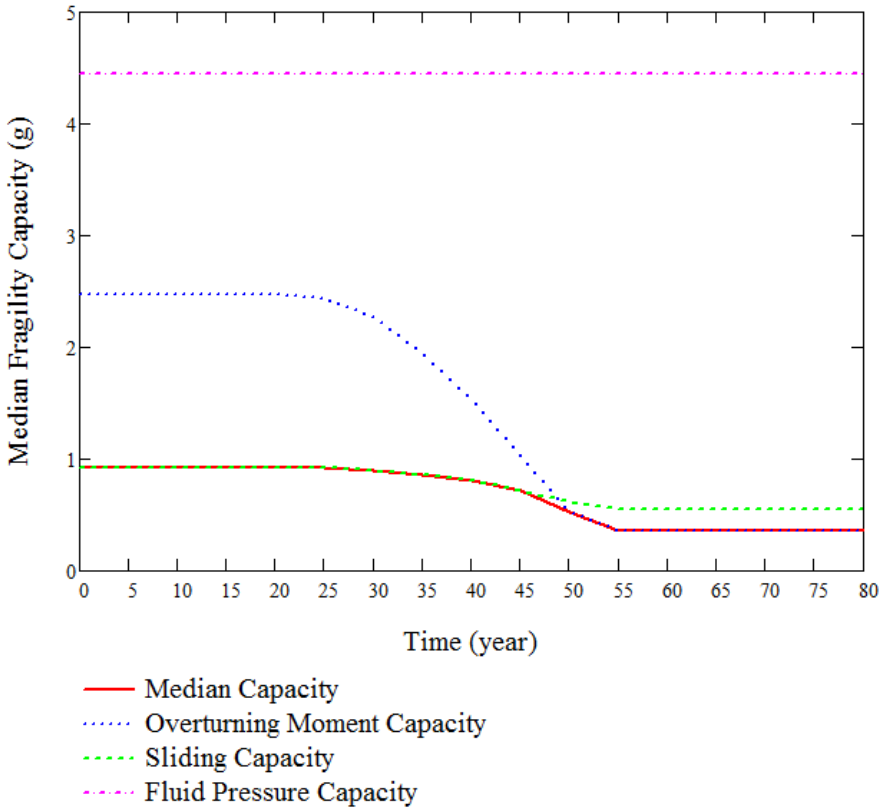

Figure 3-19 Median Capacity of the CST with Cracked Anchorage Concrete (C-2)

The deterioration of fragility capacities as a function of time can be easily observed in the HCLPF capacity and the median capacity, as shown in Figure 3-18 and Figure 3-19. There are 4 regions in these figures: (1) during 0-20 years, with a maximum crack width of 0.156 mm (about half of the crack width in the test), the fragility capacities were unchanged because of the large number of bolts that have no or moderate reduction in their bolt hold-down capacity; (2) between 20 to about 48 years, the fragility capacities were dominated by the sliding mode; (3) before 55 years, the fragility capacities were dominated by the overturning moment mode and the reduction in the bolt hold-down capacity affects the overturning moment capacity; and (4) after 55 years, the fragility capacities continue to be dominated by the overturning moment capacity, the bolts in tension appeared to have been pulled out, and the CST effectively becomes an unanchored tank. The overturning moment capacity starts to be affected dramatically by the bolt hold-down capacity after 20 years until the bolts reach a zero capacity around 55 years. The bolt hold-down capacity does not have as great an impact on the sliding capacity as on the overturning moment capacity, and it does not have any impact on the fluid pressure capacity as expected.

The slosh height become smaller as the SME becomes smaller due to degradation. The horizontal displacement at the roof level of the auxiliary building becomes larger at the end of 80 years than the base case due to the pullout of the anchor bolts that makes the CST unanchored. Even in such a case, the largest horizontal displacement at the roof level of the auxiliary building was found to be 0.314”, about 10% of the 3” gap existing between the CST and the auxiliary building.

It can be concluded that the crack growth model has a great impact on the fragility capacities of the CST. However, the model C-2 may not be accurate after about 40 years because the crack width becomes greater than 0.3 mm (crack width in the test [Klingner et al., 1998]) and the crack width estimate after 25 years is extrapolated. On the other hand, the model C-1 leads to a maximum crack width of 0.204 mm at the end of 80 years, which is still in the tested range. It is important to note that provided the linear interploation/extrapolation relation in Equation 3-8 is reasonable, a crack width of only 0.429 mm at the end of 55 years, based on the model C-2, indicates a pullout failure of the anchor bolts and a 61% reduction in seismic fragility capacity, even with a very dense array of anchor bolts (78). This observation shows the importance of concrete cracking in the CST seismic safety, and certainly leads to a recommendation of regular inspection of the concrete foundation for cracking.

It is cautioned that the above observation is based on a greatly simplified conversion from the NUREG/CR-5434 test results to the large size anchor bolts, in which many uncertain factors were not considered, for example, how the crack depth in conjunction with the crack width affect the bolt hold-down capacity. As discussed in the Year 2 Annual Report, the surface crack may not always be a good indicator of the crack depth.

3.3.4 Fragility Analysis for Degradation Case D – Perfectly Correlated Degradations

Degradation cases A, B, and C-2 were combined together to investigate the effect of multiple degradations on the seismic fragility capacities. Concrete cracking model C-2 was chosen instead of model C-1 in order to demonstrate more interesting fragility results. The three degradation cases are assumed to be perfectly correlated, i.e., the severity of each of the degradation cases is a deterministic function of the common time variable.

Figure 3-20 shows the median fragility curves for the CST with combined degradations up to 65 years. The fragility curves before the end of 45 years show equal and fine spacing between them, indicating a steady but slow degradation process. Between 45 years and 55 years, a sudden increase of the degradation severity is shown by the large spacing between the corresponding fragility curves. The very small spacing between 55 and 60 years suggest a very small drop in the fragility capacity, followed by a slightly increased drop in fragility capacity. As shown in Figure 3-21, the fragility capacity diminishes at 65 years, after which the fragility calculation in Mathcad could not reach a plausible solution.

The trend of the fragility capacity change can be better characterized by the HCLPF capacity and the median capacity, as shown in Figure 3-21 and Figure 3-22. Before the end of 45 years, the fragility capacity is dominated by the slow deterioration of the sliding capacity. Between 45 years and 55 years, the dominating failure mode switches to the overturning moment mode and the resultant deterioration rate in the fragility becomes higher. Between 55 and 60, the fragility capacity is still dominated by the overturning moment capacity, which levels to a small constant because the CST effectively becomes an unanchored tank as previously shown in the degradation case C-2. At the end of 65 years, the overturning moment capacity and the fluid pressure capacity are very close, with the latter dominating the fragility capacity. This is the only occasion among all degradation scenarios that the fluid pressure capacity dominates the fragility calculation.

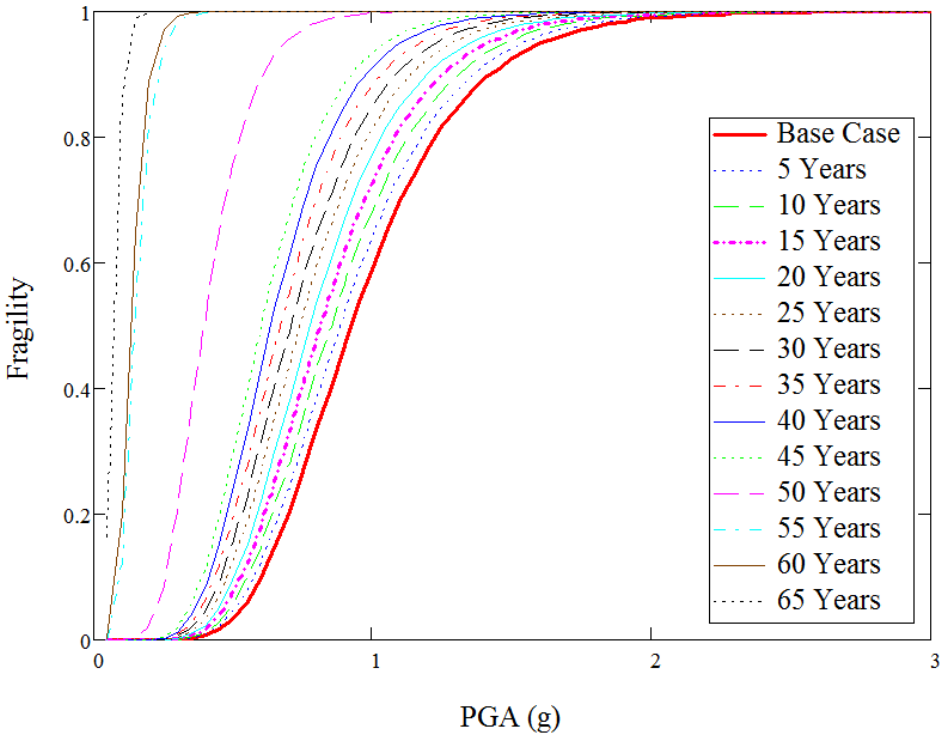

Figure 3-20 Mean Fragility Capacity of the CST with Combined Degradations

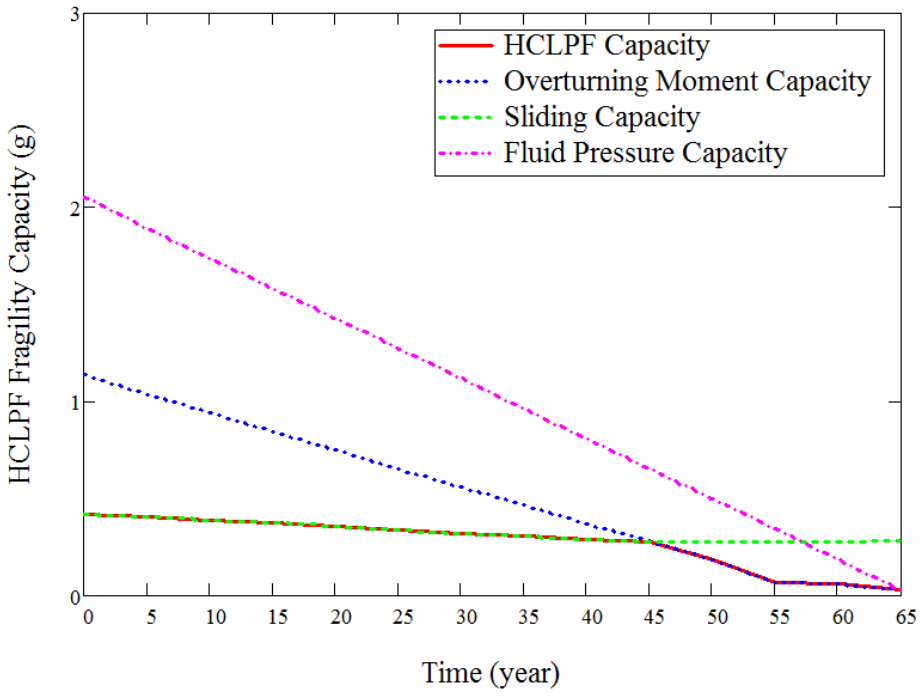

Figure 3-21 HCLPF Capacity of the CST with Combined Degradations

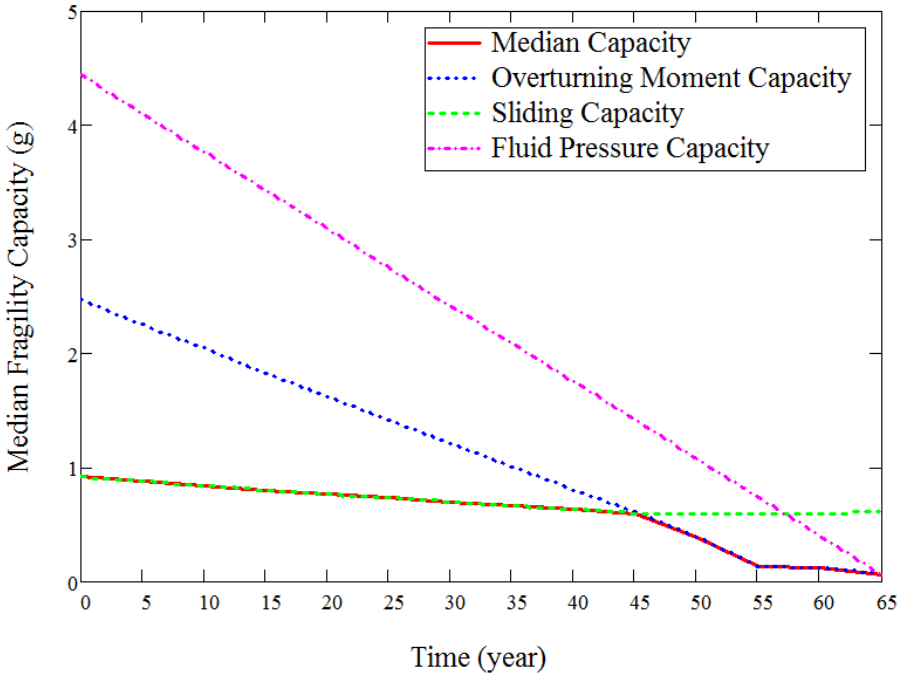

Figure 3-22 Median Capacity of the CST with Combined Degradations

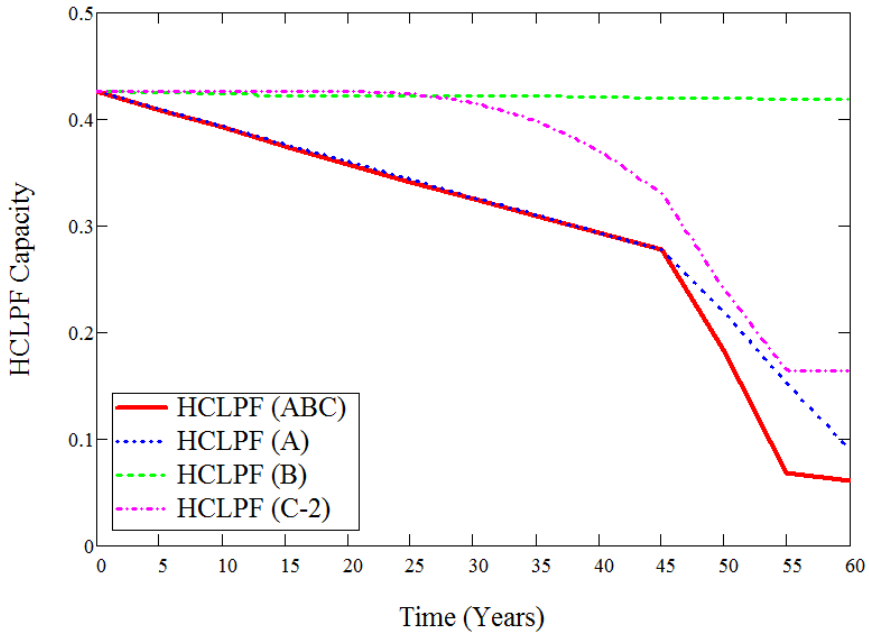

Figure 3-23 Comparison of HCLPF Capacities among All Degradation Scenarios

Figure 3-23 compares the HCLPF capacities among all 4 degradation cases (A, B, C, and D), with the solid line for the case of perfectly-correlated degradations, the dotted line for the degraded tank shell, the dashed line for the degraded anchor bolt, and the dash-dotted line for the cracked anchorage concrete using model C-2. It is interesting to note that before 45 years, the HCLPF fragility for the degradation case D is the same as that for the degradation of the tank

shell, indicating the degradation of anchor bolts and the anchorage concrete cracking have no effect on the fragility. After 45 years, it appears all three degradation scenarios contribute to the HCLPF fragility for the combined degradation case. Figure 3-23 also shows that the corrosion model for the anchor bolts, although appearing to be for the severest environment (marine) case, does not incur a significant amount of loss of cross section and the corresponding deterioration in fragility capacity is minimal.

3.4 Seismic Fragility Analyses of CST Using Operational Water Level

3.4.1 Fragility Analysis of the Undegraded CST

This subsection presents the seismic fragility analyses of the CST assuming operational water level, which is lower than the design water level. The elevation of operational water level in the CST is normally maintained by opening/closing the makeup valve. The normal range of the operational water level is between 131'-5" and 132'-3". An elevation of 132' was used as a representative operational water level, and the corresponding representative water head was calculated to be 30'-3".

The fundamental frequency of the horizontal impulsive mode was estimated to be 11.3 Hz, about 21.5% higher than 9.3 Hz as determined using the design water level. Based on the RG 1.60 horizontal spectrum shape, this change of fundamental frequency results in smaller spectral accelerations. The fundamental frequency of the horizontal convective (sloshing) mode was calculated to be 0.242 Hz, which is only slightly smaller than the original 0.244 Hz. The change of spectral acceleration due to the small frequency change is minimal. The fundamental frequency of the vertical mode was determined to be 11.8 Hz, which is about 24.0% higher than the original fundamental frequency 9.5 Hz. Based on the RG 1.60 vertical spectrum shape, this change of fundamental frequency results in smaller spectral accelerations.

The HCLPF capacity was determined to be 0.549 g, representing a 28.9% increase over the original 0.426 g estimated using the design water level. The sliding mode of the CST still dominates. At an SME of 0.549 g, the corresponding overturning moment capacity and the fluid pressure capacity are 2.0 g and 2.8 g, respectively. The influence of the auxiliary building to the two CSTs was found to be negligible; the same observation was made when the design water level was considered.

The median seismic fragility capacity was determined to be 1.2 g, by assuming the overall aleatory and epistemic uncertainties to be 0.2 and 0.27, respectively. The relative change of the median seismic fragility capacity is about 30%, compared to using the design water level. Figure 3-24 shows the mean fragility curve; and the median, 5% percentile, and 95% percentile fragility curves.

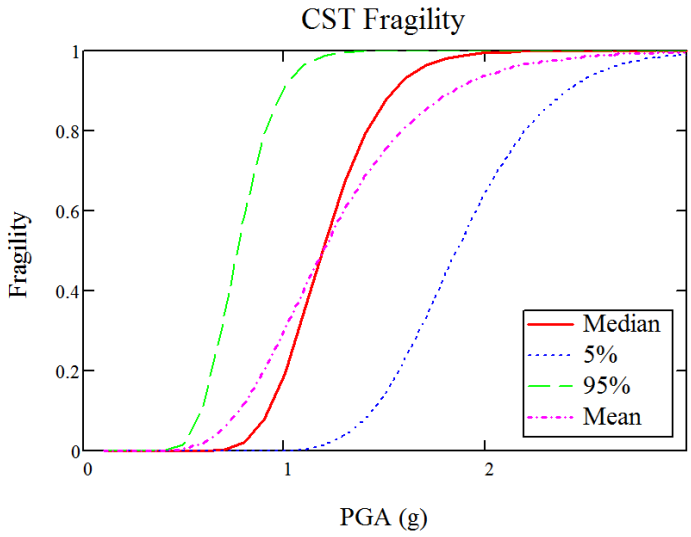

Figure 3-24 Fragility Curves of The CST with the Operational Water Level

3.4.2 Fragility Analysis with Non-Perfect Correlations between the Degradation Cases

This subsection presents seismic fragility analyses of the CST with the operational water level for two degradation cases: (D) perfectly correlated degradations and (E) non-perfectly correlated degradations. For the degradation case D: the seismic fragility deterioration behavior of the CST is expressed as a function of the three degradations that are assumed to be perfectly correlated, i.e., the degradation rates were expressed as deterministic functions of the common time variable. In reality, large uncertainties exist in the physical degradation phenomena and there is a lack of perfect knowledge on how to model them accurately. On the other hand, there is some degree of assurance in the correlations between the three degradation scenarios, namely in the tank shell, the anchor bolts, and the reinforced concrete foundation. For example, the degradations in the anchor bolts and the reinforced concrete foundation may have a higher correlation coefficient because of their similar local environment, degradation interaction, similar metallic behavior, etc. To account for these uncertainties, the co-existence of the three degradations could be better treated stochastically.

For degradation scenarios A, B, and C, let $A_0(t)$, $B_0(t)$, and $C_0(t)$ be the deterministic degradation models that are defined previously in this section, and the corresponding random degradation models $A(t)$, $B(t)$, and $C(t)$ can be defined by the following simple factored expressions,

$$\begin{aligned} A(t) &= A_0(t) \times a \\ B(t) &= B_0(t) \times b \\ C(t) &= C_0(t) \times c \end{aligned} \tag{3-12}$$

where rate factors a, b, and c are random variables with unit mean and covariance matrix Σ. These models are relatively simple because they represent the time-dependent degradation models as random variables instead of more realistic but complicated random processes.

Should a random process approach be opted, the deterministic models $A_0(t)$, $B_0(t)$, and $C_0(t)$ can be treated as the mean, but time-dependent variance models would need to be defined. In addition, the use of random processes requires separate realization of the degradation rates at each time step to determine the HCLPF capacity and carries no extra benefit for the purpose of demonstration. The simple models as shown in Equation 3-12 require much less computation. Once a set of samples are identified for random variables *a*, *b*, and *c*, a sample degradation case can be defined completely by Equation 3-12.

3.4.2.1 Development of Sample Degradation Scenarios

Each sample in the simulation requires a separate Mathcad calculation sheet because of the limitation of Mathcad in handling nested loops of multiple levels. In addition, for each sample, the calculation of the SME HCLPF capacity must be repeated manually for a series of years to obtain the deterioration behavior of the seismic fragility as a function of time. To facilitate this involved computation process, an efficient simulation scheme is required to minimize the number of Mathcad sheets. To this end, Latin Hypercube samples (LHS) were selected for this study. LHS have been widely used as alternatives to samples randomly generated by the brute-force Monte Carlo (MC) method for variance reduction.

There are a number of algorithms in the literature to generate LHS. Although they have been developed using different optimization strategies, all emphasize on distributing a smaller number of samples (than MC) with high fidelity to the underlying distribution in the hyper cube and consequently improving the simulation efficiency. The particular algorithm used in this study is the so-called Optimum LHS, which is implemented in the "lhs" package for the R statistical environment [2010]. This algorithm generates an optimal set of samples with respect to the S-optimality criterion, which seeks to maximize the mean distance from each point to all the other points in the set and effectively to scatter the points as evenly as possible [Stocki, 2005].

The generated optimum LHS, uniformly distributed in the Hypercube, need to be transformed to the correlated rate factors *a*, *b*, and *c*. In this study, the three rate factor random variables are assumed to have lognormal marginal distributions with unit mean and standard deviations 0.2, 0.25, and 0.3, respectively. The correlation coefficients between (*a*,*b*), (*a*,*c*), and (*b*,*c*) are specified as 0.4, 0.4, and 0.7, recognizing that degradations in the anchor bolts and the reinforced concrete foundation have stronger correlation than those involving the stainless steel tank shell. The procedure to transform the optimum LHS into correlated lognormal random vectors is described in detail in NUREG/CR-6922 [Nie et al., 2007].

A total number of 11 samples were generated for the rate factors for this study. It should be noted that there is some level of correlation in the independent samples because the number of samples is finite and small. For the optimum LHS generated for this study, the correlation coefficients are estimated to be 0.04, 0.09, and -0.10. As a comparison, the correlation coefficients for the resultant lognormal rate factor samples are 0.36, 0.43, and 0.7, respectively, which are very close to the specified target values. The resultant correlated rate factors are listed below in Table 3-3:

Table 3-3 Sample Rate Factors

Sample Id	*a*	*b*	*c*
1	0.892	0.666	0.717
2	0.867	1.127	1.128
3	1.111	1.254	1.525
4	0.956	0.801	0.670
5	1.062	1.847	1.496
6	1.597	1.240	1.192
7	0.728	0.861	0.690
8	0.995	1.120	0.816
9	1.254	0.877	0.992
10	0.779	0.814	0.927
11	1.030	0.894	1.375

3.4.2.2 Simulation-Based Seismic Fragility Analyses

For seismic fragility analyses of the CST considering non-perfect correlations between the three degradation scenarios, eleven Mathcad calculation sheets were developed, each of which corresponds to a row in Table 3-3. Each Mathcad calculation sheet is a sample degradation case that can be completely defined by the rate factors. For each sample degradation case, the same manual procedure used in Subsection 3.3 is applied here to determine the HCLPF capacity of the CST at every 5 years. The results are exported from all Mathcad sheets and aggregated in Excel for post processing. Similar to previous sections, the uncertainties associated with the CDFM method are assumed invariant in time, so that the median fragilities and the HCLPF capacities carry similar information. Therefore, only HCLPF capacities are considered in the following statistical analysis.

Two approaches were implemented for determining the mean curve: (1) averaging HCLPF capacities at every 5 years and (2) averaging years to reach a HCLPF level.

Figure 3-25 shows various time-dependent HCLPF capacity curves: the 11 thin curves represent the 11 sample degradation cases, the thick dotted curve is the average HCLPF capacity at every 5 years, the thick dashed curve is the average year to reach a HCLPF level, and the thick solid curve represent an additional analysis which assumed a perfect correlation between the degradation scenarios A, B, and C (i.e., rate factors $a = b = c = 1$) and used the operational water level.

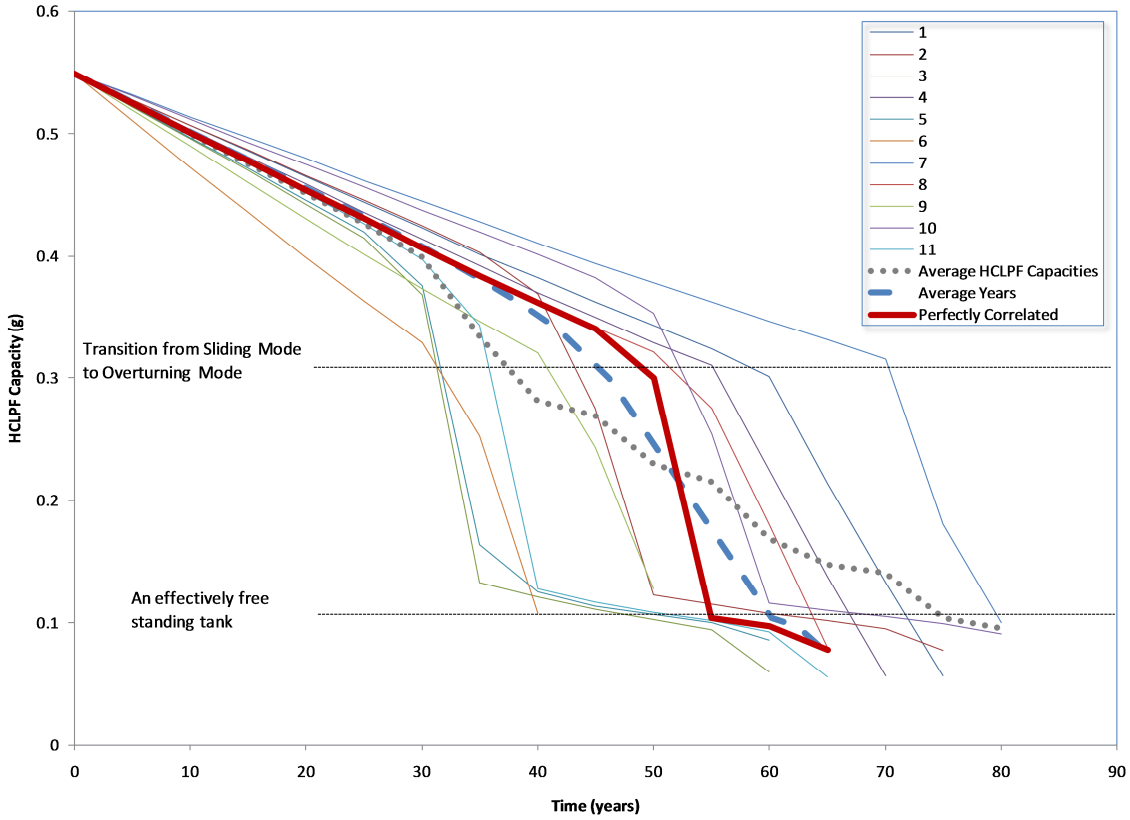

Figure 3-25 Simulated CST HCLPF Capacity vs Time

By examining the 11 simulated curves, it is clear that the deterioration characteristics of the HCLPF actually cannot be appropriately described in terms of time. Rather, there are two apparent sharp bends in the curves as indicated by the two horizontal dotted lines. The first bend occurs at a HCLPF level of about slightly higher than 0.3 g, where the controlling mode changes from the sliding mode to the overturning mode. The second bend occurs at slightly higher than a HCLPF level of 0.1 g, where the CST effectively becomes unanchored (free standing). The time for the CST to reach these two HCLPF levels varies significantly among the samples, generally from about 30 to 80 years.

Based on Figure 3-25, the average HCLPF capacity can represent well the mean curve up to 30 years but not so after 30 years. The apparent reason is that the samples at any time after 30 years can be dominated by either the sliding mode or the overturning mode, and that some even may have failed in producing a meaningful HCLPF capacity at that time. This averaging approach appears to be inappropriate in this case because of the limited number of samples. It is obvious in Figure 3-25 that averaging the years at which a given level of HCLPF capacity is achieved should lead to a much better mean curve (the thick dashed curve). Such an averaging required interpolation among data points because all HCLPF data were not produced at constant levels of HCLPF capacity, rather at each 5 years.

An additional degradation case was analyzed with all three degradation scenarios perfectly correlated. This analysis resulted in the thick solid curve in Figure 3-25, which matches very well

the two averaging curves before 30 years and apparently maintains in the middle of the simulated curves after that. It even seems to be a better mean curve than the average years curve, partly because of the limited number of samples. Therefore, this perfectly correlated case is considered as the mean curve in the following discussion.

Although determined using the operational water level, the mean curve appears to have a similar trend to that using the design water level, except for higher HCLPF capacities (see Figure 3-21 or Figure 3-23 for a comparison). Specifically, before the end of 45 years, the fragility capacity is dominated by the slow deterioration of the sliding capacity. At about 50 years, the dominating failure mode switches to the overturning moment mode and the HCLPF capacity deteriorates at a much higher rate. Between 55 and 65, the fragility capacity is still dominated by the overturning moment capacity and levels to a very small value because the CST effectively becomes an unanchored tank.

Table 3-4 shows the standard deviation in years to reach a HCLPF value, with respect to the mean curve (the perfectly correlated case). Except for the last three data points where not all samples have a feasible HCLPF capacity, the standard deviation monotonically increases. It is worthwhile to note that this increasing standard deviation occurs while the uncertainties and the correlations in the rate factors are constant. In another words, even without considering the rate factor variation in time (through random processes), the uncertainty in years to reach a HCLPF level increases. The coefficient of variation (COV) also generally increases but not as significantly as that of the standard deviation. This effect has not been able to be observed through deterministic degradation analyses such as those described in Subsection 3.3. Figure 3-26 illustrates the trend of the standard deviation in years to reach a HCLPF level.

Figure 3-27 shows the trend of the standard deviation in HCLPF at every 5 years. Similar to the standard deviation in years to reach a HCLPF level, the standard deviation in HCLPF also increases in general. The smaller standard deviation close to 80 years is due to fewer samples having a feasible HCLPF value during that period. More importantly, since the mean HCLPF becomes smaller as time proceeds, the COV in HCLPF capacity increases at an even greater rate. For example, the COV is only about 0.05 at 20 years, and increases to 0.31 at 35 years. In contrast, the COV in years to reach a HCLPF level stays in a range of 0.2 to 0.26.

The above observation is also very important in quantifying the overall uncertainties in the seismic fragility of the CST. The additional time-depended uncertainties should be properly taken into account. For example, at 20 years, the additional uncertainty β_A associated with a HCLPF capacity of 0.452 g (average HCLPF) can be estimated to be 0.05 (COV). Given the initial composite uncertainty $\beta_C = 0.34$ (using $\beta_R = 0.2$ and $\beta_U = 0.27$), the composite uncertainty in the fragility barely change. However, at 35 years, the composite uncertainty in the fragility increases to 0.46. As stated previously, the statistics in HCLPF capacity and the confidence in the additional uncertainty can be improved by increasing the number of samples.

Table 3-4 Standard Deviation in Years

Years	Mean HCLPF (g)	Standard Deviation in Years With Respect to the Mean Curve	COV
0	0.549	0.000	
5	0.525	1.048	0.21
10	0.501	2.050	0.20
15	0.478	3.044	0.20
20	0.454	4.071	0.20
25	0.431	5.047	0.20
30	0.407	6.197	0.21
35	0.384	7.401	0.21
40	0.362	8.771	0.22
45	0.340	10.587	0.24
50	0.300	13.081	0.26
55	0.104	12.558	0.23
60	0.097	11.791	0.20
65	0.078	11.986	0.18
70	NA		
75	NA		
80	NA		

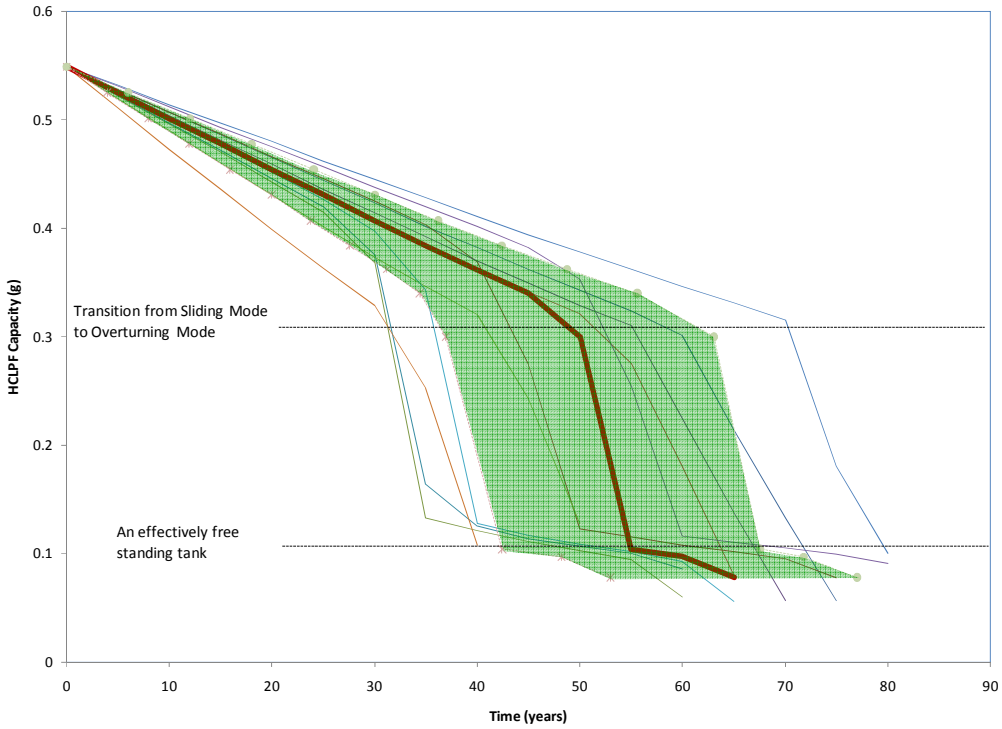

Figure 3-26 Standard Deviation in Years to Reach a HCLPF Level

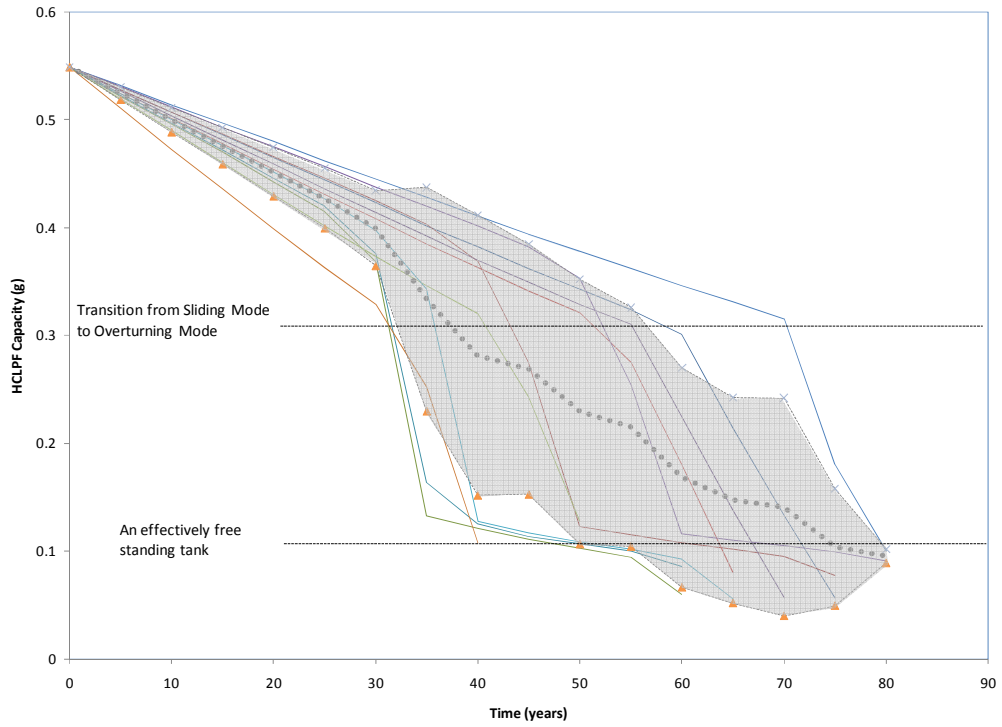

Figure 3-27 Standard Deviation in HCLPF

3.4.3 Additional Fragility Analyses of the CST with Individual Degradation Scenarios

To account for the operation water level, three additional seismic fragility analyses of the CST were performed in Year 5 to obtain the seismic fragilities of the CST for the three basic degradation scenarios A, B, and C. These analyses were necessary for the development of Tier 2 degradation acceptance criteria for the CST when individual degradation scenarios were considered.

Instead of modifying the corresponding Mathcad calculation sheet for the design water level, these three additional fragility analyses discussed in this subsection were implemented based on one sample calculation in the simulation-based fragility analysis of the CST to consider non-perfect correlation between the degradations. The sample calculation sheet utilizes the operation water level and can implement any possible combination of all three basic degradation scenarios by using proper factors, for example, any row of Table 3-3 for a sample calculation or a unit vector (1, 1, 1) for the case of perfectly-correlated degradations. Therefore, to consider the individual basic degradation scenarios A, B, and C, the factor vector was set to (1, 0, 0), (0, 1, 0), and (0, 0, 1), respectively. Appendices A through C show more details of these seismic fragility analyses.

Figure 3-28 shows the mean seismic fragility curves of the CST assuming that loss of wall thickness of the tank shell is the only degradation of the CST, for a series of years up to 65 years. Figure 3-29 compares the time-dependent seismic HCLPF capacities of the CST between the assumption of the design water level and the operational water level. For the undegraded case, the seismic HCLPF capacity of the CST assuming the operational water level is 0.549 g, higher than 0.426 g determined for the design water level. The influence of the water level on the seismic HCLPF capacity is consistent over time. Figure 3-30 through Figure 3-33 show similar plots for the degradation cases of corrosion in anchor bolts or cracking in reinforced concrete foundation. The corrosion in anchor bolts has minimal effect on the mean seismic fragility as well as the seismic HCLPF capacity, but the concrete cracking has significant effect on the fragilities. The impact of using different water levels on the seismic fragility is similar to the observation for the case of loss of wall thickness in the tank shell. It should be pointed out that all these observations are based on the assumed material degradation models.

The HCLPF capacities as a function of degradation level (e.g., loss of wall thickness) will be used in the Section 5 to develop the Tier 2 degradation acceptance criteria.

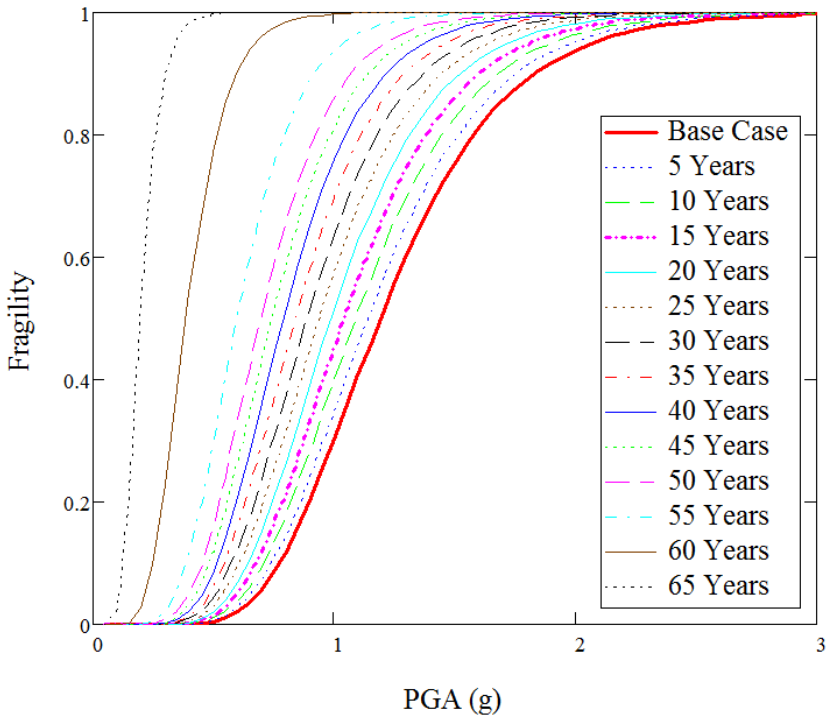

Figure 3-28 Mean Fragility Capacity of the CST with Degraded Tank Shell (Operational Water Level)

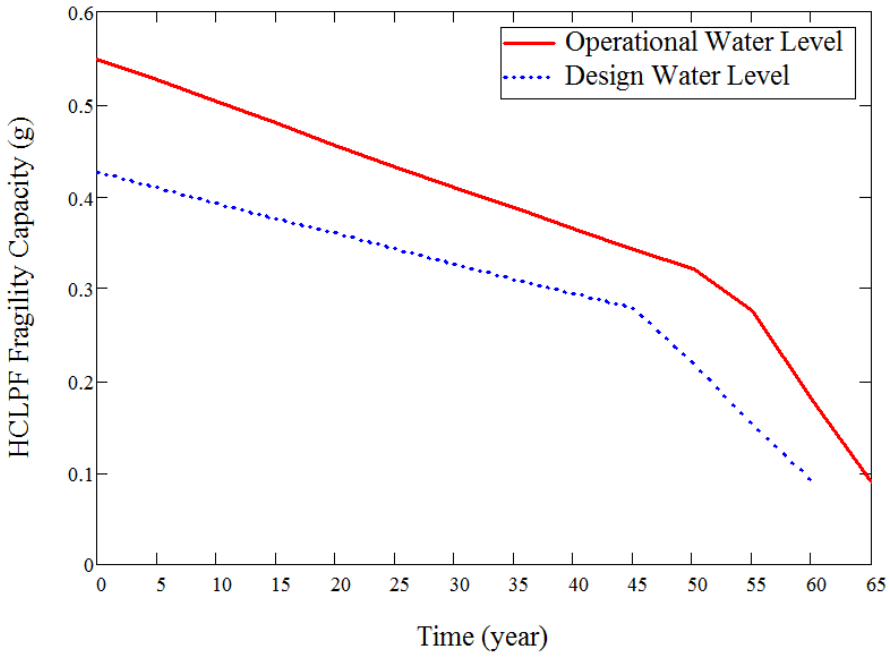

Figure 3-29 Comparison of HCLPF Capacity for Degraded Tank Shell: Operational Water Level vs. Design Water Level

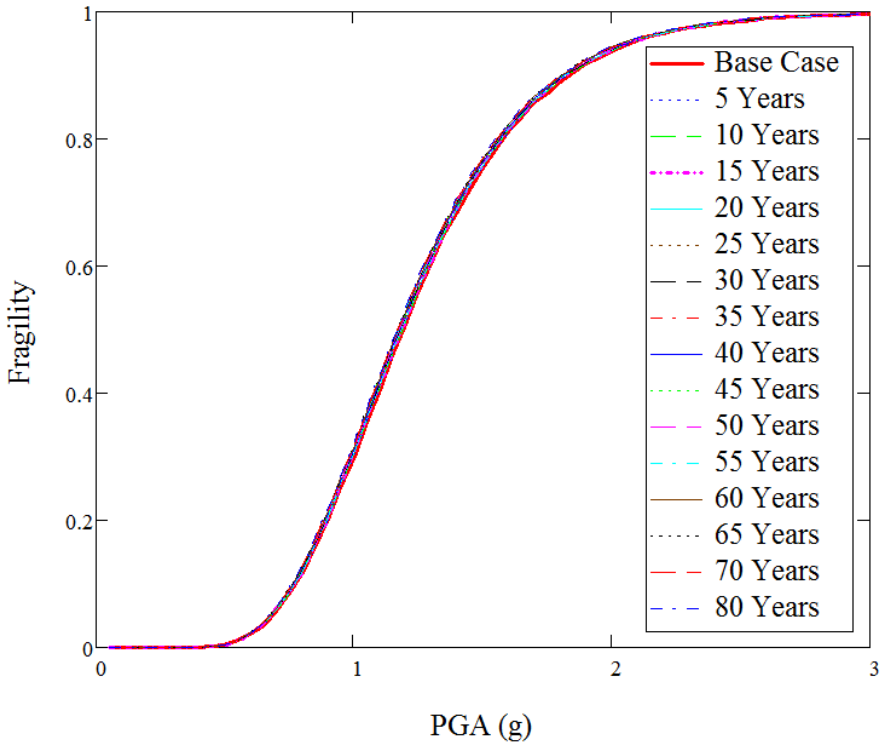

Figure 3-30 Mean Fragility Capacity of the CST with Degraded Anchor Bolts (Operational Water Level)

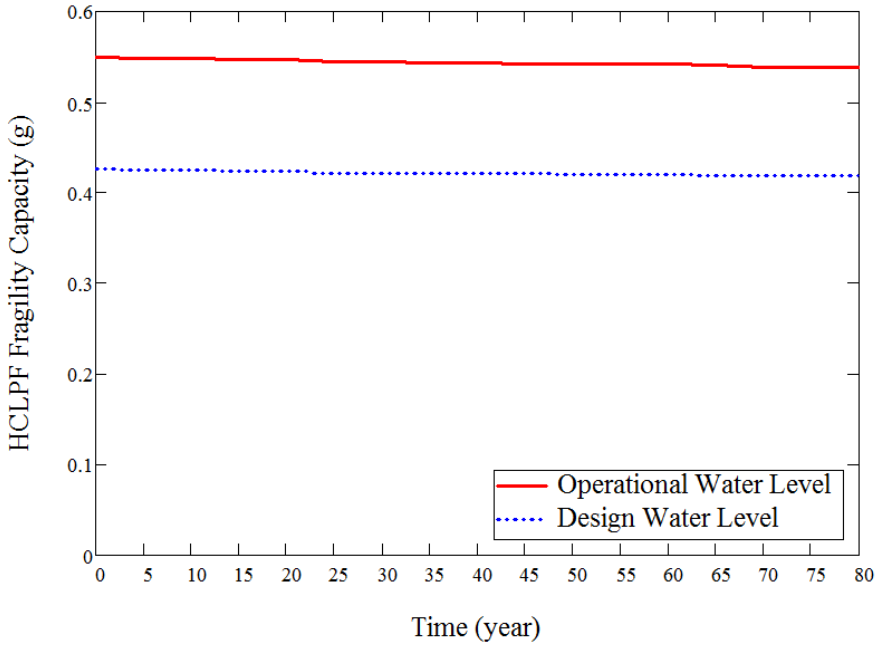

Figure 3-31 Comparison of HCLPF Capacity for Degraded Anchor Bolts: Operational Water Level vs. Design Water Level

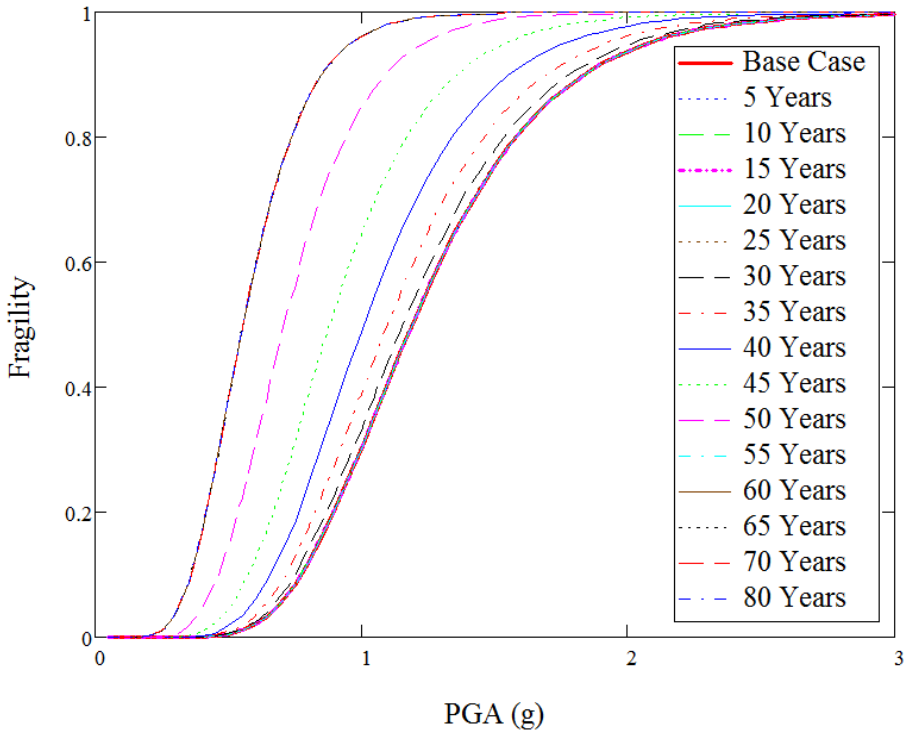

Figure 3-32 Mean Fragility Capacity of the CST with Reinforced Concrete Cracking (Operational Water Level)

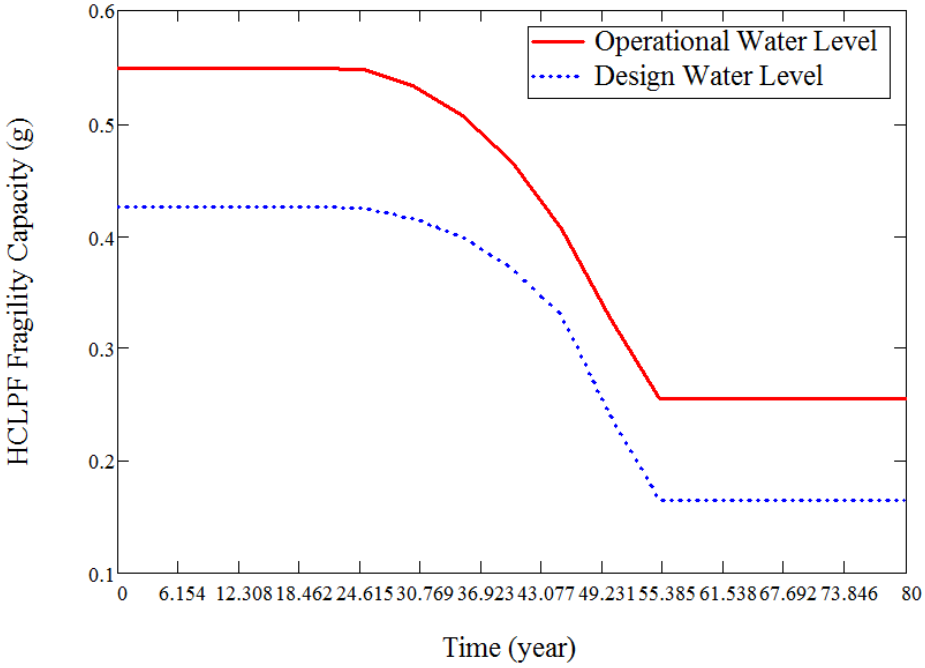

Figure 3-33 Comparison of HCLPF Capacity for Reinforced Concrete Cracking: Operational Water Level vs. Design Water Level

4 ESTIMATION OF CDF FOR THE CONDENSATE STORAGE TANK

4.1 Development of a Fragility Range for the Condensate Storage Tank

According to the procedure laid out in Section 2, a range of HCLPF values and the associated uncertainties were developed based on the Year 4 results, which were calculated using the operational water level. Two series of HCLPF values were developed in this study to consider different treatments of the uncertainties. The first series assumes that the uncertainties β_R and β_U are invariant with the magnitude of the median fragility, i.e., independent of degradation level and time. For the second series, the epistemic uncertainty is assumed to vary based on the findings in the Year 4 research when more realistic correlations were considered. Section 3 presents a summary of the seismic fragility analyses of the condensate storage tank (CST) that were performed in the Year 3 and Year 4 scope of work.

It should be noted that the term *probabilistic risk assessment* (PRA) used in all other sections of this report, is equivalently referred to as *probabilistic safety assessment* (PSA) in the rest of this section, to be consistent with the terminology custom followed by KAERI.

To consider the varying uncertainties, an additional uncertainty β_A is determined based on the COV of the HCLPF capacity (Figure 5-4 of the Year 4 report [Nie et al., 2011]), and can be approximated by the two regression equations as shown in Figure 4-1, where x = (0.549 – HCLPF) and β_A can be approximated as the COV. The additional uncertainties β_A are combined to the epistemic uncertainty β_U because β_A represents the imperfect knowledge about the variations and correlations of the rate factors that are described in Section 3. β'_U is the SRSS of β_U and β_A, and was used in place of β_U in the PSA for the case of varying uncertainties. The maximum value of β'_U in the list is 0.84, which is about twice as large as the maximum uncertainty value of the undegraded components in the literature. It appears that this level of uncertainty does not cause a problem in the PSA calculation. This series will be used as a sensitivity study of the first series where uncertainties do not change.

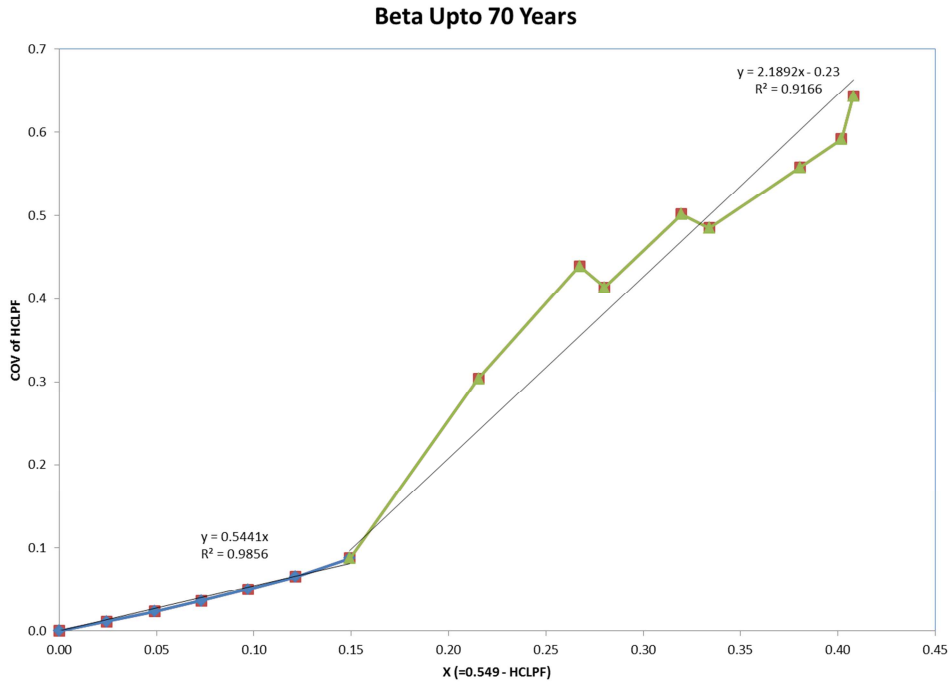

Figure 4-1 Approximation of the Additional Uncertainty

Both series have the same HCLPF capacities, which range from a maximum of 0.549 g to a minimum of 0.078 g, respectively for the undegraded case and for a perfectly correlated case. The choice of these two bounding values was to minimize the communication effort between the fragility analyst and the PSA analyst, who are located in different continents for this study. However, if convenient in other situations, a narrower range can be used to reduce the number of PSA calculations. In this study, the computational cost of a PSA calculation was not so great and this large range of HCLPF values allowed the demonstration of the overall behavior of the HCLPF-CDF relationship. Between these two bounding HCLPF values, eight HCLPF values were added to evenly divide the range, as well as two additional values, 0.300 g and 0.100g, indicating the points at which the failure mode switches (see Figure 3-25). The total number of HCLPF values for each series is 12.

Table 4-1 and Table 4-2 show the HCLPF values and the associated uncertainties for the cases of constant uncertainties and varying uncertainties, respectively. These data were used in KAERI's PSA to estimate the corresponding CDFs and ΔCDFs.

Table 4-1 HCLPF and CDF for Constant Uncertainties

Cases	HCLPF (g)	β_R	β_U
Base case	0.549	0.20	0.27
	0.500	0.20	0.27
	0.444	0.20	0.27
	0.392	0.20	0.27
	0.340	0.20	0.27
Sliding to Overturning	0.300	0.20	0.27
	0.287	0.20	0.27
	0.235	0.20	0.27
	0.183	0.20	0.27
	0.130	0.20	0.27
Free Standing Tank	0.100	0.20	0.27
Minimum case	0.078	0.20	0.27

Table 4-2 HCLPF and CDF for Varying Uncertainties

Cases	HCLPF (g)	β_R	β_U	β_A	β'_U
Base case	0.549	0.20	0.27	0.00	0.27
	0.500	0.20	0.27	0.03	0.27
	0.444	0.20	0.27	0.06	0.28
	0.392	0.20	0.27	0.11	0.29
	0.340	0.20	0.27	0.23	0.35
Sliding to Overturning	0.300	0.20	0.27	0.32	0.42
	0.287	0.20	0.27	0.34	0.43
	0.235	0.20	0.27	0.46	0.53
	0.183	0.20	0.27	0.57	0.63
	0.130	0.20	0.27	0.69	0.74
Free Standing Tank	0.100	0.20	0.27	0.75	0.80
Minimum case	0.078	0.20	0.27	0.80	0.84

4.2 Estimation of CDFs and ΔCDFs

The Ulchin NPP units 5&6, where the CST is located, were selected by KAERI for its PSA to estimate the CDFs and ΔCDFs for various HCLPF values and uncertainties as listed in Table 4-1

and Table 4-2. The scope of the PSA included internal and external PSAs. Except for the degradation of the CST, the PSA model did not include the degradation of other structures, systems, and components (SSCs). The total CDF was defined as the summation of the CDFs induced by internal events and external events such as earthquakes, fire, and flood. A brief description of the seismic PSA procedure is provided below, as the degradation of the CST was taken into account in the seismic PSA.

To facilitate the seismic PSA, many structures and components were screened out based on a detailed walkdown, their generic fragility data, and fragility analyses. More specifically, those structures and components that have a HCLPF capacity larger than 0.65 g were screened out based on the guidelines proposed by Prassionos et al. [1987] and Budnitz et al. [1985]. As a result, 18 seismic risk significant components were kept in the seismic PSA model after the screening, as shown in Table 4-3 together with their median (A_m) and HCLPF capacities and uncertainties.

Table 4-3 Capacities & Uncertainties of Selected Components

Component	**A_m (g)**	**β_U**	**β_R**	**HCLPF (g)**
Offsite Power [SLOOP]	0.30	0.22	0.20	0.15
Battery Charger [SBCRC/SBCSF]	1.03	0.28	0.28	0.41
Switch [SSWIT]	2.33	0.41	0.45	0.55
4.16kV Switchgear [SSWRC]	1.33	0.33	0.29	0.48
Inverter [SNIRC]	1.37	0.33	0.30	0.49
Battery Rack [SBRSF]	1.46	0.33	0.31	0.51
480V AC Load Center [SLCRC]	1.50	0.32	0.29	0.57
125V DC Control System [SDCSF]	1.58	0.33	0.29	0.57
Regulating Transformer [SRTRC]	1.30	0.33	0.30	0.46
Condensate Storage Tank [SCST]	*1.29*	*0.27*	*0.20*	*0.55*
Diesel Generator [SDGSF]	1.03	0.28	0.28	0.41
Essential Coolant Water (ECW) Compression Tank [SECT]	2.33	0.41	0.45	0.55
ECW Chiller [SECH]	1.33	0.33	0.29	0.48
ECW Pump [SECP]	1.37	0.33	0.30	0.49
ESW Pump [SEWP]	1.46	0.33	0.31	0.51
CCW Surge Tank [SCCST]	1.50	0.32	0.29	0.57
Instrumentation Tube [SITSF]	1.50	0.30	0.30	0.56
HVAC Ducting and Supports [SHVAC]	2.06	0.32	0.41	0.62

The components listed in Table 4-3 were used for the failure mode and effect analysis (FMEA) of the selected plant. The FMEA can identify initiating events that are caused by the seismic-induced failures of the structures and components. For this study, the following seismic-induced initiating events were identified through the FMEA:

- Loss of Essential Power (LEP)
- Loss of Secondary Heat Removal (LHR)
- Loss of Component Cooling Water (LCCW)
- Small Loss of Coolant Accident (SLOCA)
- Loss of Off-site Power (LOOP)
- Seismic induced General Transient (GTRN)

Figure 4-2 shows the event tree of the above initiating events, where PDS means the plant damage state, TR the damage to be transferred to the internal system, and CD the core damage. Figure 4-3 shows the components grouped by their corresponding seismic-induced initiating events. Fault trees were constructed for each seismic-induced initiating event, for example, the fault tree for the LEP due to seismic event is shown in Figure 4-4.

From the event tree and fault trees, the Boolean equations for the seismic-induced initiating events can be derived. Finally, the initiating event frequency and the corresponding core damage frequency can be determined by solving the Boolean equations or transferring the initiating event to the internal PSA process in the cases of LOOP and GTRN. The computer codes PRASSE (Probabilistic Risk Assessment of Systems for Seismic Events) [Kim et al., 2011] and AIMS-PSA (Advanced Integrated Management System for PSA) [Han et al., 2010] were used for seismic PSA and internal PSA, respectively.

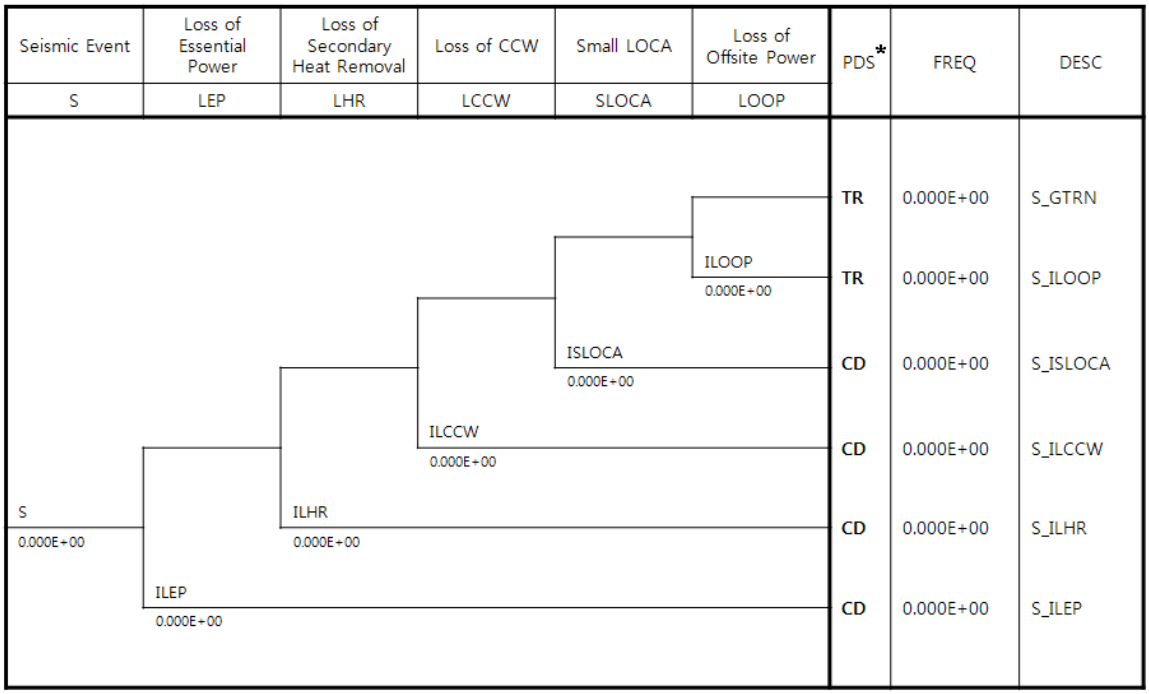

Figure 4-2 Event Tree for Seismic Event

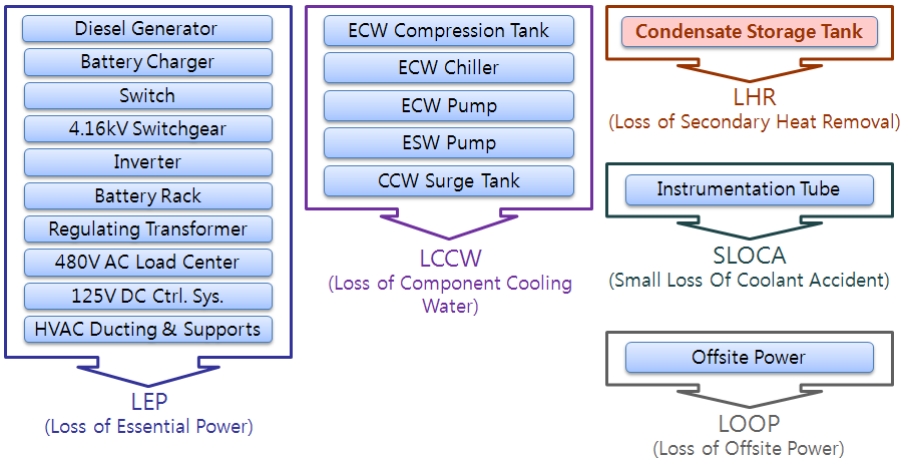

Figure 4-3 Seismic-Induced Initiating Events and Their Components

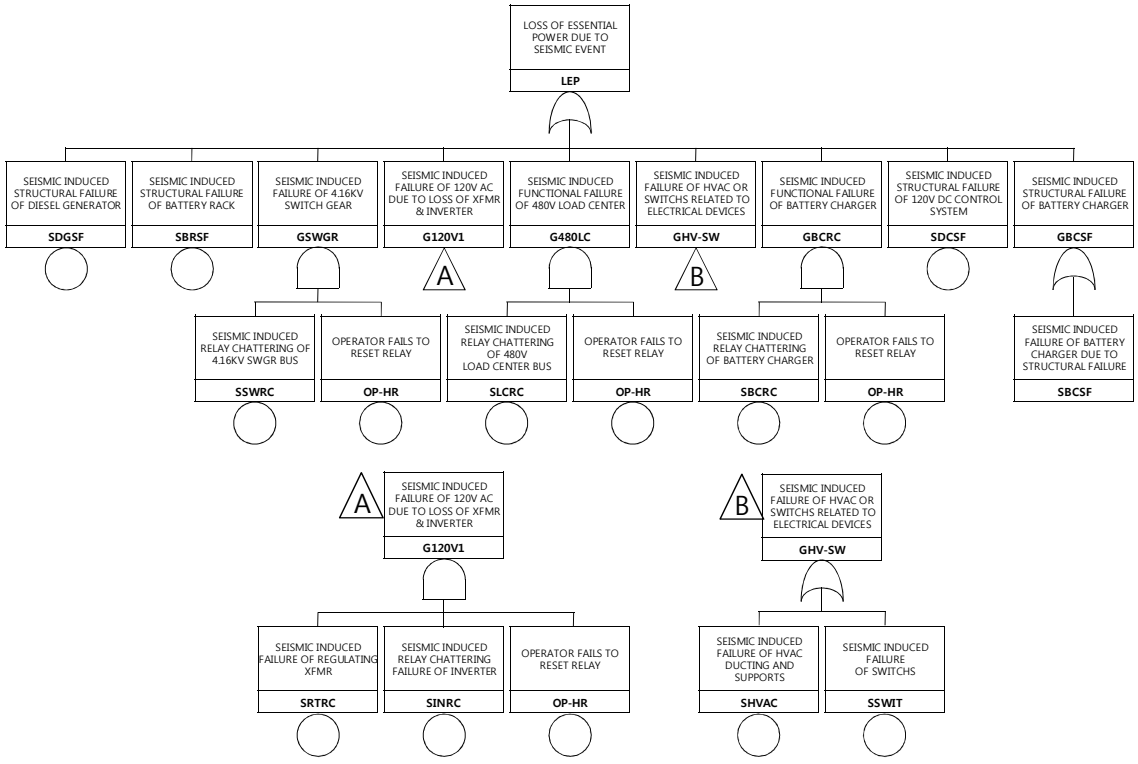

Figure 4-4 Fault Tree for Initiating Event LEP

The seismic-induced initiating event frequencies and CDFs for an undegraded case (baseline) are summarized in Table 4-4, in which the total seismic-induced CDF is identified to be 6.00E-6. According to the internal and external PSA reports for the Ulchin NPP units 5&6, the CDFs due to internal events and fire are 5.65E-6 and 2.30E-6, respectively. The flood-induced CDF is reported to be less than 1.0E-12, and is negligible in the total CDF compared to other internal or external CDFs. Therefore, the total baseline CDF was calculated to be 1.395E-5.

The CDFs and ΔCDFs for degraded CST were estimated by the same procedure as for the baseline CDF calculation, and are shown in Table 4-5 for the constant uncertainty case and the varying uncertainty case. The ΔCDF values versus the baseline CDF are plotted in Figure 4-5, overlapping the risk acceptance regions as prescribed in the U.S. Regulatory Guide 1.174, Rev. 2.

Table 4-4 Seismic-Induced Initiating Event Frequencies and CDFs

Initiating Events	Frequency	Seismic-Induced CDF
LEP	2.64E-6	2.64E-6
LHR	2.65E-7	2.65E-7
LCCW	1.64E-6	1.64E-6
SLOCA	2.74E-8	2.74E-8
LOOP	4.95E-5	6.12E-7
GTRN	6.54E-4	8.16E-7
Total Seismic-Induced CDF		6.00E-6

Table 4-5 CDF and ΔCDF for the Cases of Constant and Varying Uncertainties

Cases	HCLPF (g)	Constant Uncertainty		Varying Uncertainty	
		CDF (E-5.0)	ΔCDF (E-7.0)	CDF (E-5.0)	ΔCDF (E-7.0)
Base case	0.549	1.395	-	1.395	-
	0.500	1.413	1.834	1.415	2.036
	0.444	1.460	6.520	1.460	6.570
	0.392	1.553	15.82	1.541	14.68
	0.340	1.724	33.00	1.640	24.58
Sliding to Overturning	0.300	1.952	55.79	1.784	39.00
	0.287	2.053	65.83	1.830	43.52
	0.235	2.752	135.8	2.154	75.98
	0.183	4.274	288.0	2.869	147.5
	0.130	8.212	681.8	4.592	319.8
Free Standing Tank	0.100	13.64	1,224	6.966	557.2
Minimum case	0.078	21.87	2,047	9.990	859.6

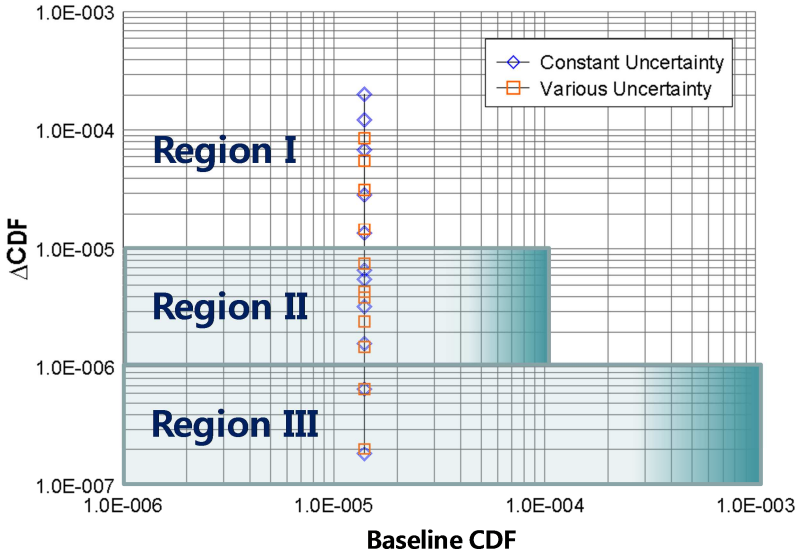

Figure 4-5 ΔCDF and NRC RG 1.174 Risk Acceptance Guideline

4.3 Assessment of the HCLPF-CDF Relation

Figure 4-6 and Figure 4-7 show that the relations between the CDF/ΔCDF and the HCLPF capacity are very smooth, regardless of whether constant uncertainties or varying uncertainties have been assumed. Therefore, there is no need for more data points to achieve an accurate estimate of the HCLPF capacity for a given level of CDF through interpolation. These curves also suggest that there might be a possibility to develop an analytical relationship between the CDF/ΔCDF and the HCLPF through proper regression analysis. However, after testing several different models in Excel, it is believed that the development of an analytical model may require more advanced tools if there is such a model at all. Therefore, the development of DAC for the CST in the next section will rely on interpolation.

Overall, the use of constant uncertainties leads to larger CDF/ΔCDF than using the varying uncertainties, with the level of difference increasing to a factor of greater than two. However, in the range close to $\Delta CDF_{cr} = 10^{-6}$/reactor year, the difference is minimal. In another words, the use of constant uncertainties or varying uncertainties does not significantly affect the development of DAC for the CST based on a $\Delta CDF_{cr} = 10^{-6}$/reactor year.

The baseline CDF is 1.395×10^{-5} /reactor year, which is about a magnitude smaller than the NRC safety goal (CDF = 10^{-4} /reactor year). Therefore, the acceptable level of risk increase due to degradation as developed in Section 2.1 is plausible.

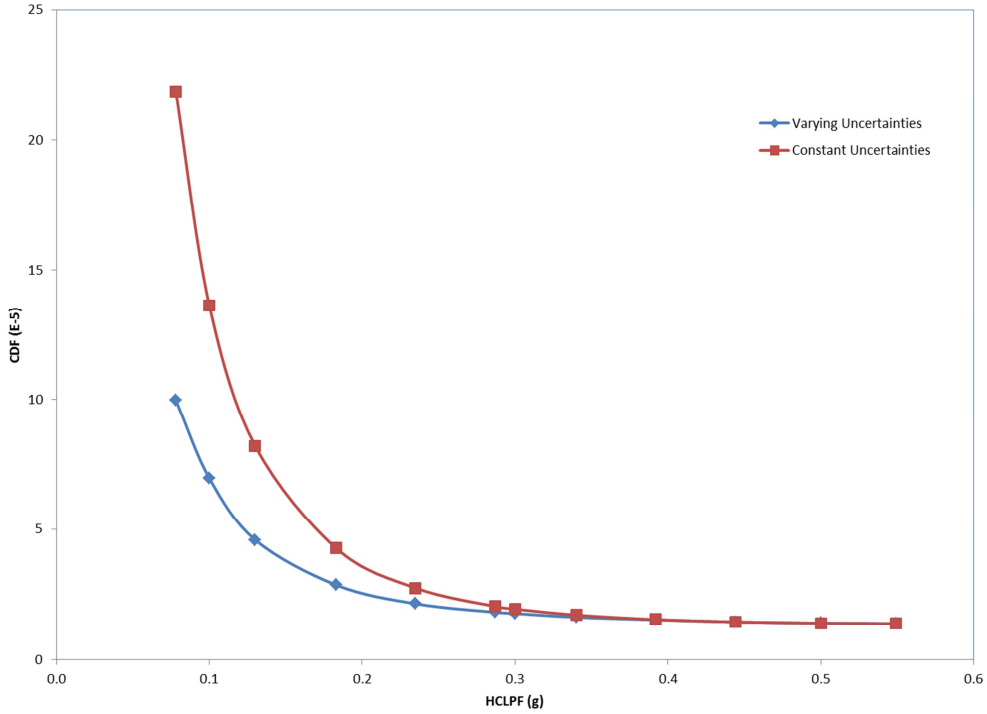

Figure 4-6 HCLPF vs. CDF

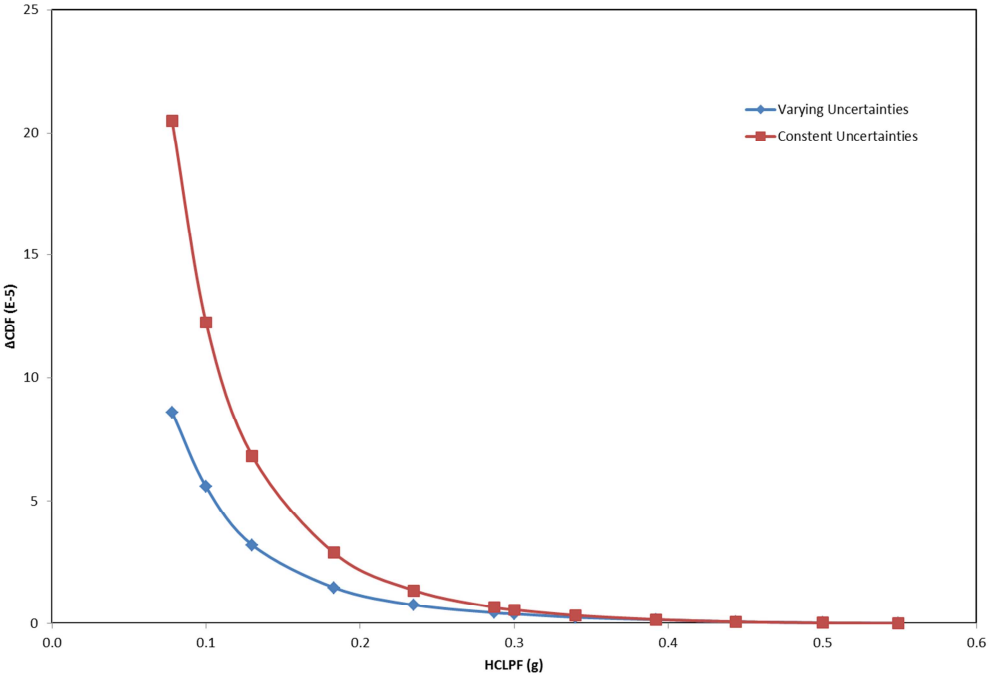

Figure 4-7 HCLPF vs. ΔCDF

5 THREE-TIER DAC FOR THE CST

This section presents an application of the three-tier DAC approach described in Section 2 to the CST. These DAC were determined using cubic splines to closely fit the results of the probabilistic safety assessment. Section 6 discusses how these DAC can be used in the inspection/ maintenance process.

Before the description of the development of the three-tier DAC, a summary of the resultant degradation models is provided below to assist the development of DAC in terms of time.

5.1 Resultant Degradation Formulations for the Five Degradation Cases

For the fragility analyses of the condensate storage tank (CST), three basic degradation scenarios were considered: (A) degraded stainless tank shell, (B) degraded anchor bolts, and (C) cracked reinforced concrete foundation. Two cases of degradation combinations were considered as well: (D) a perfect correlation of the degradation scenarios A, B, and C; and (E) non-perfectly correlated these degradation scenarios.

For degradation scenarios A and B, age-related degradation models were taken from the Year 2 report for demonstration purposes and the parameters required to define these models were determined to consider the CST condition [Nie et al., 2011]. For degradation scenario C, a hybrid degradation model was developed based on available anchorage test results for cracked concrete and regression models based on measured data at Korean NPPs. The resultant models are summarized below to facilitate the development of DAC in terms of time in this section; more details about the background of these models can be found in Section 3 as well as the Year 3 and Year 4 annual reports [Nie et al., 2009, 2010, 2011].

Degradation Scenario (A): Degraded Stainless Tank Shell:

$$A_0(t) = 7.494 \times 10^{-3} \times t$$
$$ts(t) = \frac{5}{8} - A_0(t) \quad (5\text{-}1)$$

in which time t is in years, and the tank shell thickness ts in inches. $A_0(t)$ is the time-dependent loss of the tank shell thickness.

Degradation Scenario (B): Degraded Anchor Bolts:

$$B_0(t) = 5.559 \times 10^{-3} \times t^{0.79}$$
$$D(t) = 2.5 - B_0(t) \quad (5\text{-}2)$$

In which time t is in years, and the diameter of the bolts D in inches. $B_0(t)$ is the time-dependent diameter reduction.

Degradation Scenario (C): Cracked Reinforced Concrete Foundation:

$$C_0(t) = 0.0078 \times t$$
$$T = 200 + \frac{C_0(t)}{0.3}(54.4 - 200) \quad (5\text{-}3)$$

In which time t is in years, the crack width W in mm, and the tensile capacity T in kips. In addition, T is set to 0 kips as a lower bound value when Equation 5-3 results in an impractical negative tensile strength. $C_0(t)$ is the time-depended crack width. This model is the C-2 model introduced in Section 3.

Degradation Case (D): Perfectly-Correlated Degradations A, B, and C:

Degradation models A, B, and C as described by Equations 5-1 through 5-3 are assumed to progress with the same time parameter.

Degradation Case (E): Non-Perfectly-Correlated Degradations A, B, and C:

$$\begin{aligned} A(t) &= A_0(t) \times a \\ B(t) &= B_0(t) \times b \\ C(t) &= C_0(t) \times c \end{aligned} \quad (5\text{-}4)$$

In which A, B, and C refer to the random degradation models, with respect to the basic deterministic degradation models A_0, B_0, and C_0. The rate factors a, b, and c are random variables with lognormal marginal distributions of unit means and standard deviations 0.2, 0.25, and 0.3, respectively. The correlation coefficients between (a,b), (a,c), and (b,c) are specified as 0.4, 0.4, and 0.7, recognizing that degradations in the anchor bolts and the reinforced concrete foundation have stronger correlation than those involving the stainless steel tank shell. A total number of 11 optimum Latin Hypercube samples (LHS) were generated for the rate factors. The empirical correlation coefficients for the resultant lognormal rate factor samples are 0.36, 0.43, and 0.7, respectively, which are very close to the specified values. The resultant correlated rate factors are listed below in Table 3-3 [Nie et al., 2011].

These degradation models are used in this section to develop degradation acceptance criteria in terms of time (DAC_T) based on the degradation acceptance criteria in terms of degradation level (DAC_D).

5.2 Tier 1: Degradation Acceptance Criterion in Terms of HCLPF (DAC_{HCLPF})

The relationships between the core damage frequency (CDF) and the HCLPF were interpolated at $\Delta CDF_{cr} = 10^{-6}$/reactor year to obtain the DAC_{HCLPF}. The HCLPF-CDF curves were obtained by KAERI through PRAs as discussed in Section 4. Figure 5-1 and Figure 5-2 show the results of the cubic spline interpolation, respectively for the cases of constant uncertainties and varying uncertainties. The green lines indicate the location of the interpolation corresponding to a $\Delta CDF_{cr} = 10^{-6}$/reactor year. DAC_{HCLPF} is estimated to be 0.422 g for the case of constant uncertainties and 0.419 g for the case of varying uncertainties. The difference of these two

cases is minimal (0.7%) because the HCLPF-CDF relations of these two cases are very similar at lower levels of degradation, as observed in Section 4.

As a check on the cubic spline interpolation method, linear interpolations were also performed and the resultant DAC_{HCLPF} was calculated to be 0.425 g and 0.422 g for the case of constant uncertainties and the case of varying uncertainties, respectively. The differences are only about 0.7% in both cases. However, if the interpolation point was located elsewhere, for example, at 0.2 g, the difference would be somewhat bigger and the cubic spline interpolation would lead to more accurate estimates because the cubic spline is smoother. It should be noted that interpolation for HCLPF at around $\Delta CDF_{cr} = 10^{-6}$/reactor year is very sensitive to the value of ΔCDF_{cr} because the curves are very flat.

For the rest of this report, DAC_{HCLPF} of 0.422 g will be used as the degradation acceptance criterion for the CST as a representative value, with other values also being considered to assess various sensitivities as applicable. One may think at a first impression that the DAC_{HCLPF} is not immediately useful because HCLPF is not readily available in the inspection process. However, DAC_{HCLPF} can be viewed as a surrogate of ΔCDF_{cr} for the subject component, the CST in this case, for the calculation of DAC_D and DAC_T, regardless of any specific physical degradation. If a level of degradation is observed somewhere in the CST, one can determine whether the level of degradation is safety-significant by checking the fragility value without performing PRA, which may not always be accessible in many cases. Moreover, if the degradation is observed at a different location or at more than one location, the same DAC_{HCLPF} is still valid for the assessment of safety-significance of the observed degradation(s) and can be used to compute DAC_D and DAC_T, as well.

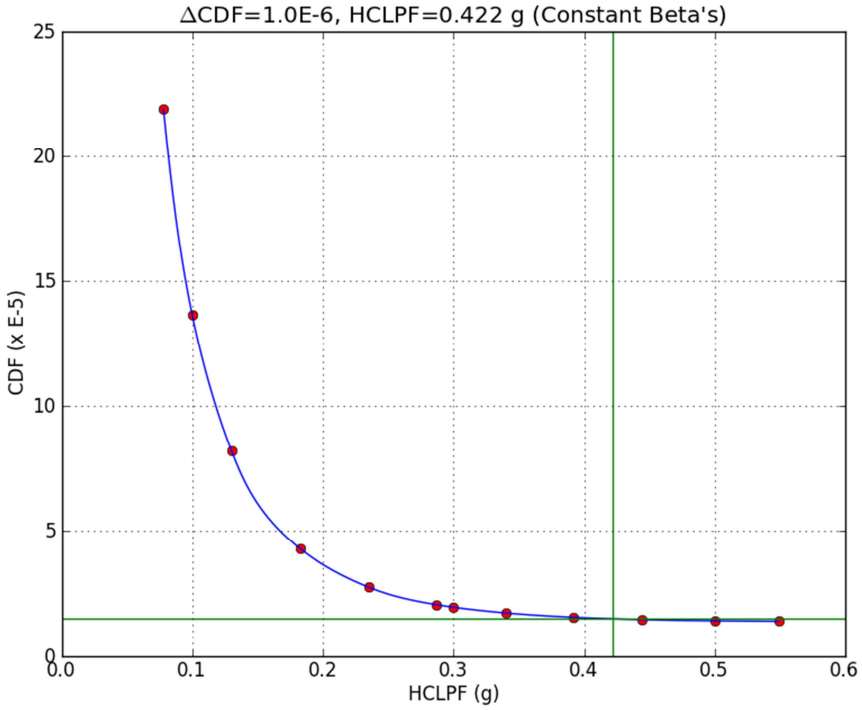

Figure 5-1 Interpolation of CDF-HCLPF at $\Delta CDF=10^{-6}$ /Reactor Year (Constant Uncertainties)

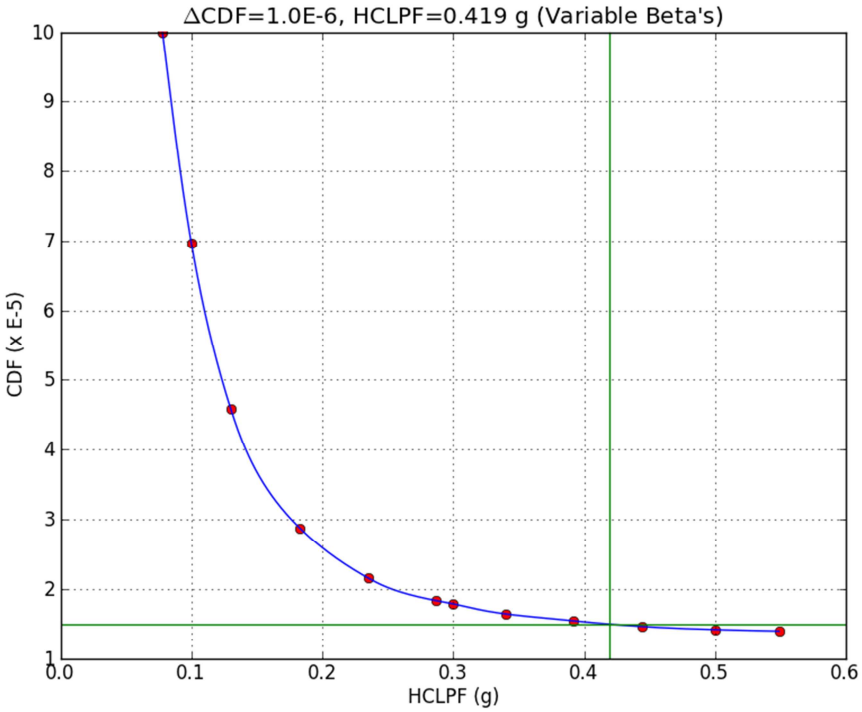

Figure 5-2 Interpolation of CDF-HCLPF at ΔCDF=10^{-6} /Reactor Year (Varying Uncertainties)

5.3 Tier 2: DAC in Terms of Degradation Levels (DAC_D)

In order to be consistent with the seismic fragility analyses in the Year 4 study that utilized the operational water level (as compared to the design water level in the Year 3 study), three additional fragility analyses were performed to obtain the seismic HCLPF capacities for the three individual degradation scenarios A, B, and C. These fragility results are summarized in Section 3 and Appendices A through C.

These fragility results are required in this section to develop various DAC_D's, any of which can only consider one basic degradation scenario, i.e., any one of A, B, or C. In the following subsections, the curves showing the relationship between the HCLPF capacity and various degradation levels were determined at a constant spacing in time (5 years), although time is not used in these curves.

5.3.1 DAC in Terms of Tank Shell Thickness (DAC_{ts})

As shown in Figure 5-3, a cubic spline interpolation of the HCLPF-ts curve at DAC_{HCLPF} = 0.422 g led to an estimate of the DAC_{ts} of 0.420 in. It can be seen that the cubic spline can represent the entire data range very well. The green horizontal and vertical lines in this figure indicate the interpolation points for both cases of constant uncertainties and varying uncertainties. The critical thickness reduction due to degradation can be calculated to be 0.203 in., which is about a third of the original tank shell thickness of 0.625 in. This level of thickness reduction shows that the CST can undertake a relatively large amount of corrosion in the tank shell, and any level

of thickness reduction less than 0.203 in. would not be of any safety concern. This finding was reached by assuming there is no other degradation scenario affecting the CST at the same time. Although DAC_{ts}, as well as other DAC_D, can be used to determine the relative severity of an observed level of degradation, it cannot by itself be used to predict the remaining time until which the next inspection/maintenance would be needed. Life prediction requires a reliable time-dependent degradation model for the tank shell material and its environment.

For reference, if the DAC_{HCLPF} is 0.419 g (corresponding to varying uncertainties), the DAC_{ts} is found to be 0.415 in.

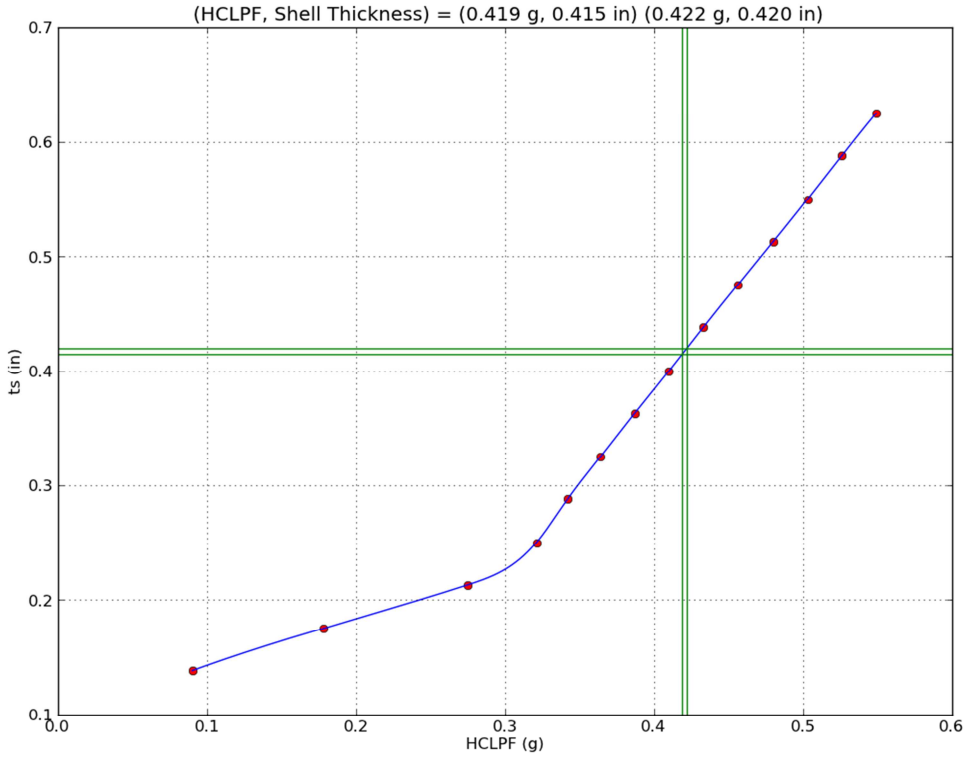

Figure 5-3 DAC_{ts} through Interpolation of the HCLPF-ts Relationship

5.3.2 DAC in Terms of Anchor Bolt Diameter (DAC_{dbolt})

Similarly, DAC in terms of the diameter of the anchor bolts DAC_{dbolt} can be determined to be 1.248 in., by interpolating the HCLPF-dbolt relationship at DAC_{HCLPF} = 0.422 g (see Figure 5-4). The cubic spline as shown in Figure 5-4 represents the HCLPF-dbolt data very well. The green lines in this figure show the interpolation points for both cases of constant uncertainties and varying uncertainties. Using the original diameter of the anchor bolts (2.5 in.), the critical diameter reduction due to degradation can be calculated to be 1.252 in., which is about more than half of the original bolt diameter. Therefore, the capacity of the CST in maintaining the plant safety is even less vulnerable to anchor bolt degradation than the tank shell corrosion, as was similarly concluded using the results of the fragility analyses [Nie et al., 2010, 2011]. This high level of tolerance of the anchor bolts to corrosion regarding their contribution to plant risk

is due to the large number (78) of anchor bolts that were placed for the CST. This observation is based on an assumption that there is no other degradation scenarios affecting the CST at the same time. DAC_{dbolt} can be used to estimate the relative severity of an observed level of degradation in the anchor bolt, but cannot by itself be used to predict the remaining time for the degraded anchor bolts to be replaced. Life prediction for the anchor bolts requires a reliable time-dependent degradation model for the anchor bolts under the specific environment of the Ulchin plant.

For reference, if DAC_{HCLPF} is 0.419 g (the case of varying uncertainties), the DAC_{dbolt} is found to be 1.229 in., which is 1.5% less than 1.248 in. determined at DAC_{HCLPF} = 0.422 g for the case of constant uncertainties.

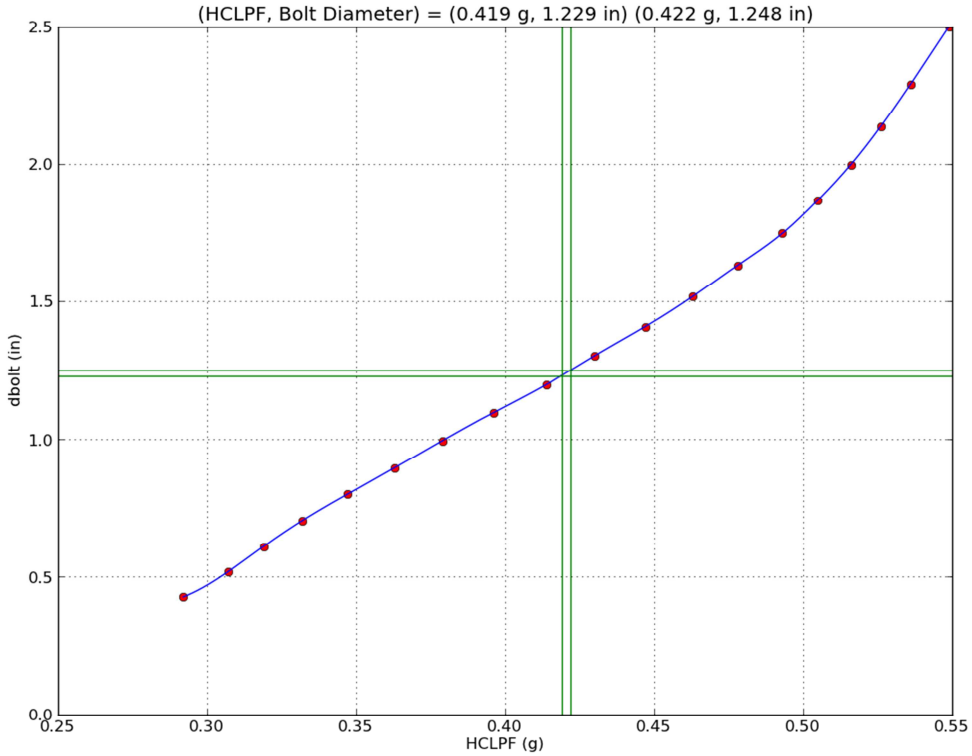

Figure 5-4 DAC_{dbolt} through Interpolation of the HCLPF-dbolt Relationship

5.3.3 DAC in Terms of Cracking in Concrete Foundation (DAC_{crack})

For the degradation case of cracking in the reinforced concrete foundation of the CST, DAC in terms of the cracking width DAC_{crack} can be determined to be 0.342 mm, by interpolating the HCLPF-Crack Width relationship at DAC_{HCLPF} = 0.422 g (see Figure 5-5). As can be seen in this figure, the cubic spline can only represent well the middle part of the HCLPF-Crack Width data; the sudden changes at both ends of the data points (corresponding to failure mode changes) cannot be represented by the same cubic spline without large distortion in the resultant curve. However, as shown by the green lines in the figure, the interpolation points occur on the smooth middle part and there should be no concern in the accuracy of the interpolation.

DAC_{crack} can be used to estimate the relative severity of an observed crack width in the reinforced concrete foundation, but cannot be used to predict the remaining time until which the foundation needs to be repaired. Life prediction of the reinforced concrete foundation requires a reliable time-dependent degradation models for the crack width and the pullout capacity of the anchor bolt.

For reference, if DAC_{HCLPF} is 0.419 g, the DAC_{crack} is found to be 0.344 mm, which is very close to 0.342 mm (determined using DAC_{HCLPF} = 0.422 g), because the HCLPF-Crack Width curve is relatively flat in the middle part of the data range.

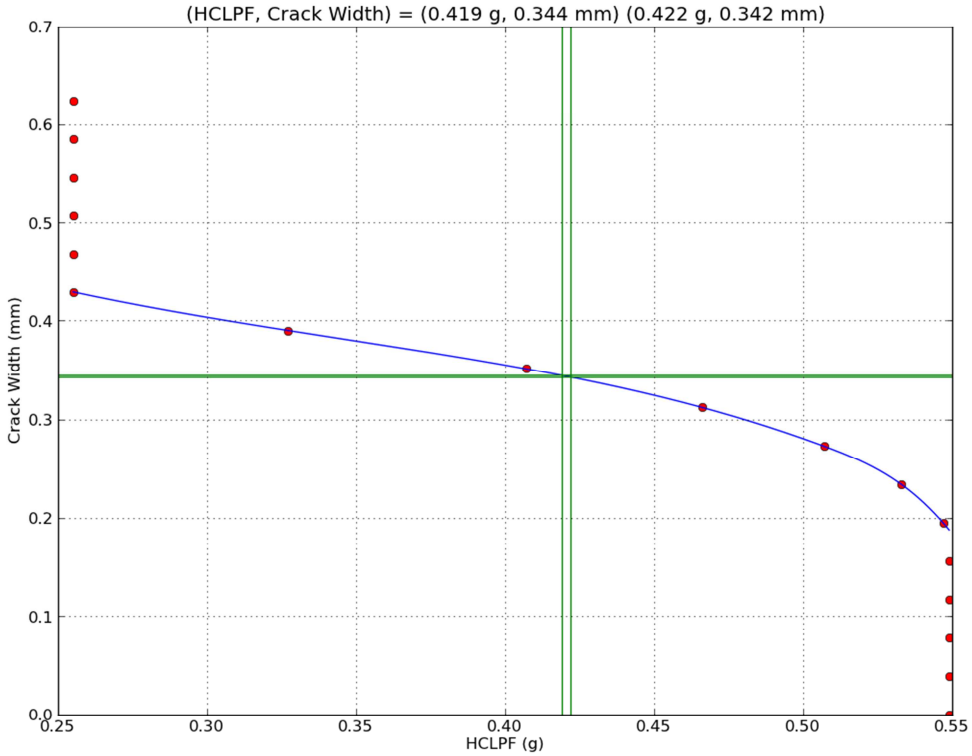

Figure 5-5 DAC_{crack} through Interpolation of HCLPF-Crack Width

5.4 Tier 3: DAC in Terms of Time (DAC_T)

It should be reiterated that the introduction of time in the development of the degradation acceptance criteria relies on the availability and reliability of the age-related degradation models for the individual degradation scenarios and combined degradation cases. Measured degradation data over a long period of time are highly valuable for developing such models or validating existing models. Unfortunately, high quality data for degradation monitoring and suitable for degradation model development are currently rare. If observed degradation data are not sufficient for developing reliable degradation models or deriving reliable parameters for existing degradation models, these data can be used to compare with the various DAC_D's or

DAC_{HCLPF} to determine whether the observed degradation is safety significant. To estimate the remaining life without a sound understanding of the degradation process over a long period of time, multiple time-dependent degradation models can be assumed based on available degradation information for sensitivity analysis.

In this section, all DAC_T's are developed based on the degradation models described in Section 5.1, mainly for the purpose of demonstration. Without careful justification of the suitability of these degradation models for the real degradation situations, the use of these DAC_T's may not be appropriate.

5.4.1 DAC_T for the Degradation Scenarios A, B, and C

In the previous section, DAC_{ts}, DAC_{dbolt}, and DAC_{crack} have been developed without considering the time after construction for these critical degradation levels to be reached. However, using the degradation models as summarized in Section 5.1, the time to reach these critical degradation levels can be easily calculated.

For Degradation Scenario (A), the critical tank shell thickness reduction was found to be 0.203 in. Using Equation 5-1 that is a linear function of the time variable *t*, the time to reach this level of thickness reduction, $DAC_{T\text{-}ts}$, can be calculated to be 27.1 years.

For Degradation Scenario B, the critical diameter reduction was determined to be 1.252 in., which corresponds to, based on Equation 5-2, a life of 950.6 years before its degradation significantly affect the plant risk. This very long life span is a result of the assumed degradation model for the anchor bolts, and in this case, is also due to the large number of anchor bolts placed for the CST. This observation is in line with what was identified in the Year 3 annual report [Nie et al., 2010].

For Degradation Scenario C, the DAC_{crack} was determined to be 0.342 mm. Substituting $C_0(t)$ with DAC_{crack} in Equation 5-3 yields t = 43.8 years, which is close to the initial licensed operation period for the U.S. NPPs.

5.4.2 DAC_T for the Perfectly-Correlated Degradation Scenarios A, B, and C

For the case of perfectly-correlated degradation scenarios A, B, and C, since these degradation scenarios proceed in the same pace according to their degradation models, a common variable can be used to represent this degradation progress. Although not necessary, time is a natural and convenient choice for such a common variable.

Figure 5-6 shows the HCLPF-time relation for the combined degradation case that perfectly correlates the three basic degradation scenarios. Similar to Figure 5-5, the cubic spline used for interpolation does not connect all data points to avoid overly distorting the curve. However, the interpolation at DAC_{HCLPF} should be accurate because the cubic spline is very smooth around DAC_{HCLPF} as indicated by the green horizontal and vertical lines in Figure 5-6. The DAC in terms of time, $DAC_{T\text{-}Perfect}$ is calculated to be 26.9 years at the DAC_{HCLPF} = 0.422 g (27.5 years if DAC_{HCLPF} = 0.419 g), very similar to that for the case of degradation in the tank shell. This suggests that the degradation in the tank shell dominates the degradation process up to the critical time $DAC_{T\text{-}Perfect}$, by which the degradations may not cause significant increase in plant risk ($\Delta CDF \leqslant$

10^{-6}/reactor year). This observation was also identified in the Year 3 research that focused on the seismic fragility analyses of the CST [Nie et al., 2010].

It should be noted that the critical time DAC_T is predicted by assuming that there is no intermediate inspections/maintenance and that the degradation models adequately represent the reality. In case that degradation levels observed in inspections are not consistent with the degradation models, one can adjust the degradation models and recalculate the remaining life.

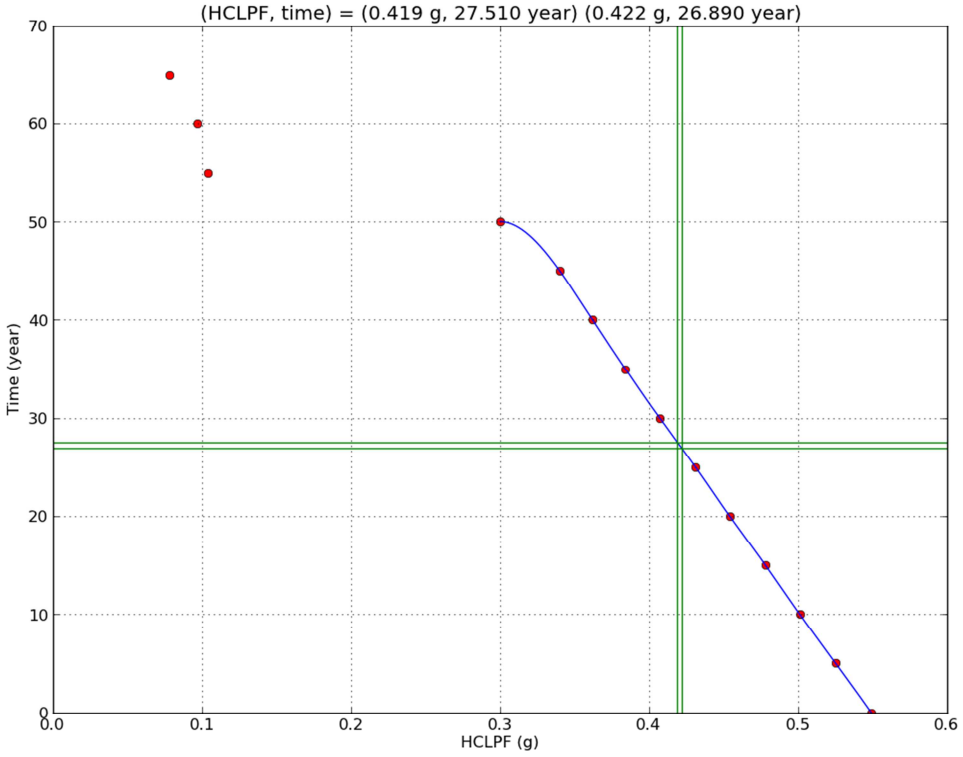

Figure 5-6 $DAC_{T\text{-}Perfect}$ through Interpolation of HCLPF-Time

5.4.3 DAC_T for the Non-Perfectly Correlated Degradation Scenarios A, B, and C

For the case of non-perfectly correlated degradation scenarios A, B, and C, simulations had to be carried out to characterizes the seismic fragility performance of the CST, which resulted in 11 sample degradation cases based on assumed variances and coefficients of correlation (see Section 3 for details). Each sample case during simulation is a combined degradation case of sample degradation models (the original degradation models multiplied by sample factors) for the tank shell, anchor bolts, and the cracked reinforced concrete foundation. Figure 5-7 through Figure 5-17 show the interpolation of the sample HCLPF-time relations using cubic splines. It can be seen that only some of the cubic splines can cover the entire data range in order to avoid severe distortion in the interpolated curves. Nevertheless, the cubic splines are all very smooth at the interpolation points as shown in these figures, assuring the accuracy of the interpolations for all 11 sample cases.

Table 5-1 and Table 5-2 show the statistical results of the $DAC_{T\text{-}SIM}$ for the cases of constant uncertainties and varying uncertainties, respectively. Both cases are very similar; so the discussion below is based on DAC_{HCLPF} = 0.422 g. This level of DAC_{HCLPF} occurs in the region dominated by the sliding failure mode, as shown in Figure 3-25. The mean $DAC_{T\text{-}SIM}$ is about 27.3 years, which is very similar to the perfectly-correlated case (26.9 years) and the case of degradation in the tank shell only (27.1 years). The standard deviation in the $DAC_{T\text{-}SIM}$ is 5.7 years and the coefficient of variation (COV) was calculated to be 0.209.

The COV of the crack width is 0.264, which is in good agreement with the theoretical value of 0.3. Since the degradation levels in the tank shell and the anchor bolts are significantly less than the original sizes at the times corresponding to DAC_{HCLPF} = 0.422 g, the COVs of the tank shell thickness and the bolt diameter (0.005 and 0.009, respectively) are much smaller than those specified to the corresponding degradation models (0.2 and 0.25, respectively). The COVs for the loss of the tank shell thickness and the diameter reduction of the anchor bolts were estimated to be 0.01, and 0.278, respectively (calculated from the values shown in Table 5-1). It appears that variations in the crack width and the diameter reduction of the anchor bolt have a strong influence on the variation in the $DAC_{T\text{-}SIM}$, although it has been determined that the degradation of the tank shell dominates the deterioration of the fragility capacity of the CST up to the $DAC_{T\text{-}SIM}$.

Table 5-1 $DAC_{T\text{-}SIM}$ for Constant Uncertainties (DAC_{HCLPF}=0.422 g)

Simulation ID	$DAC_{T\text{-}SIM}$ (years)	ts (in)	dbolt (in)	Crack (mm)
Sim 1	30.236	0.423	2.445	0.169
Sim 2	30.705	0.426	2.406	0.270
Sim 3	23.812	0.427	2.415	0.283
Sim 4	28.160	0.423	2.438	0.147
Sim 5	24.657	0.429	2.371	0.288
Sim 6	16.897	0.423	2.436	0.157
Sim 7	36.768	0.424	2.417	0.198
Sim 8	26.968	0.424	2.416	0.172
Sim 9	21.558	0.422	2.445	0.167
Sim 10	34.435	0.424	2.426	0.249
Sim 11	25.925	0.425	2.435	0.278
mean	27.284	0.425	2.423	0.216
Sample Std	5.691	0.002	0.022	0.057
Cov	0.209	0.005	0.009	0.264

Table 5-2 $DAC_{T\text{-}SIM}$ for Varying Uncertainties (DAC_{HCLPF} = 0.419 g)

Simulation ID	$DAC_{T\text{-}SIM}$ (years)	ts (in)	dbolt (in)	Crack (mm)
Sim 1	30.944	0.418	2.444	0.173
Sim 2	31.408	0.421	2.405	0.276
Sim 3	24.329	0.422	2.413	0.289
Sim 4	28.849	0.418	2.437	0.151
Sim 5	25.167	0.425	2.369	0.294
Sim 6	17.303	0.418	2.434	0.161
Sim 7	37.652	0.420	2.416	0.203
Sim 8	27.621	0.419	2.414	0.176
Sim 9	22.076	0.418	2.444	0.171
Sim 10	35.282	0.419	2.424	0.255
Sim 11	26.463	0.421	2.434	0.284
mean	27.918	0.420	2.421	0.221
Sample Std	5.836	0.002	0.022	0.058
Cov	0.209	0.005	0.009	0.263

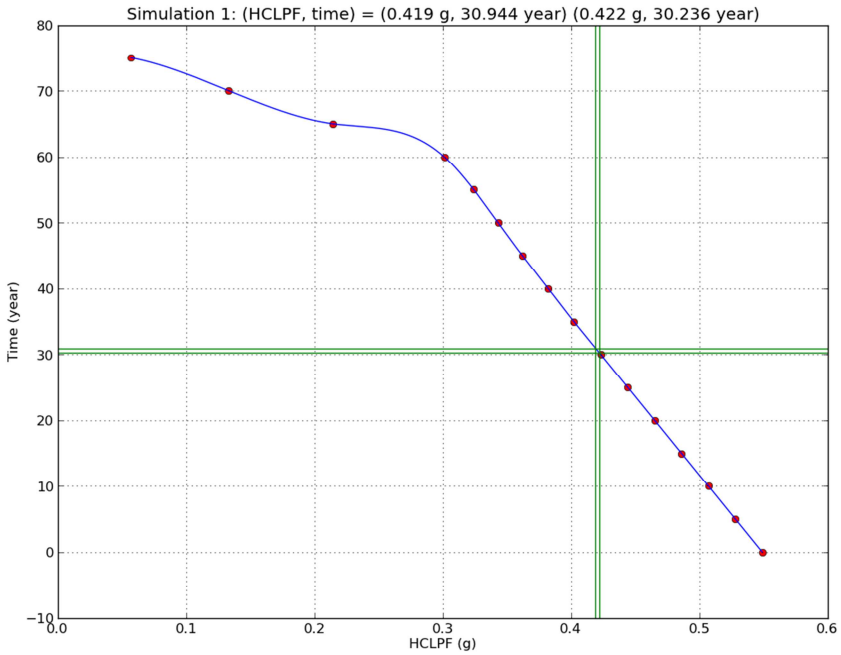

Figure 5-7 $DAC_{T\text{-}Sim1}$ through Interpolation of HCLPF-Time for Sample One

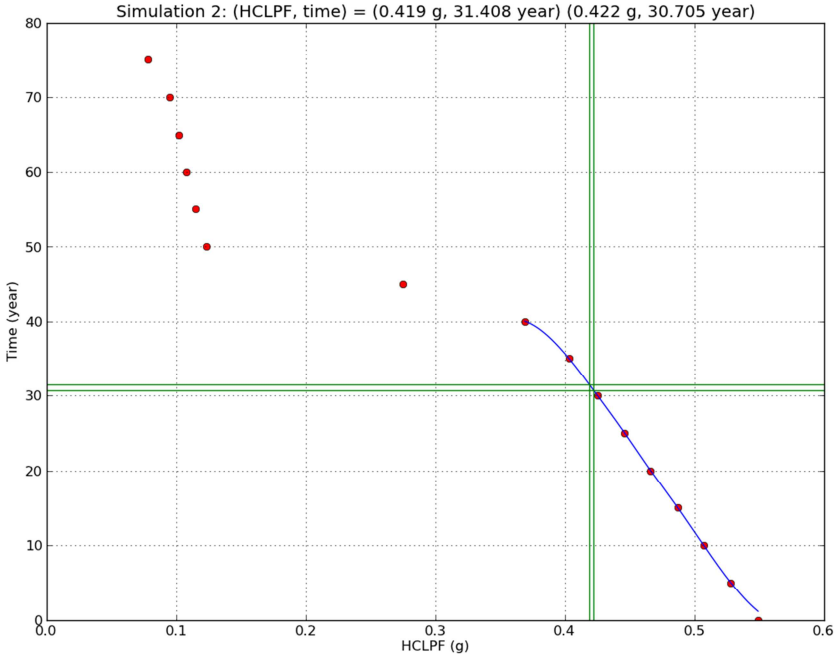

Figure 5-8 $DAC_{T\text{-}Sim2}$ through Interpolation of HCLPF-Time for Sample Two

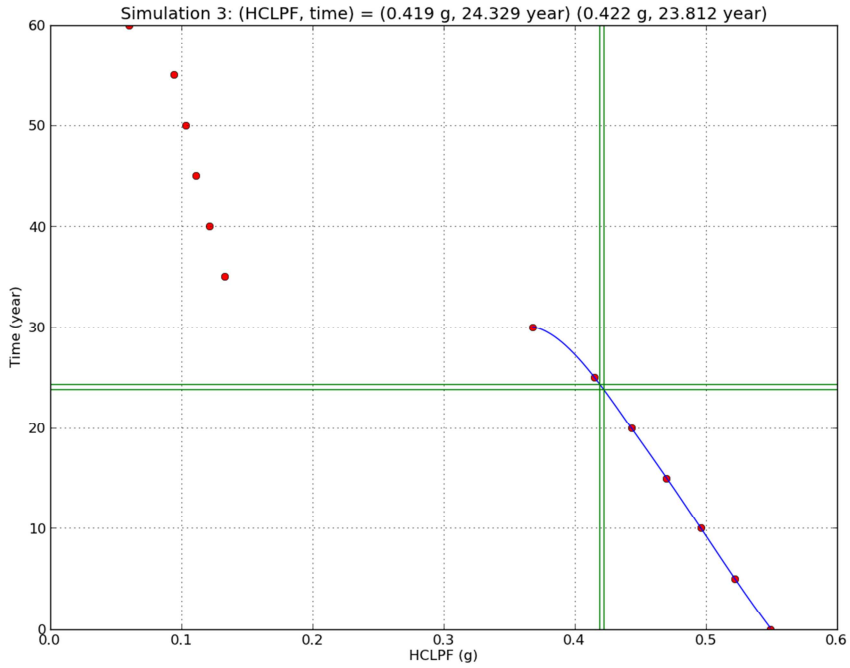

Figure 5-9 $DAC_{T\text{-}Sim3}$ through Interpolation of HCLPF-Time for Sample Three

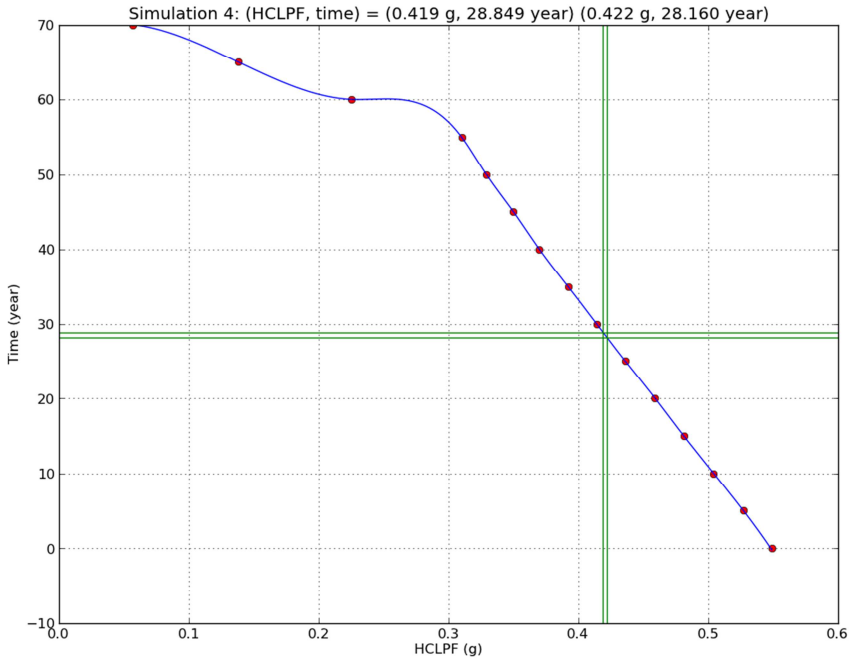

Figure 5-10 $DAC_{T\text{-}Sim4}$ through Interpolation of HCLPF-Time for Sample Four

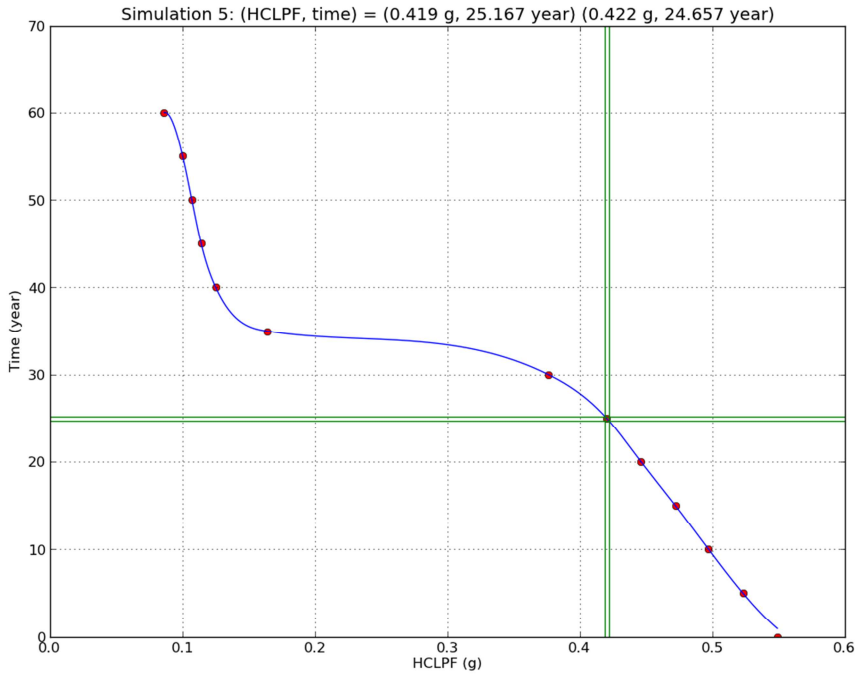

Figure 5-11 $DAC_{T\text{-}Sim5}$ through Interpolation of HCLPF-Time for Sample Five

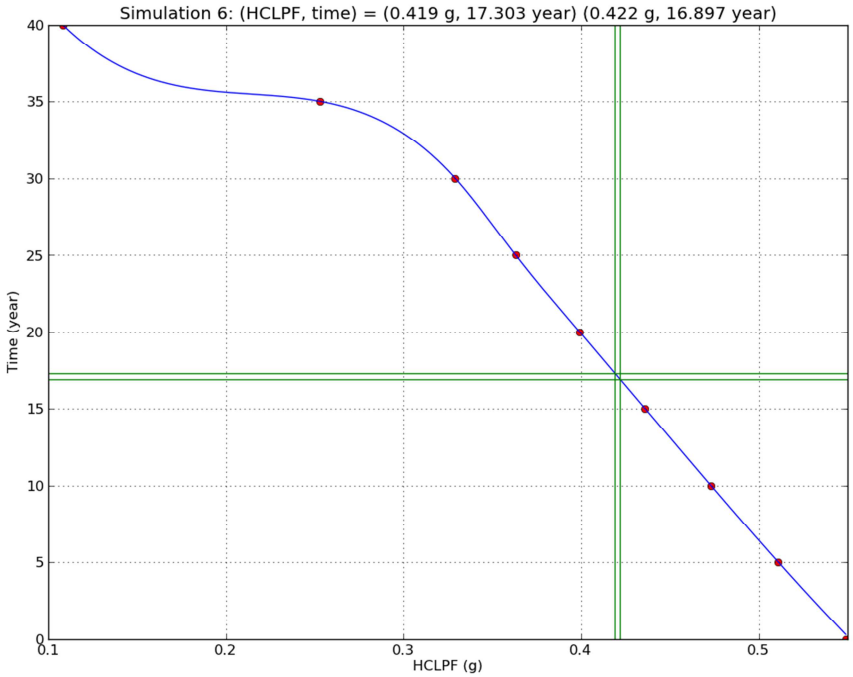

Figure 5-12 $DAC_{T\text{-}Sim6}$ through Interpolation of HCLPF-Time for Sample Six

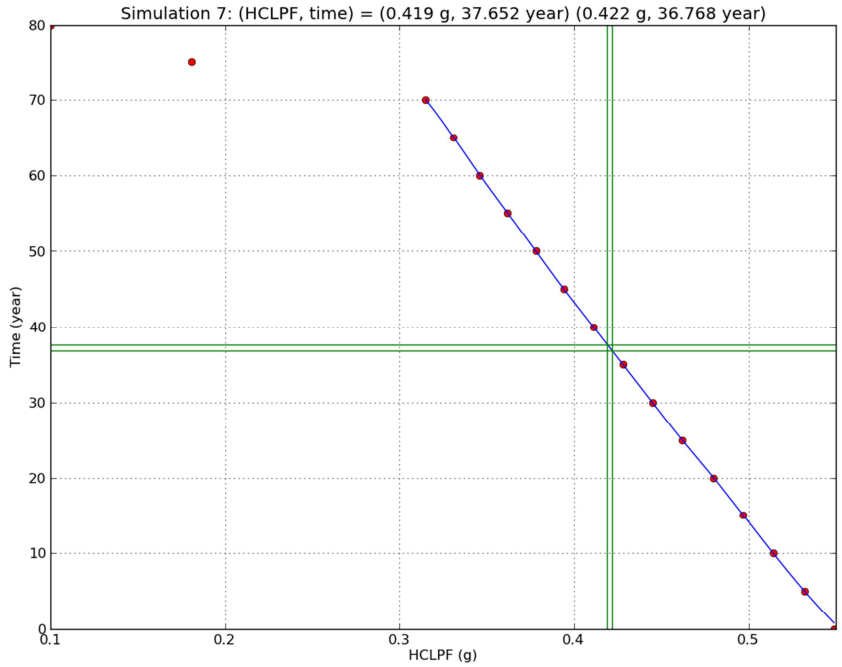

Figure 5-13 $DAC_{T\text{-}Sim7}$ through Interpolation of HCLPF-Time for Sample Seven

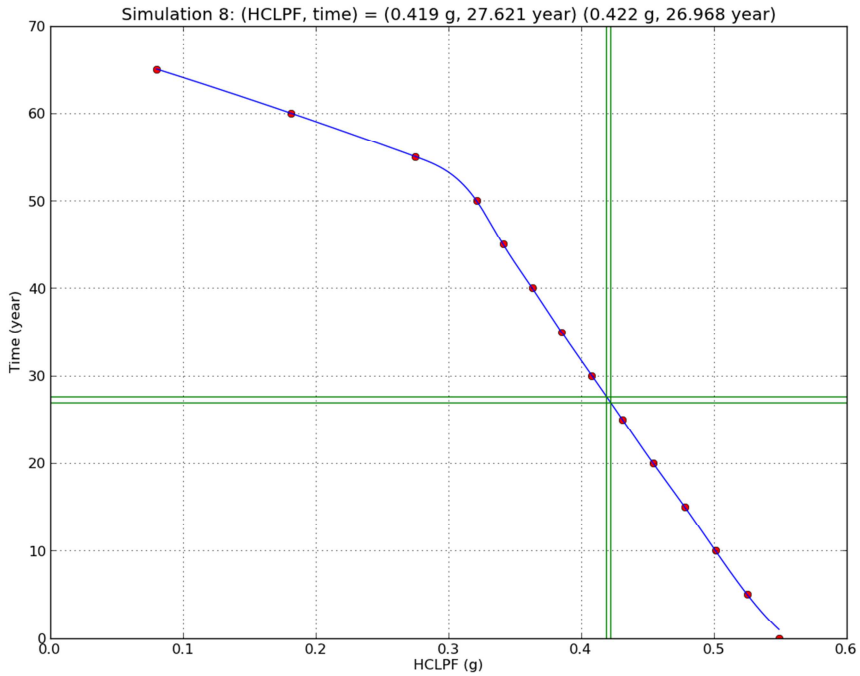

Figure 5-14 $DAC_{T\text{-}Sim8}$ through Interpolation of HCLPF-Time for Sample Eight

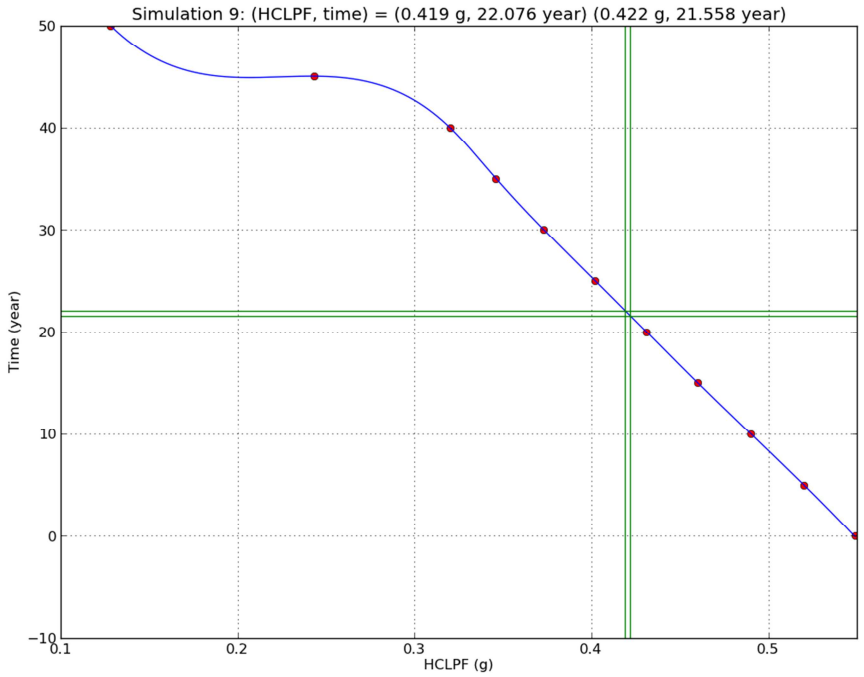

Figure 5-15 $DAC_{T\text{-}Sim9}$ through Interpolation of HCLPF-Time for Sample Nine

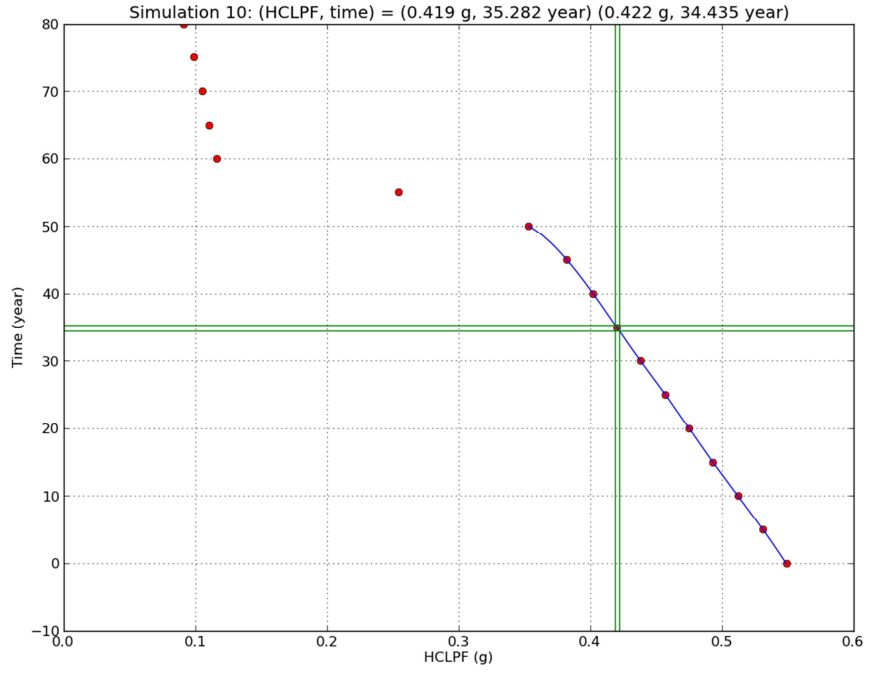

Figure 5-16 $DAC_{T\text{-}Sim10}$ through Interpolation of HCLPF-Time for Sample Ten

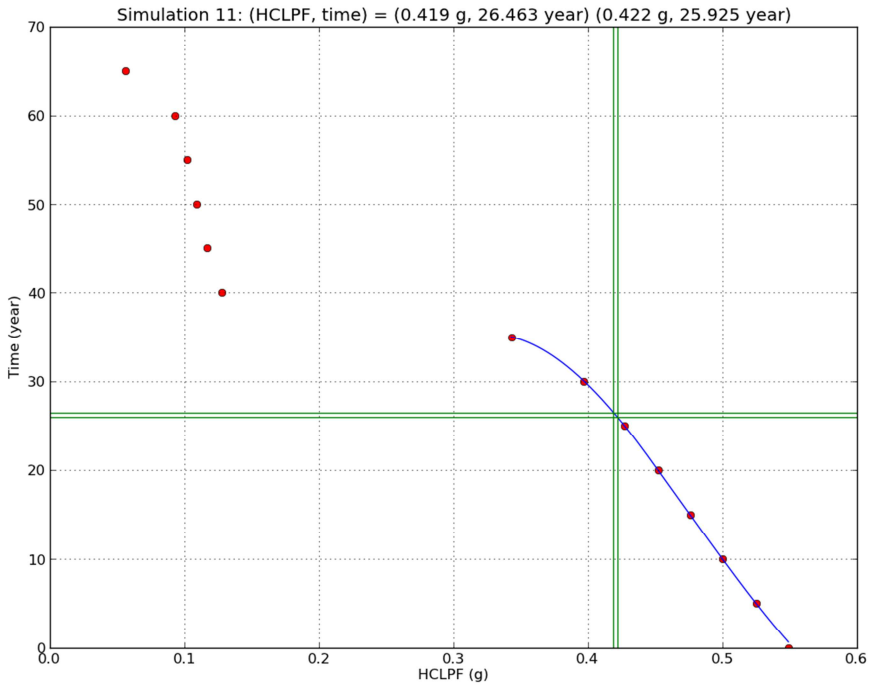

Figure 5-17 $DAC_{T\text{-}Sim11}$ through Interpolation of HCLPF-Time for Sample Eleven

5.5 DAC for $\Delta CDF_{cr}=10^{-5}$ / Reactor Year

5.5.1 DAC_{HCLPF}

A risk criterion of $\Delta CDF_{cr} = 10^{-6}$/reactor year, the upper bound of Region III in Figure 2-1, has been determined to be appropriate for the development of various DAC in this report. For the particular case of the subject CST, NRC RG 1.174 also allows a higher ΔCDF_{cr}, as depicted by Region II in Figure 2-1, which can be used for the development of DAC because the total CDF is 1.395×10^{-5} /reactor year for the Ulchin plant is less than 10^{-4}/reactor year. However, as stated in Section 2, to permit the higher ΔCDF_{cr} in Region II, the quality of the PRA in calculation of the total CDF and LERF would have to be full-scope; with sufficient level of detail; technically adequate; and representing well the as-built, as-operated, and as-degraded plant. This translates to a significant requirement on the PRA implementation, which is often not sophisticated enough in practice. Therefore, instead of using a higher level ΔCDF_{cr} as a risk criterion for the development of various DAC in this report, a sensitivity analysis was performed using a higher risk criterion of $\Delta CDF_{cr} = 10^{-5}$/reactor year to assess its impact on the various DAC. It should be pointed out that such a level of ΔCDF_{cr} is about the same level as the baseline CDF, implying that multiple degraded components with a similar risk increase allowance could result in significantly increased CDF exceeding the NRC risk goal of CDF=10^{-4}/reactor year. Therefore, the use of $\Delta CDF_{cr} = 10^{-5}$/reactor year in this section is purely for sensitivity assessment.

As shown in Figure 5-18, a cubic spline interpolation of the CDF-HCLPF relationship using ΔCDF_{cr} = 10^{-5}/reactor year yielded a DAC_{HCLPF} = 0.255 g for the case of constant uncertainties, which is about 60% of that based on ΔCDF_{cr} = 10^{-6}/reactor year. For the case of varying uncertainties, the DAC_{HCLPF} was estimated to be 0.214 g, as shown in Figure 5-19. The difference is about 16%, which is much broader than 0.7% as determined using ΔCDF_{cr} = 10^{-6}/reactor year. Therefore, the varying uncertainties as a result of the degradation process have a significant impact on the DAC when the risk criterion is taken as the upper bound of Region II in Figure 2-1. On the other hand, the assumption of constant (degradation-independent) uncertainties in the development of various DAC is conservative in the case of the CST because the varying (increasing) uncertainties lead to smaller DAC_{HCLPF}. It should be pointed out that the difference in DAC between the assumptions of constant uncertainties and varying uncertainties is negligible when the stricter risk criterion of ΔCDF_{cr} = 10^{-6}/reactor year is used for the rest of this report.

Linear interpolations of the CDF-HCLPF relations, performed separately, yielded a DAC_{HCLPF} of 0.262 g and 0.218 g, for the cases of constant uncertainties and varying uncertainties, respectively. The differences from those determined using cubic spline interpolations are about 2-3%.

These levels of DAC_{HCLPF}, either 0.255 g or 0.214 g, occur in the region dominated by the overturning moment failure mode, as shown in Figure 3-25.

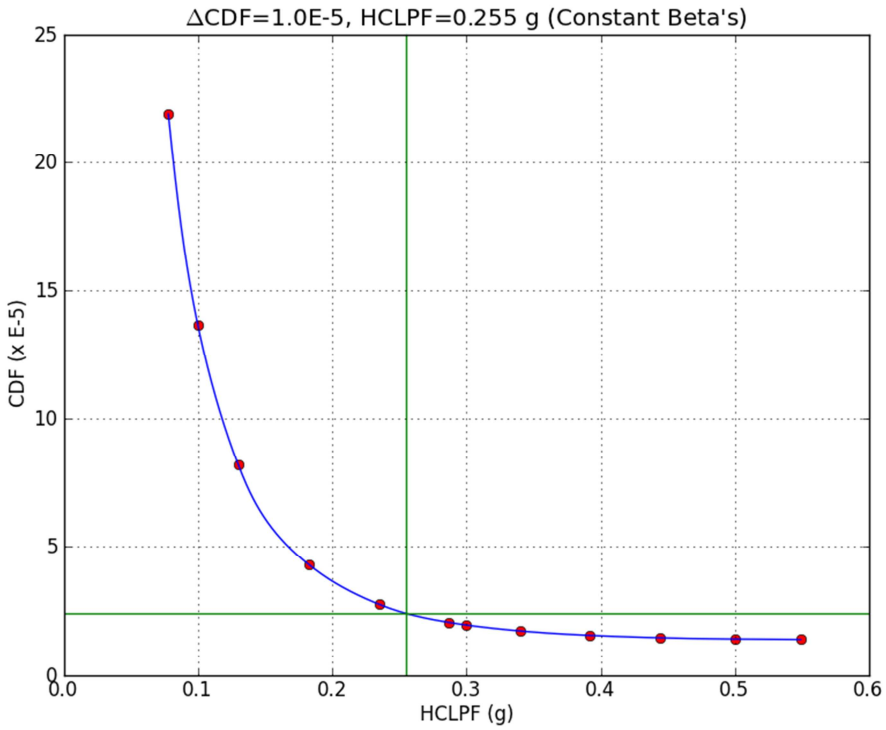

Figure 5-18 DAC_{HCLPF} for ΔCDF_{cr} =10^{-5} /Reactor Year (Constant Uncertainties)

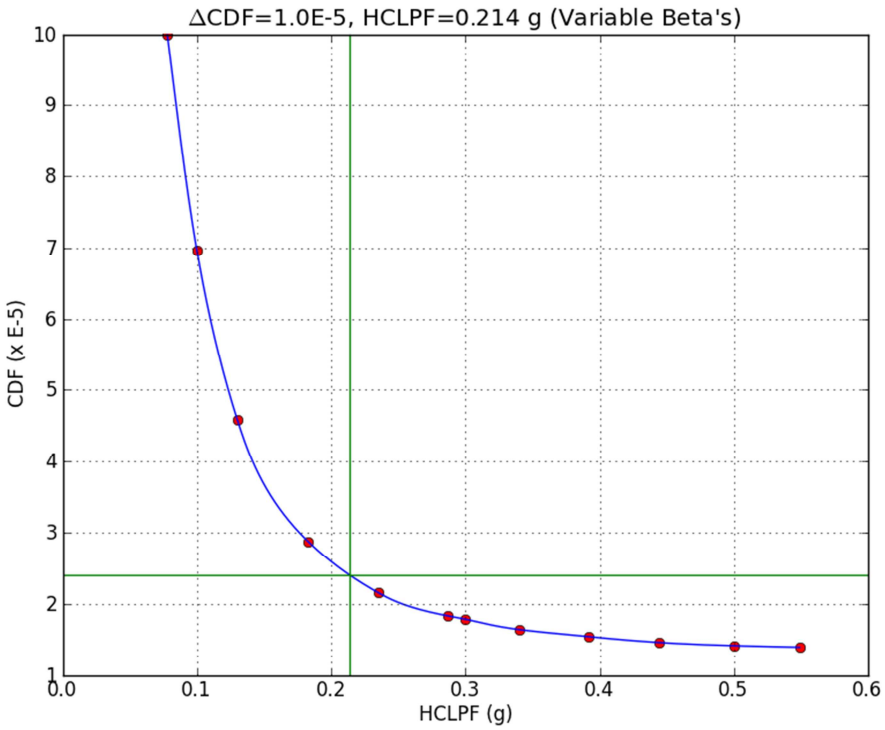

Figure 5-19 DAC_{HCLPF} for $\Delta CDF_{cr} = 10^{-5}$ /Reactor Year (Varying Uncertainties)

5.5.2 DAC for a Single Degradation Scenario A, B, or C

Using $\Delta CDF_{cr} = 10^{-5}$ /reactor year, DAC_{ts} (in terms of tank shell thickness) can be estimated to be 0.205 in. and 0.189 in., as shown in Figure 5-20, for the cases of constant uncertainties and varying uncertainties, respectively. The loss of wall thickness is about more than 2/3 of the original thickness, as compared to about 1/3 when using $\Delta CDF_{cr} = 10^{-6}$ /reactor year. The corresponding DAC_T (in terms of time) can be estimated to be 56.0 years and 58.2 years, respectively for the two uncertainty cases, as compared to 27.1 years when using $\Delta CDF_{cr} = 10^{-6}$ /reactor year.

For both cases of only corrosion in the anchor bolts or only cracking in the reinforced concrete foundation, the use of $\Delta CDF_{cr} = 10^{-5}$ /reactor year is not feasible because the DAC_{HCLPF} falls outside of the data ranges as shown Figure 5-21 and Figure 5-22. The lower limit of the range of HCLPF values corresponds to a free-standing condition of the CST.

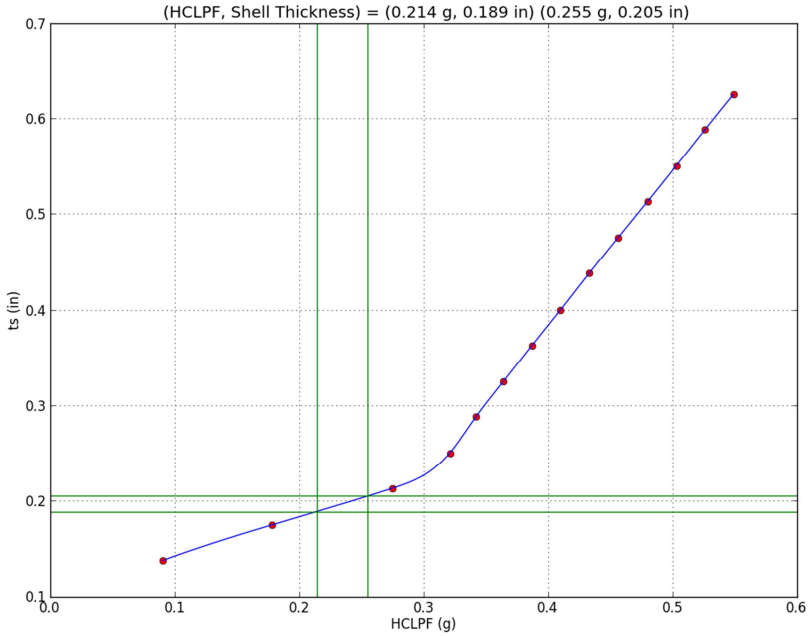

Figure 5-20 DAC_{ts} for $\Delta CDF_{cr} = 10^{-5}$ /Reactor Year

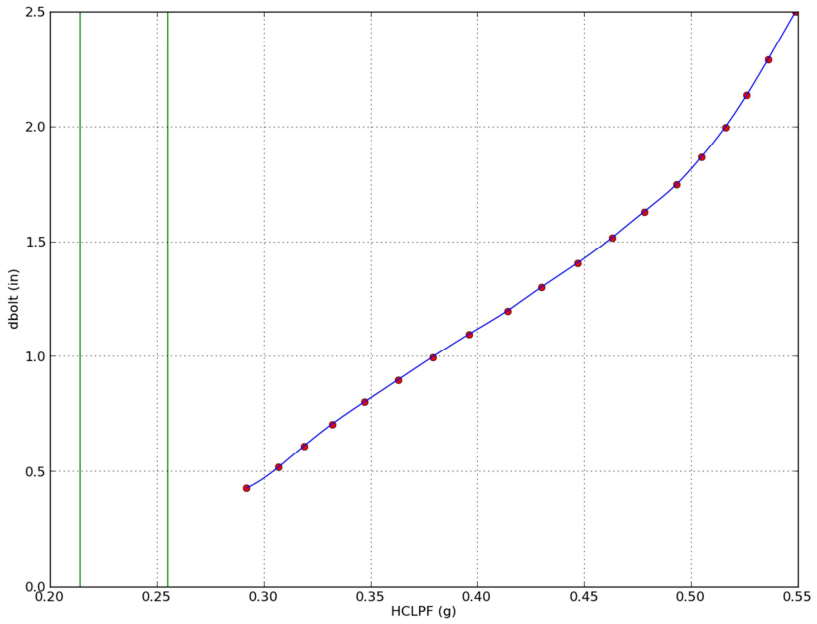

Figure 5-21 Development of DAC_{dbolt} for $\Delta CDF_{cr} = 10^{-5}$ /Reactor Year Exceeding Data Range

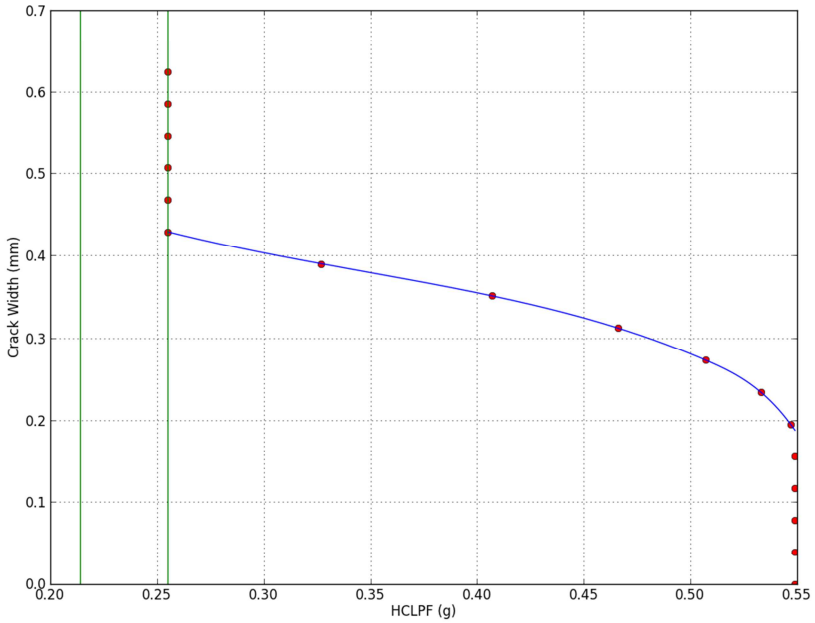

Figure 5-22 Development of DAC_{crack} for $\Delta CDF_{cr} = 10^{-5}$ /Reactor Year Exceeding Data Range

5.5.3 DAC_T for the Perfectly Correlated Degradation Scenarios A, B, and C

For the case of perfectly correlated degradation combination of A, B, and C, the use of $\Delta CDF_{cr} = 10^{-5}$/reactor year yields 51.1 years and 52.2 years, respectively for the case of constant uncertainties and varying uncertainties. The difference between the life predictions (2%) is much smaller than the difference between the DAC_{HCLPF}'s (16%) because the time-HCLPF curve is relatively flat at the points of interpolation as shown in Figure 5-23. It should be pointed out that the life-predictions were achieved using linear interpolations (on the blue line) because the cubic spline (in black) is overly distorted as shown in Figure 5-23. A proper use of cubic spline in this case requires additional data points around the interpolation points, which however is not necessary since liner interpolations are sufficient for the purpose of sensitivity study.

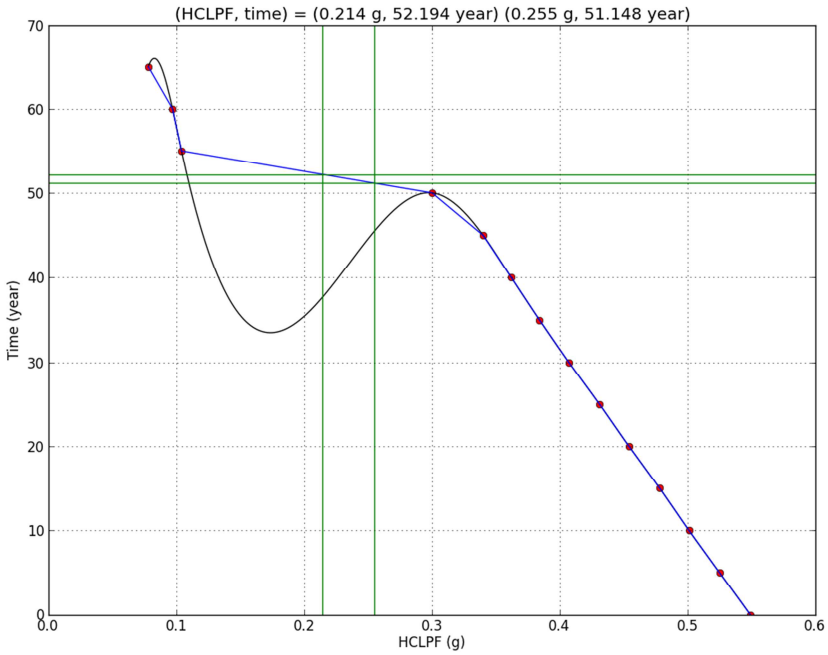

Figure 5-23 $DAC_{T\text{-}Perfect}$ for ΔCDF_{cr} =10^{-5} /Reactor Year

5.5.4 DAC_T for the Non-Perfectly Correlated Degradation Scenarios A, B, and C

For the case of non-perfectly correlated degradation combination of A, B, and C, the time-HCLPF relations from the 11 simulations were interpolated separately using either cubic spline interpolation or linear interpolation if the cubic spline for a simulation data is overly distorted at the interpolation point, as shown in Figure 5-24 through Figure 5-34. Table 5-3 and Table 5-4 show the $DAC_{T\text{-}SIM}$ (in terms of time) estimated from the results of the 11 simulations performed in the Year 4 study. The mean life is estimated to be 48.7 years and 49.9 years for the cases of constant uncertainties and varying uncertainties, respectively, which are close to the case of perfectly correlated degradation combination. The difference in these mean life estimates (2%) are much smaller than that in the DAC_{HCLPF} (16%), as observed similarly in the case of perfectly correlated degradation combination. The standard deviations and COVs associated with these mean life predictions are about 14 years and 28%, respectively, the latter of which is higher than the COV (20.9%) when a risk criterion of ΔCDF_{cr} = 10^{-6}/reactor year was used.

It should be pointed out that the reduced difference in mean life predictions from that in the DAC_{HCLPF}, due to aging-induced uncertainty increase, is only pertinent to the particular case of the CST because the time-HCLPF curves are all very flat at the points of interpolation. Therefore, the importance of the aging-related increase in uncertainties should not be downplayed in general.

In summary, the life prediction assuming only corrosion in the tank shell was estimated to be 56 to 58 years, 51 to 52 years for the case of perfectly correlated degradation combination, and about 49 to 50 years for the case of non-perfectly correlated degradation combination. It

clearly indicates that multiple degradations impact more the expected life span than a single degradation scenario when the higher risk criterion of $\Delta CDF_{cr} = 10^{-5}$/reactor year is used, as compared to the stricter risk criterion of $\Delta CDF_{cr} = 10^{-6}$/reactor year where the corrosion in the tank shell dominates the life prediction. This is because the higher risk criterion leads to a region dominated by the overturning moment failure mode, where all degradations contribute to the deterioration of the HCLPF capacity, as discovered in Section 3.

Table 5-3 $DAC_{T\text{-}SIM}$ for Constant Uncertainties (DAC_{HCLPF}=0.255 g)

Simulation ID	$DAC_{T\text{-}SIM}$ (years)	ts (in)	dbolt (in)	Crack (mm)
Sim 1	64.182	0.196	2.401	0.359
Sim 2	45.658	0.328	2.372	0.402
Sim 3	32.404	0.355	2.391	0.385
Sim 4	60.061	0.195	2.387	0.314
Sim 5	34.000	0.354	2.334	0.397
Sim 6	34.868	0.208	2.386	0.324
Sim 7	72.239	0.231	2.359	0.389
Sim 8	56.090	0.207	2.350	0.357
Sim 9	44.221	0.209	2.403	0.342
Sim 10	54.949	0.304	2.393	0.397
Sim 11	37.047	0.339	2.414	0.397
mean	48.702	0.266	2.381	0.369
Sample Std	13.618	0.069	0.025	0.032
Cov	0.280	0.259	0.010	0.086

Table 5-4 $DAC_{T\text{-}SIM}$ for Varying Uncertainties (DAC_{HCLPF}=0.214 g)

Simulation ID	$DAC_{T\text{-}SIM}$ (years)	ts (in)	dbolt (in)	Crack (mm)
Sim 1	65.000	0.190	2.400	0.364
Sim 2	47.007	0.320	2.369	0.414
Sim 3	33.277	0.348	2.389	0.396
Sim 4	60.188	0.194	2.387	0.315
Sim 5	34.279	0.352	2.332	0.400
Sim 6	36.345	0.190	2.382	0.338
Sim 7	73.769	0.223	2.357	0.397
Sim 8	58.281	0.190	2.345	0.371
Sim 9	46.261	0.190	2.399	0.358
Sim 10	56.449	0.295	2.390	0.408
Sim 11	38.000	0.332	2.412	0.408
mean	49.896	0.257	2.378	0.379
Sample Std	13.726	0.072	0.025	0.032
Cov	0.275	0.279	0.010	0.085

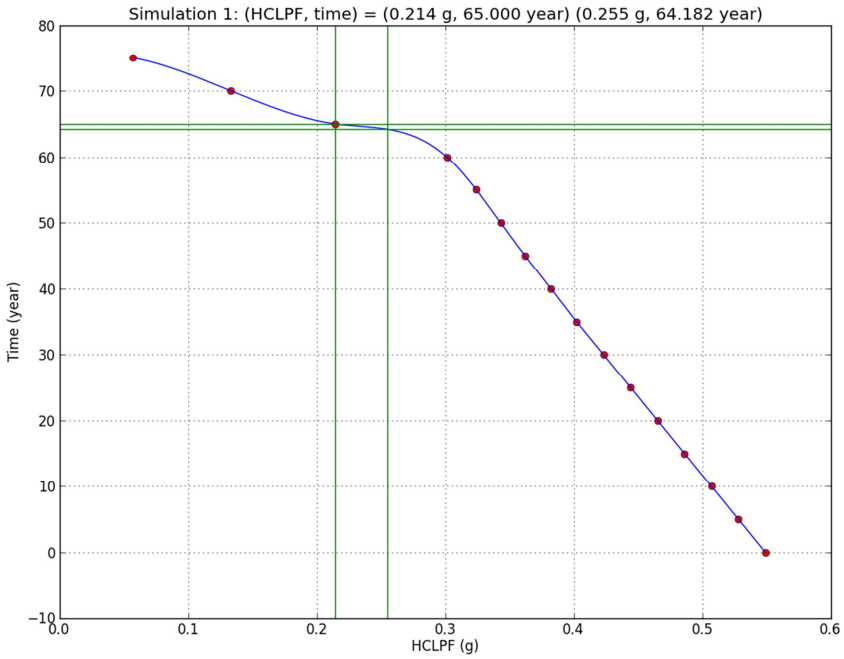

Figure 5-24 $DAC_{T\text{-}Sim1}$ for Sample One for $\Delta CDF_{cr}=10^{-5}$ /Reactor Year

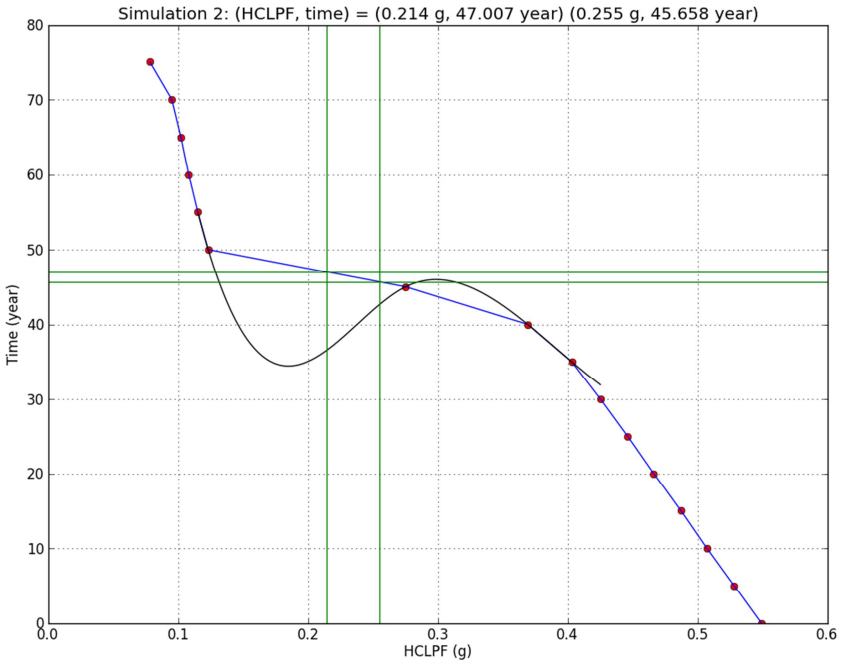

Figure 5-25 $DAC_{T\text{-}Sim2}$ for Sample One for $\Delta CDF_{cr}=10^{-5}$ /Reactor Year

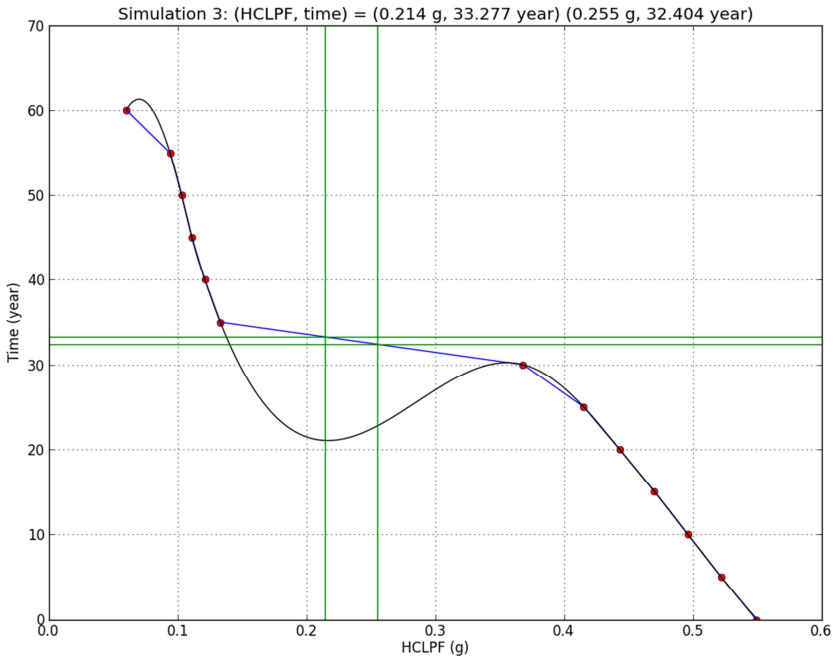

Figure 5-26 $DAC_{T\text{-}Sim3}$ for Sample One for $\Delta CDF_{cr}=10^{-5}$ /Reactor Year

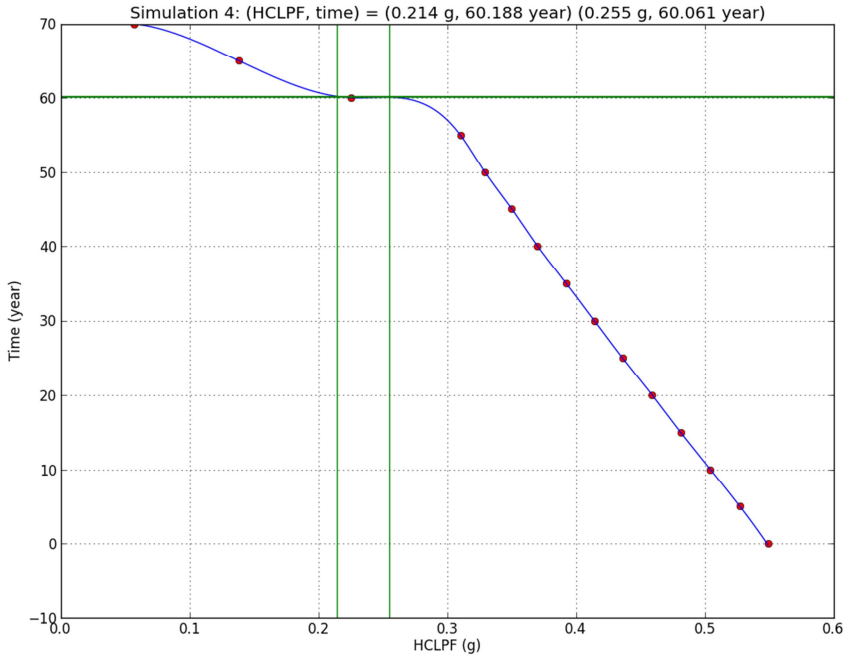

Figure 5-27 $DAC_{T\text{-}Sim4}$ for Sample One for $\Delta CDF_{cr}=10^{-5}$ /Reactor Year

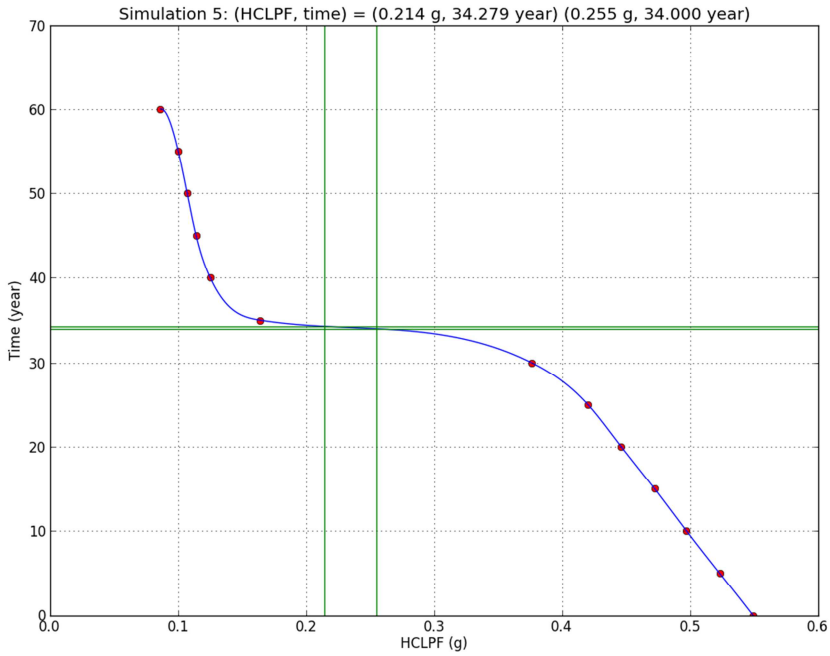

Figure 5-28 $DAC_{T\text{-}Sim5}$ for Sample One for $\Delta CDF_{cr}=10^{-5}$ /Reactor Year

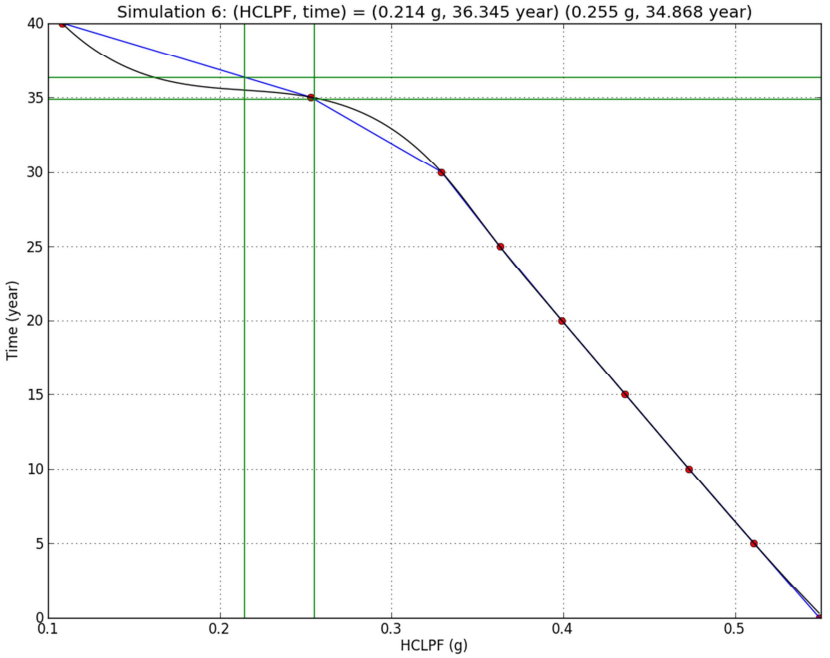

Figure 5-29 $DAC_{T\text{-}Sim6}$ for Sample One for $\Delta CDF_{cr}=10^{-5}$ /Reactor Year

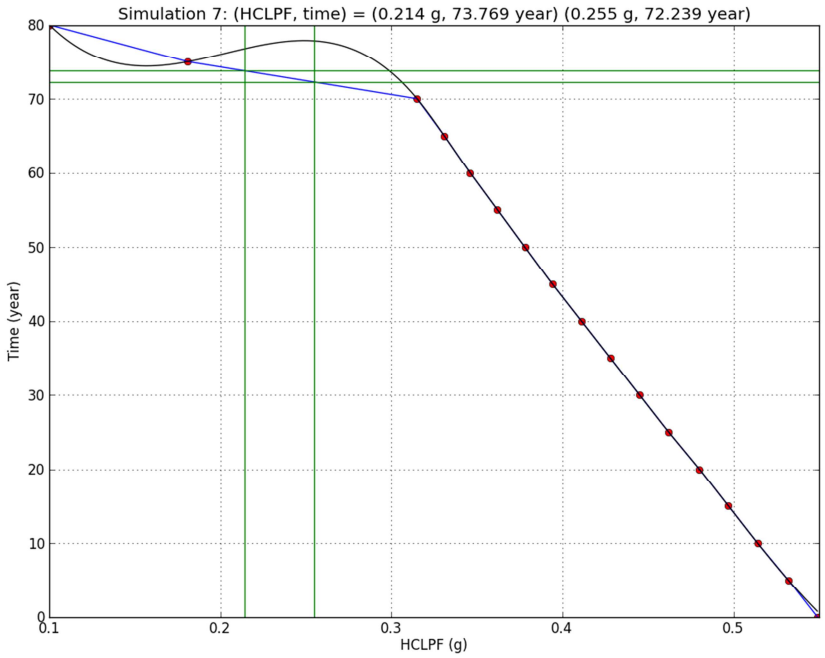

Figure 5-30 $DAC_{T\text{-}Sim7}$ for Sample One for $\Delta CDF_{cr}=10^{-5}$ /Reactor Year

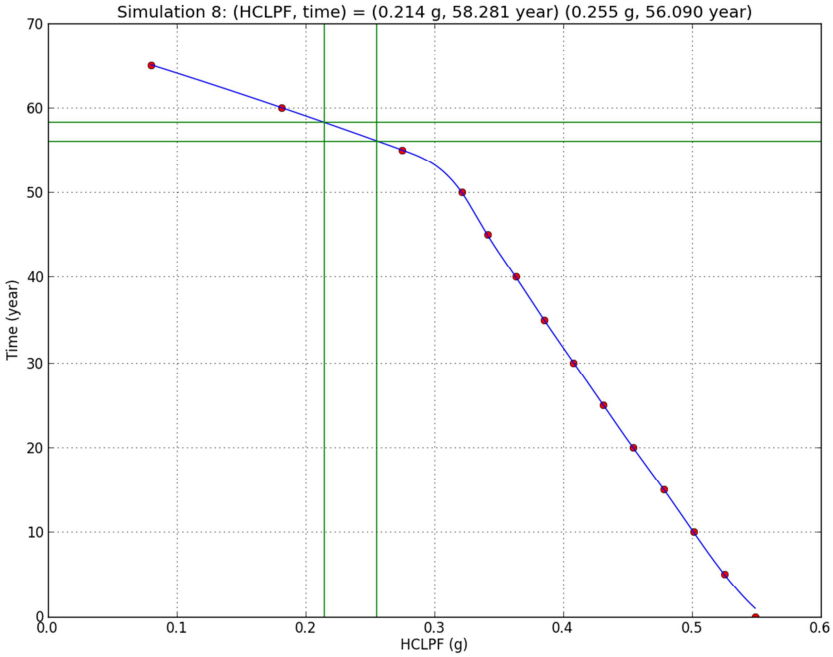

Figure 5-31 $DAC_{T\text{-}Sim8}$ for Sample One for $\Delta CDF_{cr}=10^{-5}$ /Reactor Year

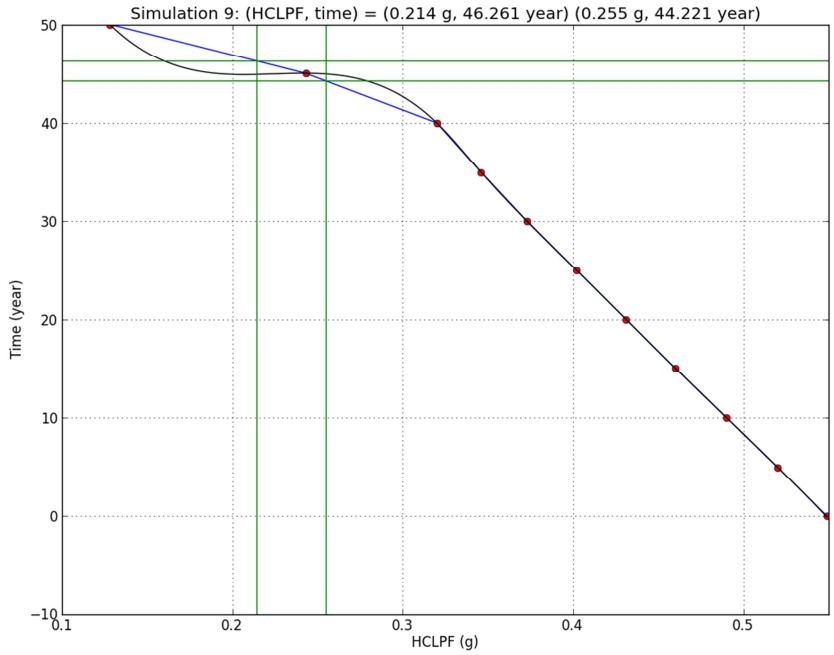

Figure 5-32 $DAC_{T\text{-}Sim9}$ for Sample One for $\Delta CDF_{cr}=10^{-5}$ /Reactor Year

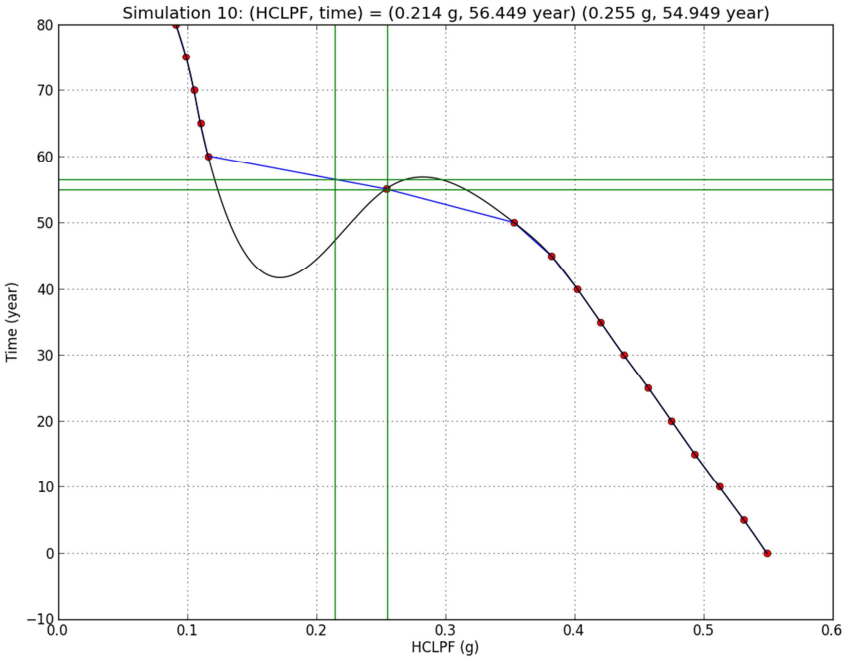

Figure 5-33 $DAC_{T\text{-}Sim10}$ for Sample One for $\Delta CDF_{cr}=10^{-5}$ /Reactor Year

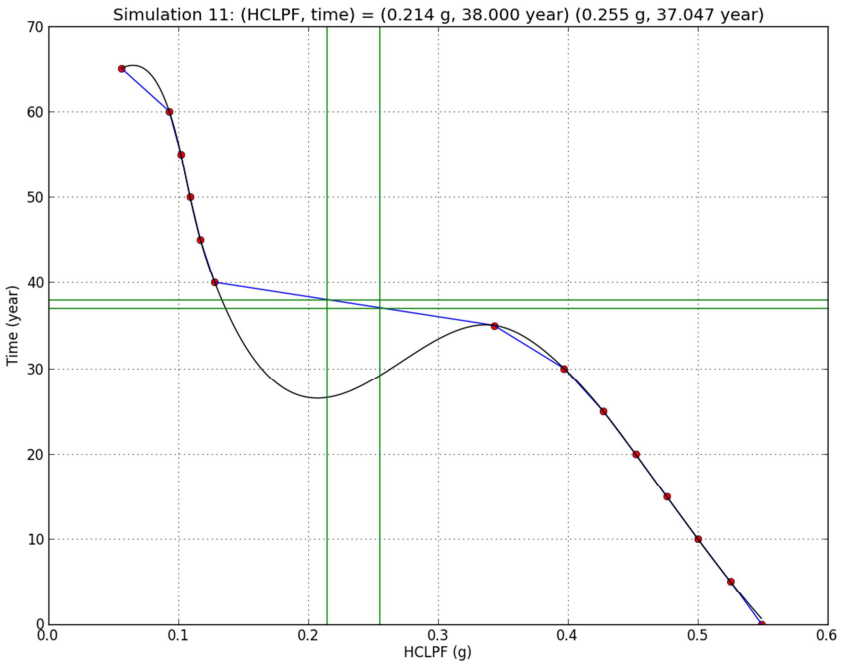

Figure 5-34 $DAC_{T\text{-}Sim11}$ for Sample One for $\Delta CDF_{cr}=10^{-5}$ /Reactor Year

5.6 Summary of the Three-Tier DAC

The relationship between the three-tier DAC and the ΔCDF_{cr} for the CST at the Ulchin NPP is summarized in Figure 5-35. The risk criterion $\Delta CDF_{cr} = 10^{-6}$/reactor year is categorized in this figure as Tier 0, which is the foundation for defining various DAC for any component in an NPP, such as a CST or a diesel generator. In general, more information is required to develop higher tier DAC.

The Tier 1 DAC_{HCLPF} (in terms of HCLPF) can then be determined for a subject component, for example the CST in this report, through a sufficiently detailed PRA analysis following the guidelines described in Section 2. DAC_{HCLPF} is independent of any particular degradation scenario(s) in the subject component and is a function of the ΔCDF_{cr} and the role of the component in the plant logic. Therefore, DAC_{HCLPF} can be viewed as a surrogate to the ΔCDF_{cr} in developing other DAC in terms of either levels of degradation or time (life prediction). For the CST, DAC_{HCLPF} was determined to be 0.422 g. As shown in Figure 3-25, a DAC_{HCLPF} = 0.422 g corresponds to a region where the sliding failure mode dominates.

The Tier 2 DAC_D (in terms of degradation level) can be developed for a component if a specific or a dominating degradation scenario is identified for that component. For the case of the CST, three individual degradation scenarios were assumed: (A) corrosion in tank shell, (B) corrosion in anchor bolts, and (C) cracking of the reinforced concrete foundation. The corresponding DAC_D's are shown below:

DAC_{ts} = 0.420 in. (1/3 corrosion allowance),

DAC_{dbolt} = 1.248 in. (half of the anchor bolt diameter or ¾ loss of the cross section),

DAC_{crack} = 0.342 mm.

It should be pointed out that DAC_D cannot by themselves be properly defined for the case of multiple co-existing degradation scenarios.

The Tier 3 DAC_T (in terms of time or life prediction) can be defined for a single degradation scenario or multiple co-existing degradation scenarios. However, the development of DAC_T requires reliable time-dependent degradation models that represent well the real degradation situation of the subject component.

Based on the degradation models assumed in Equations 5-1 through 5-3, the DAC_T can be determined for the three individual degradation scenarios A, B, and C based on the corresponding Tier 2 DAC_D:

$DAC_{T\text{-}ts}$ = 27.1 years,

$DAC_{T\text{-}dbolt}$ = 950.6 years,

$DAC_{T\text{-}crack}$ = 43.8 years.

Both the $DAC_{T\text{-}ts}$ and $DAC_{T\text{-}crack}$ appear to be reasonable values as compared to the typical initial licensing period of an NPP. It can be seen that corrosion in tank shell is more important than the other two, provided that the assumed degradation models are accurate. As for the anchor bolts, another factor in contributing to the extremely long life prediction is that there are a large number of the anchor bolts (78).

For the case of perfectly correlated degradation scenarios A, B, and C, $DAC_{T\text{-}Perfect}$ was determined directly from the DAC_{HCLPF} for the CST and it is estimated to be 26.9 years. $DAC_{T\text{-}Perfect}$ is very close to $DAC_{T\text{-}ts}$, suggesting that corrosion in the tank shell dominates the deterioration behavior of the HCLPF as compared to corrosion in anchor bolts and cracking in the reinforced concrete foundation.

For the case of non-perfectly correlated degradation scenarios A, B, and C, $DAC_{T\text{-}sim}$ was determined to be 27.3 years, which is the mean life prediction based on the results of the 11 simulations performed in the Year 4 study. $DAC_{T\text{-}sim}$ is very close to both $DAC_{T\text{-}Perfect}$ and $DAC_{T\text{-}ts}$. The COV of $DAC_{T\text{-}sim}$ is about 21%.

The difference in the assumptions of degradation-related uncertainty change, i.e., whether the uncertainties should be varied (increased) as previously observed regarding their dependency on degradation, has a minimal effect on the various DAC because of the choice of the strict risk criterion $\Delta CDF_{cr} = 10^{-6}$/reactor year.

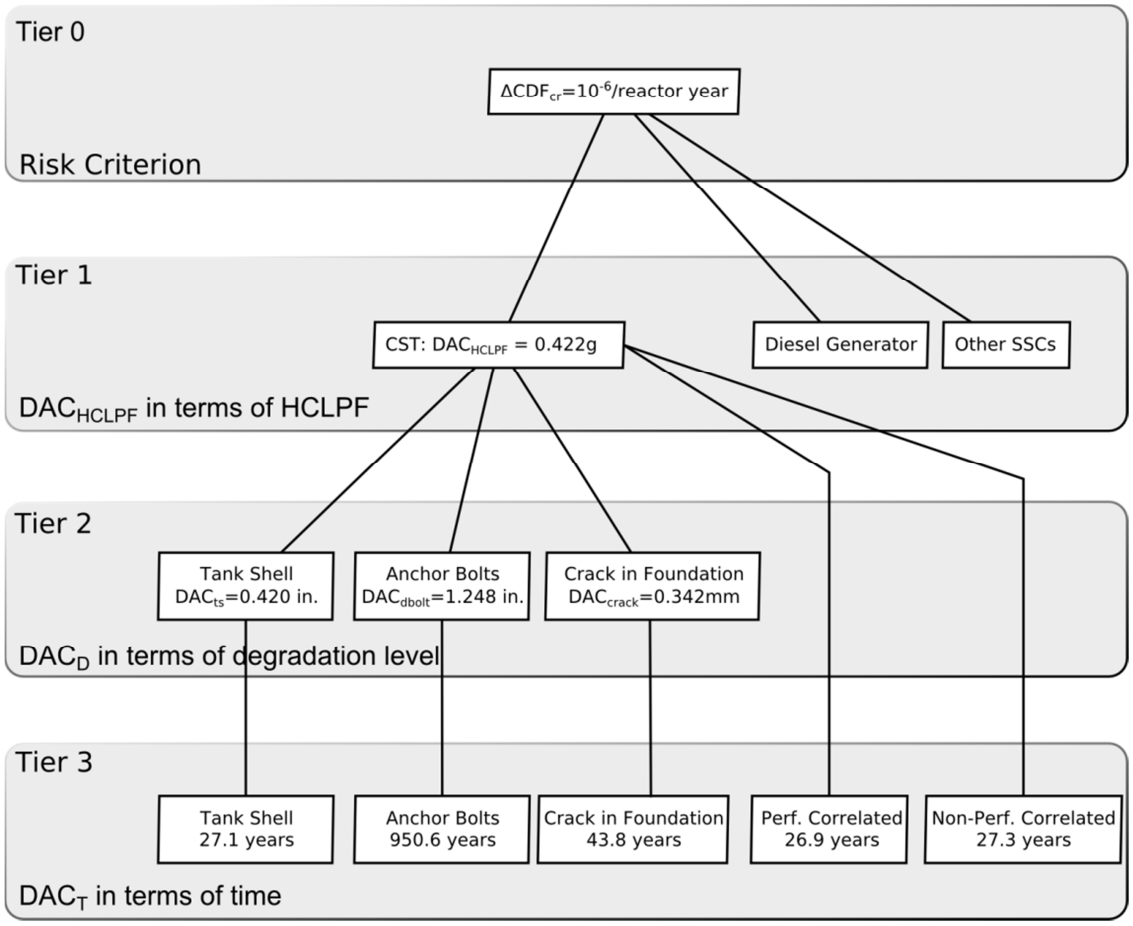

Figure 5-35 Summary of Degradation Acceptance Criteria

6 GUIDELINES ON THE APPLICATION OF VARIOUS DAC TO INSPECTION/ MAINTENANCE PLANNING

The purpose of separating the degradation acceptance criteria (DAC) into three tiers is to maximize their use in optimizing inspection/maintenance planning and minimizing the associated cost throughout the life span of the NPPs. The current practice in the inspection and maintenance programs implemented in NPPs is to follow industry standards and codes and regulation rules, including:

- 10 CFR 50.65, "Requirements for Monitoring the Effectiveness of Maintenance at Nuclear Power Plants"
- NRC Inspection Procedure 62706, "Maintenance Rule"
- NRC Inspection Procedure 62002, "Inspection of Structures, Passive Components, and Civil Features at Nuclear Power Plants"
- 10 CFR Part 54, "Requirements for Renewal of Operating Licenses for Nuclear Power Plants"
- SRP-LR (NUREG-1800), "Standard Review Plan for Review of License Renewal Applications for Nuclear Power Plants"
- NUREG 1801, "Generic Aging Lessons Learned (GALL)"
- NUMARC 93-01, "Industry Guideline for Monitoring the Effectiveness of Maintenance at Nuclear Power Plants"
- NEI 95-10, "Industry Guideline for Implementing the Requirements of 10 CFR Part 54 – The License Renewal Rule"

However, these requirements and guidelines have mostly been developed based on experience and in a deterministic manner, and have seldom been rigorously substantiated by explicit and thorough analysis of their risk significance. As an example for risk-informed inspection/ maintenance planning, this section provides guidelines on how to apply the various DAC developed for the CST in this report to the inspection/maintenance planning.

As indicated in Section 5.6, the development of higher tier DAC requires more information regarding the degradation condition, so does the application of higher tier DAC. A plant at different stages may require different DAC based on the available information at the moment of analysis. For a newly constructed nuclear power plant, there is not much plant-specific degradation data available for the development of DAC and consequently generic data and degradation models have to be used to provide a general and conservative schedule of inspection of various safety-significant components. As a plant gets older, more experience data become available through inspections and these data can be used to assess the imminent safety implication of an observed degradation and benchmark/develop degradation models for remaining life prediction. Therefore, the application of the various DAC should be strategized base on the availability of degradation information.

6.1 General Guidelines

First of all, since the basis for the various DAC so developed in this report according to the NRC RG 1.174, Rev. 2 is the core damage frequency (CDF) of the plant as a function of the degradation condition of the CST, the quality of the probabilistic risk assessment (PRA) or probabilistic safety assessment (PSA) should be full-scope, with sufficient level of detail, technically adequate, and representing well the as-built, as-operated, and as-degraded plant, as stated in Section 2. It is especially important to ensure that the PRA represents the as-degraded condition of a plant. Multiple co-existing degraded components in an NPP could significantly change its baseline CDF or LERF so that a different ΔCDF_{cr} may be needed or even immediate action must be taken if the baseline CDF or LERF does not satisfy any more the NRC risk goal. However, the current practice of PRA may not have sufficient emphasis on representing the degradation status of the plants; therefore, proper consideration of multiple degraded components in a plant remains to be a future exploration. Throughout this report, the CST is assumed to be the only component with safety-significant degradation(s) in the Ulchin NPP of Korea.

It should be reiterated that the guidelines on the use of the DAC for the CST are applicable only to the Ulchin NPP where the CST is located and which KAERI's PRA was based on. It should also be emphasized that any conclusions made in terms of time (life prediction) are only for reference because the assumed material degradation models and combination methods have not been benchmarked using real data measured at the Ulchin NPP. Any inference beyond these assumptions should be discouraged or requires case-specific scrutiny for its suitability.

The age-related degradations considered for the CST were found to have a large impact on the uncertainties in the HCLPF capacity, which led to the consideration of two cases: constant uncertainties and varying uncertainties, in the development of DAC in this report. However, because the identified risk criterion $\Delta CDF_{cr} = 10^{-6}$/reactor year is relatively strict, the impact of the constant and varying uncertainties on the final DAC for the CST was found to be negligible. In addition, for the CST in the Ulchin NPP, the use of constant uncertainties in the PRA was shown to be conservative compared to the use of varying uncertainties. However, extension of this observation to other components and other NPPs requires additional investigation.

Without further complication of the discussion, the following demonstrative application of DAC to inspection planning assumes any recommended scheduling will be adjusted somewhat to accommodate other physical requirements, such as permission of in-service inspection and refueling scheduling.

Although the following discussion is specific to the CST in the Ulchin NPP, the general procedure proposed and demonstrated in this report is applicable to other components and other NPPs.

6.2 Initial Planning for Newly Constructed NPPs

Based on the $DAC_{T\text{-}ts}$, $DAC_{T\text{-}dbolt}$, $DAC_{T\text{-}crack}$, $DAC_{T\text{-}Perfect}$, and $DAC_{T\text{-}sim}$ as shown in Figure 5-35, the minimum life prediction is about 27 years, determined using the assumed degradation models as summarized in Section 5.1. This estimate appears to be in a general agreement with the initial licensing period of 40 years for the U.S. NPPs. With the assumed statistical parameters for the case of non-perfectly correlated degradation scenarios, the resultant coefficient of variation

(COV) in $DAC_{T\text{-}sim}$ was found to be 20.9%. However, the actual uncertainty in the minimum life prediction should be higher, potentially to a large degree because of many uncertain factors, including: (1) the basic material degradation models may not have high fidelity to the actual operational environment, (2) there may be additional degradation scenarios in the CST during operation, (3) the statistical parameters for the non-perfectly correlated degradation scenarios may be not represent well the reality, and (4) the conservative deterministic failure margin (CDFM) method [Kennedy et al., 1989] for calculation of the HCLPF capacity is an approximate method. Therefore, to conservatively compensate these largely unknown uncertainties in the DAC_T's, a period of 10 years is recommended as the initial inspection interval for the CST in the Ulchin NPP, with an apparent overall conservative factor of 2.7. This recommendation may be well consistent with some current practice based on industry standards and regulation rules.

However, this recommendation should not be viewed as a stopper to the exercise of common judgment during the operation. For example, since the CST is a large component constructed without other shielding structures, any sign of significant degradation in the CST might be detected visually and the degradation should be investigated even though it is before the first planned formal inspection.

This recommendation should be enveloped by other guidelines as prescribed in the current industry standards and regulation rules, to maintain the required conservativeness in those documents. However, as more data become available during later inspections to support or revise the recommendation, it may become unnecessary to strictly follow those guidelines in the industry standards and regulation rules if such an action can be technically justified.

For a newly constructed NPP, it is recommended to develop DAC for those risk-significant components and establish their individual inspection schedules. The schedules of individual components can be grouped into several well separated time periods for management convenience, or can be adjusted to optimize the inspection cost.

6.3 Risk Assessment and Planning With Data from Inspections

Data from inspections are valuable to assess the safety significance of any observed degradations, benchmark and update the material degradation models, and make better future inspection planning based on updated models. The following subsections discuss the application scenarios based on whether degradation is observed and the number and/or location of the observed degradations.

6.3.1 No Significant Degradation

If no degradation in the CST can be identified as significant, the recommended initial interval can be increased, for instance to 15 years, which is about half of the original predicted life. It is understandable that the significance of a degradation case is difficult to be determined without checking the risk consequence, but in general if a degradation case is only a small fraction of the DAC_D or very small in the sense of measurement, this degradation case can be viewed as insignificant.

Although it is often difficult in practice to lift the requirement of being enveloped by the industry standards and regulation rules without updating these documents, many of them allow

alternative approaches as long as they can be technically justified. For this case of no observed significant degradations at an inspection, the DAC developed in this report can be used as a technical justification for accepting the new inspection interval, provided that existing regulations, codes, and standards do not preclude this from being done.

6.3.2 Single Degradation Scenarios

If only one of the three individual degradation scenarios is determined to have a significant level of degradation during an inspection, the corresponding DAC_D can be used to assess the risk significance of the observed degradation level and make adjustment to the inspection interval based on an updated life prediction.

For example, an observed loss of wall thickness of 0.1 in. may be claimed not to be a significant risk concern because it is less than the critical loss of wall thickness of 0.205 in. To update the inspection interval, the degradation rate can be updated or a new degradation model can be defined if enough data are available. If this level of degradation was observed at the first inspection (10 years after construction), the rate would be higher than the assumed rate (7.494×10^{-3} in./year) in Equation 5-1, and the next inspection is recommended in 5 years (with a conservative factor approximately 2). On the other hand, if this level of degradation was observed at the second inspections (20 years), the average rate is less than the assumed rate. Since there are two data points, a new degradation model can be developed to predict the remaining life before the next inspection. It is important to include a conservative factor of at least 2 to cover uncertainties.

If the loss of wall thickness exceeds 0.205 in., the increase of the CDF exceeds the $\Delta CDF_{cr} = 10^{-6}$/ reactor year and the CST should be repaired promptly. The urgency of the repair depends on the extent of the loss of wall thickness, but the margin is sufficiently large when considering the corrosion allowance of 0.420 in. to reach a ΔCDF of 10^{-5}/reactor year.

6.3.3 Multiple Degradation Scenarios

It is usually not obvious whether observed levels of degradation at three locations represent a risk concern if none of them appears to be absolutely dominant. Since the description of DAC in terms of multiple degradation scenarios is difficult, one generally must compute the HCLPF capacity considering the observed levels of degradation in the CST and compare that to DAC_{HCLPF} = 0.422 g to determine the risk significance. Degradation models can be updated using the observed data and a new life prediction can be calculated based on DAC_{HLCPF} and the updated degradation models.

As a simplified alternative to the actual calculation of HCLPF, one could use the simulation results in the Year 4 research to generate a 3D table that maps the degradation levels to the estimated HCLPF capacity for the CST, i.e., (ts, dbolt, crack with) → HCLPF, and use the closest point in the 3D space (ts, dbolt, crack with) to determine an approximate HCLPF. Another improvement is to use 3D liner interpolation in place of search of closest match. It should be pointed out that the 11 simulations generated a relatively large number of data points which constitute a good coverage of the data range. The perfectly correlated degradation case can be used as additional data points in this method.

6.3.4 Other Degradations

Although the three basic degradation scenarios were identified to be the most likely ones, there is a possibility that degradations occur at other locations. In that case, one has to utilize the lowest level DAC, which is DAC_{HCLPF}, to assess the imminent risk implication of the observed degradations and make proper life predictions to establish a new inspection interval. As stated previously, DAC_{HCLPF} is independent of the actual degradation situation. Fortunately, a PRA is not needed because DAC_{HCLPF} is the surrogate to the ΔCDF_{cr}, which solely defines the acceptable risk increase as long as the baseline CDF has not dramatically changed.

7 CONCLUSIONS AND RECOMMENDATIONS

7.1 Summary and Conclusions

This report presents the research results of the last task in the 5-year BNL-KAERI collaboration program, the goal of which is to develop a realistic seismic risk evaluation system which includes the consideration of aging of structures and components in nuclear power plants (NPPs). The previous four tasks of the collaboration program have each contributed to the later tasks by providing necessary information, insights, data, and models. In particular, the last three tasks, Year 3 through Year 5, constitute a coherent methodology to assess the seismic risk of a degraded component in an NPP through the evaluation of the seismic fragility of the component under undegraded and various degraded conditions and the development of degradation acceptance criteria (DAC) for the component. A condensate storage tank (CST) located at the Ulchin NPP of Korea was selected to demonstrate the methodology. This report covers the development of a general procedure for the risk-based DAC development, probabilistic safety analyses to obtain the core damage frequencies for a series of fragility capacities, development of DAC for the CST, and guidelines on the application of the various DAC in inspection/maintenance planning. This report also includes an extended summary of the seismic fragility analyses performed as part of the Year 3 and Year 4 tasks to complete the entire picture of the seismic risk evaluation methodology, as well as to support the DAC development in the rest of the report.

U.S. NRC Regulatory Guide (RG) 1.174, Rev. 2, "An Approach for Using Probabilistic Risk-Informed Decisions on Plant-Specific Changes to the Licensing Basis," was used to develop the acceptable level of risk increase due to age-related degradation of structures and passive components (SPCs). Age-related degradation of an SPC in a nuclear power plant (NPP) can be viewed as a permanent modification to a plant and could be viewed as a change to the licensing basis of the NPP if the degradation level is significant. Based on this NRC guidance, acceptable risk criteria $\Delta CDF_{cr} = 10^{-6}$/reactor year and $\Delta LERF_{cr} = 10^{-7}$/reactor year were determined in this study for use in the development of DAC for SPCs. If the total CDF < 10^{-4}/reactor year and LERF < 10^{-5} / reactor year, NRC RG 1.174 also allows the use of risk criteria of $\Delta CDF_{cr} = 10^{-5}$/reactor year and $\Delta LERF_{cr} = 10^{-6}$/reactor year. However, the quality of the PRA in the calculation of the total CDF and LERF would have to be full-scope; with sufficient level of detail; technically adequate; and representing well the as-built, as-operated, and as-degraded plant. In this study, only ΔCDF_{cr} was used for simplicity, partly because of the unavailability of a Level-2 PRA for the LERF calculation. RG 1.174 also recognizes that there may not be a Level-2 PRA for some plants.

A fundamental procedure for the development of the DAC for an SPC was developed considering a common practical situation where the fragility analysis and the PRA are performed separately and normally by different groups of people. This procedure includes three major steps which are largely decoupled:

(1) Develop a range of the fragility values of the subject SPC that various levels of degradation can potentially result in,

(2) Perform PRAs of the plant using these fragility values to obtain a range of corresponding CDFs,

(3) Interpolate the fragility-CDF curve using the $\Delta CDF_{cr} = 10^{-6}$/reactor year to determine a critical fragility capacity F_{cr}.

A generic system of DAC in three-tiers was proposed in this procedure to best use available information of the subject SPC, consisting of: (Tier 1) DAC_F in terms of the fragility capacity, (Tier 2) DAC_D in terms of the level of degradation, and (Tier 3) DAC_T in terms of time. The purpose of separating the degradation acceptance criteria (DAC) into three tiers is to maximize their use in optimizing inspection/maintenance planning and minimizing the associated cost throughout the life span of the NPPs. DAC_F can be viewed as a surrogate to ΔCDF_{cr} for the subject SPC. DAC_D is especially useful when a specific level of degradation is observed during an inspection and the inspector wants to assess how the observed level of degradation impacts the seismic CDF. One disadvantage in using DAC_D is that multiple degradation scenarios in an SPC are difficult to be described. DAC_T can be developed from DAC_F or DAC_D when there are reliable time-dependent degradation models for an SPC. DAC_T allows a proper treatment of multiple co-existing degradation scenarios in the subject SPC. It should be noted that time-dependent degradation models are rare and difficult to be developed for a particular SPC, as discovered previously in this collaboration program.

A range of HCLPF values and the associated uncertainties were developed based on the Year 4 results, which were calculated using the operational water level. Two series of HCLPF values were developed in this study to consider different treatments of the uncertainties. The first series assumes that the uncertainties β_R and β_U are invariant with the magnitude of the median fragility, i.e., independent of degradation level and time. For the second series, the epistemic uncertainty is assumed to vary based on the findings in the Year 4 research when more realistic correlations were considered.

KAERI performed the PRA of the Ulchin NPP units 5 & 6, where the CST is located, for the two cases of uncertainty assumptions. The scope included internal and external PRAs. Except for the degradation of the CST, the PRA model did not include the degradation of other structures, systems, and components (SSCs). The total CDF was defined as the summation of the CDFs induced by internal events and external events such as earthquakes, fire, and flood. To facilitate the seismic PRA, many structures and components that have a HCLPF capacity larger than 0.65 g were screened out and 18 seismic risk significant components remained in the seismic PRA model. As a comparison, the HCLPF capacity for the CST under undegraded condition was found to be 0.549 g using the operational water level and 0.426 g using the design water level, the former of which was used for the DAC development. The total baseline CDF was calculated to be 1.395×10^{-5} /reactor year, including 6.00×10^{-6} due to seismic events, 5.65×10^{-6} due to internal events, and 2.30×10^{-6} due to fire. The baseline CDF is about a magnitude smaller than the NRC safety goal (CDF = 10^{-4} /reactor year).

The relations between the CDF/ΔCDF and the HCLPF capacity are very smooth, regardless of whether constant uncertainties or varying uncertainties have been assumed. Overall, the use of constant uncertainties leads to larger CDF/ΔCDF than using the varying uncertainties, with the level of difference increasing to a factor of somewhat greater than two. However, in the range close to $\Delta CDF_{cr} = 10^{-6}$/reactor year, the difference is minimal. In another words, the use of constant uncertainties or varying uncertainties does not significantly affect the development of DAC for the CST based on a $\Delta CDF_{cr} = 10^{-6}$/reactor year.

For the fragility analyses of the CST and the development of DAC for the CST, three basic degradation scenarios were considered: (A) degraded stainless tank shell, (B) degraded anchor bolts, and (C) cracked reinforced concrete foundation. Two cases of degradation combinations were considered as well: (D) a perfect correlation of the degradation scenarios A, B, and C; and (E) a non-perfect correlation of these degradation scenarios.

A whole system of three-tier DAC were determined using cubic spline interpolations, as shown in the following figure (reproduction of Figure 5-35):

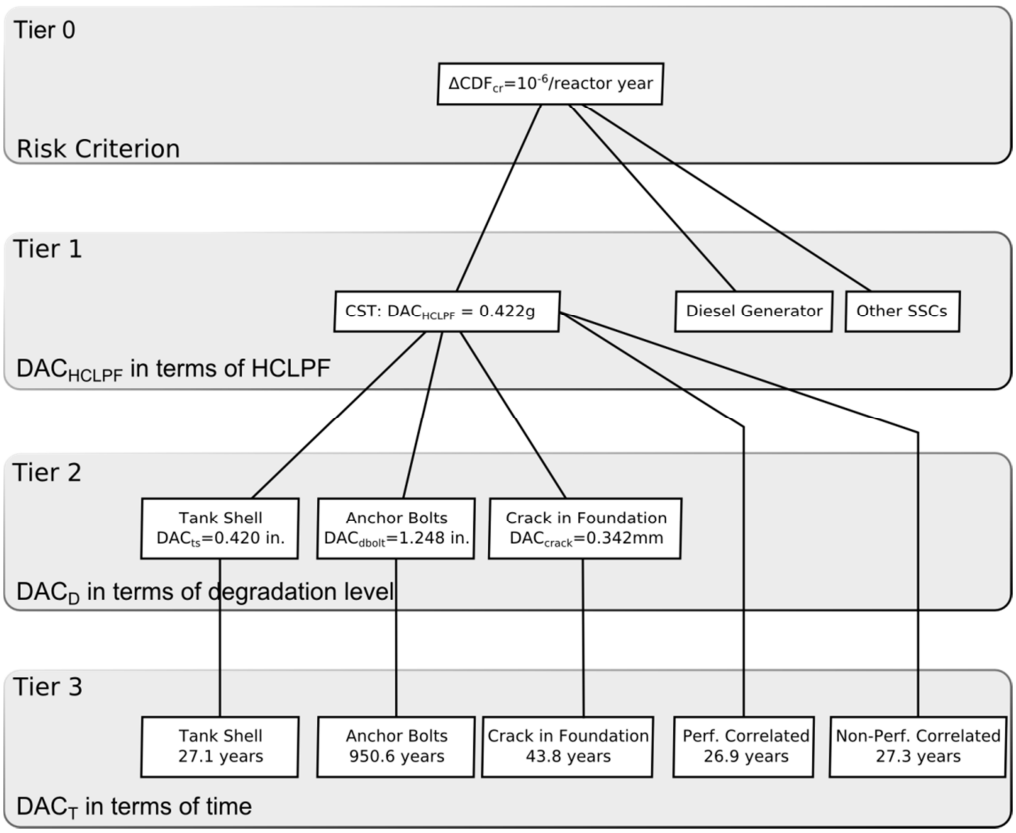

Tier 0 refers to the risk criterion $\Delta CDF_{cr} = 10^{-6}$/reactor year, the foundation for defining various DAC for any component in an NPP. In general, higher tier DAC require more information.

The Tier 1 DAC_{HCLPF} (in terms of HCLPF) for the CST was determined to be 0.422 g. DAC_{HCLPF} is independent of any particular degradation scenario(s) and is a function of the ΔCDF_{cr} and the role of the component in the plant logic. Therefore, DAC_{HCLPF} can be viewed as a surrogate to the ΔCDF_{cr} in developing other DAC for the CST. A DAC_{HCLPF} = 0.422 g corresponds to a region where the sliding failure mode dominates.

The Tier 2 DAC_D (in terms of degradation level) developed for the CST are shown below:

DAC_{ts} = 0.420 in. (1/3 corrosion allowance of tank shell),
DAC_{dbolt} = 1.248 in. (half of the anchor bolt diameter or ¾ loss of the cross section),
DAC_{crack} = 0.342 mm (cracking in reinforced concrete foundation).

The Tier 3 DAC_T (in terms of time or life prediction) can be defined for a single degradation scenario or multiple co-existing degradation scenarios, provided that reliable time-dependent degradation models are available to represent well the real degradation situation of the subject component. For the three individual degradation scenarios A, B, and C assumed for the CST, the Tier 2 DAC_D were determined as:

$DAC_{T\text{-}ts}$ = 27.1 years,
$DAC_{T\text{-}dbolt}$ = 950.6 years,
$DAC_{T\text{-}crack}$ = 43.8 years.

Both the $DAC_{T\text{-}ts}$ and $DAC_{T\text{-}crack}$ appear to be reasonable values as compared to the typical initial operating period of an NPP. It can be seen that corrosion in the tank shell is more important than the other two degradations, provided that the assumed degradation models are accurate. As for the anchor bolts, another factor in contributing to the extremely long life prediction is that there are a large number of the anchor bolts (78).

For the case of perfectly correlated degradation scenarios A, B, and C, $DAC_{T\text{-}Perfect}$ was determined directly from the DAC_{HCLPF} for the CST and it is estimated to be 26.9 years. For the case of non-perfectly correlated degradation scenarios A, B, and C, $DAC_{T\text{-}sim}$ was determined to be 27.3 years, which is the mean life prediction based on the results of the 11 simulations performed in the Year 4 study. Both $DAC_{T\text{-}Perfect}$ and $DAC_{T\text{-}sim}$ are very close to $DAC_{T\text{-}ts}$, suggesting that corrosion in the tank shell dominates the deterioration behavior of the HCLPF as compared to corrosion in the anchor bolts and cracking in the reinforced concrete foundation.

A sensitivity analysis was performed using a higher risk criterion of $\Delta CDF_{cr} = 10^{-5}$/reactor year to assess its impact on the various DAC. For the particular case of the subject CST, NRC RG 1.174 also allows a higher ΔCDF_{cr}, which can be used for the development of DAC because the total CDF is less than 10^{-4}/reactor year. It should be pointed out that such a level of ΔCDF_{cr} is about the same level of the baseline CDF, implying that multiple degraded components with a similar risk increase allowance could result in significantly increased CDF exceeding the NRC risk goal of CDF=10^{-4}/reactor year. Therefore, the use of $\Delta CDF_{cr} = 10^{-5}$/reactor year in this section is purely for sensitivity assessment.

From this sensitivity analysis, DAC_{HCLPF} was estimated to be 0.255 g for the case of constant uncertainties, which is about 60% of that based on $\Delta CDF_{cr} = 10^{-6}$/reactor year. For the case of varying uncertainties, the DAC_{HCLPF} was estimated to be 0.214 g. The difference between the two uncertainty cases is about 16%, which is much broader than using $\Delta CDF_{cr} = 10^{-6}$/reactor year. The assumption of constant uncertainties in the development of various DAC is conservative in the case of the CST because the varying (increasing) uncertainties lead to smaller DAC_{HCLPF}. These levels of DAC_{HCLPF} occur in the region dominated by the overturning moment failure mode.

This sensitivity analysis also showed that the acceptable loss of wall thickness can be more than 2/3 of the original thickness, as compared to about 1/3 when using $\Delta CDF_{cr} = 10^{-6}$ /reactor year. DAC_T was determined to be 56 to 58 years for the case of only corrosion in the tank shell, 51 to 52 years for the case of perfectly correlated degradation combination, and about 49 to 50 years for the case of non-perfectly correlated degradation combination.

Using the CST as an example, specific guidance was provided in this report on the application of the various DAC to inspection/maintenance planning. It should be reiterated that the guidelines on the use of the DAC for the CST are applicable only to the Ulchin NPP where the CST is located and which KAERI's PRA was based on. It should also be emphasized that any conclusions made in terms of time (life prediction) are only for reference because the assumed material degradation models and combination methods have not been benchmarked using real data measured at the Ulchin NPP. Any inference beyond these assumptions should be discouraged or requires case-specific scrutiny for its suitability.

7.2 Recommendation for Future Study

The various DAC developed in this report are based on the guidance in NRC RG 1.174, Rev. 2 using the core damage frequency of the plant. The PRA model used to calculate the CDFs should represent adequately the as-degraded plant condition. Multiple co-existing degraded components in an NPP could significantly change its baseline CDF or LERF so that a different ΔCDF_{cr} may be needed or even immediate action must be taken if the baseline CDF or LERF no longer satisfies the NRC risk goal. However, the current practice of PRA (or PSA) may not have sufficient emphasis on representing the degradation status; therefore, proper consideration of multiple degraded components in a plant should be explored in the future.

Development of DAC for all safety significant components in an NPP can be very costly because that involves the fragility analyses of those components for many different degradation scenarios, a series of PRAs, and a sizable effort to determine the various DAC and to use them for inspection/maintenance planning. It is therefore recommended to develop tools that can automate the entire process.

In addition, due to the approximations in the various degradation models for the materials of components used in NPPs, further research in improving these models would be extremely beneficial.

8 REFERENCES

10 CFR 50.65, *Requirements for Monitoring the Effectiveness of Maintenance at Nuclear Power Plants*, Code of Federal Regulations.

10 CFR Part 54, *Requiremetns for Renewal of Operating Licenses for Nuclear Power Plants*, Code of Federal Regulations.

51 FR 30028 (1986). "Safety goals for the operations of nuclear power plants; policy statement," *Federal Register*, Vol. 5, P. 30028, Washington, DC.

AISC (1989). *Manual of Steel Construction - Allowable Stress Design*, 9th Edition, American Institute of Steel Construction, Chicago, IL.

Albrecht, P. and Naeemi, A.H. (1984). *Performance of Weathering Steel in Bridges*, Report 272, Nat. Cooperative Highway Res. Program.

ASCE 4-98 (2000). *Seismic Analysis Of Safety-Related Nuclear Structures And Commentary*, American Society of Civil Engineers, Reston, VA.

Bandyopadhyay, K., A. Cornell, C. Costantino, R.P. Kennedy, C. Miller, and A. Veletsos (1995). *Seismic Design and Evaluation Guidelines for the Department of Energy High-Level Waste Storage Tanks and appurtenances*, BNL 52361, Brookhaven National Laboratory, Upton, NY.

Braverman, J.I., C.A. Miller, B.R. Ellingwood, D.J. Naus, C.H. Hofmayer, S. Shteyngart, and P. Bezler (2001). *Probability-Based on Evaluation of Degraded Reinforced Concrete Components in Nuclear Power Plants*, NUREG/CR-6715, U.S. Nuclear Regulatory Commission, Washington, D.C.

Braverman, J.I., G. DeGrassi, G. Martinez-Guridi, R.J. Morante, and C.H. Hofmayer (2005). *Risk-Informed Assessment of Degraded Buried Piping Systems in Nuclear Power Plants*, NUREG/CR-6876, U.S. Nuclear Regulatory Commission, Washington, D.C.

Budnitz, R.J. et al. (1985). *An Approach to the Quantification of Seimic Margins in Nuclear Power Plants*, NUREG/CR-4334, U.S. Nuclear Regulatory Commission, Washington, D.C.

Choun, Y.S., I.K. Choi, and J.M. Seo (2008). "Improvement of the seismic safety of existing nuclear power plants by an increase of the component seismic capacity: a case study," *Nuclear Engineering and Design*, **238**, 1410-1420.

Ellingwood, B.R. (1994). *Validation of Seismic Probabilistic Risk Assessments of Nuclear Power Plants*, NUREG/GR-0008, U.S. Nuclear Regulatory Commission, Washington, D.C.

Ellingwood, B.R. and J. Song (1996). *Impact of Structural Aging on Seismic Risk Assessment of Reinforced Concrete Structures in Nuclear Power Plants*, NUREG/CR-6425, U.S. Nuclear Regulatory Commission, Washington, D.C.

Generic Issue 199 (GI-199) (2010). *Implications Of Updated Probabilistic Seismic Hazard Estimates In Central And Eastern United States On Existing Plants, Safety/Risk Assessment*, August 2010, U.S. Nuclear Regulatory Commission, Washington, D.C.

Han, S.H., S.W. Lee, S.-C. Jang, H.-G. Lim, and J.-E.Yang (2010). "Improved features in a PSA software AIMS-PSA," *Transactions of the Korean Nuclear Society Spring Meeting, Pyeongchang, Korea, May 27-28.*

Iman, R.L., and W.J. Conover (1980). "Small sample sensitivity analysis techniques for computer models with an application to risk assessment," *Communications in Statistics - Theory and Methods*, **9**(17), 1749-1842.

Kaplan, S., V.M. Bier, and D.C. Bley (1989). "A note on families of fragility curves – is the composite curve equivalent to the mean curve?" Transactions, *10th International Conference on Structural Mechanics in Reactor Technology*, Vol. **P**, 163-168.

Kennedy, R.P. and M.K. Ravindra (1984). "Seismic fragilities for nuclear power plant risk studies," *Nuclear Engineering and Design*, **79**, 47-68.

Kennedy, R.P., C.A. Cornell, R.D. Campbell, S. Kaplan and H.F. Perla (1984). "Probabilistic seismic safety study of an existing nuclear power plant," *Nuclear Engineering and Design*, **59**, 315-338.

Kennedy, R.P., R.C. Murray, M.K. Ravindra, J.W. Reed, and J.D. Stevenson (1989). *Assessment of seismic margin calculation methods* and *Supplement 1*, NUREG/CR-5270, U.S. Nuclear Regulatory Commission, Washington, D.C.

Kim, J.H., I.-K. Choi, and J.-H. Park (2011). "Uncertainty analysis of system fragility for seismic safety evaluation of NPP," *Nuclear Engineering and Design*, **241**(7), 2570–2579.

Klingner, R.E., J.M. Hallowell, D. Lotze, H.G. Park, M. Rodriguez, and Y.G. Zhang (1998). *Anchor Bolt Behavior and Strength During Earthquakes*, NUREG/CR-5434, U.S. Nuclear Regulatory Commission, Washington, D.C.

Lee, N.H., I.H. Moon, and I.S. Ju (2001). "Failure mechanism for large-sized grouted anchor bolt under tensile load," *16th International Conference on Structural Mechanics in Reactor Technology*, SMiRT-16, Washington, D.C.

Mathcad 14.0 User's Manual (2007).

Mori, Y. (2005). "Reliability-based service life prediction and durability in structural safety assessment." Chapter 7, *Structural Safety and Its Quality Assurance*, Editors: B.R. Ellingwood and J. Kanda, ASCE.

NASA SP-8007 (1968). "Buckling of thin-walled circular cylinders," *NASA Space Vehicle Design Criteria*, National Aeronautics and Space Administration, Washington, D.C.

Naus, D.J., C.B. Oland, and B.R. Ellingwood (1996). *Report on Aging of Nuclear Power Plant Reinforced Concrete Structures*, NUREG/CR-6424, U.S. Nuclear Regulatory Commission, Washington, D.C.

Naus, D.J., C.B. Oland, and E.G. Arndt (1991). "Ageing management of safety-related concrete structures to provide improved bases for continuing the service of nuclear power plants," *Materials and Structures*, **24**, 308-316.

NEI 95-10 (1996). *Industry Guideline for Implementing the Requirements of 10 CFR Part 54 – The License Renewal Rule*, Nuclear Energy Institute.

Newmark, N.M. and W.J. Hall (1978). *Development of Criteria for Seismic Review of Selected Nuclear Power Plants*, NUREG/CR-0098, U.S. Nuclear Regulatory Commission, Washington, D.C.

Nie, J., J. Xu, and C. Costantino (2007). *P-CARES: Probabilistic Computer Analysis for Rapid Evaluation of Structures*, NUREG/CR-6922, U.S. Nuclear Regulatory Commission, Washington, D.C.

Nie, J., J.I. Braverman, C.H. Hofmayer, M.K. Kim, and I.K. Choi (2009). *Identification and Assessment of Material Models for Age-Related Degradation of Structures and Passive Components In Nuclear Power Plants*, Annual Report for Year 2 Task. BNL Report-82249-2009, Brookhaven National Laboratory; KAERI/TR-3757/2009, Korea Atomic Energy Research Institute.

Nie, J., J.I. Braverman, C.H. Hofmayer, Y.S. Choun, M.K. Kim, and I.K. Choi (2008). *Identification and Assessment of Recent Aging-Related Degradation Occurrences in U.S. Nuclear Power Plants*, Annual Report for Year 1 Task. BNL Report-81741-2008, Brookhaven National Laboratory; KAERI/RR-2931/2008, Korea Atomic Energy Research Institute.

Nie, J., J.I. Braverman, C.H. Hofmayer, Y.S. Choun, M.K. Kim, and I.K. Choi (2010). *Fragility Analysis Methodology for Degraded Structures and Passive Components in Nuclear Power Plants – Illustrated Using a Condensate Storage Tank*, Annual Report for Year 3 Task. BNL Report-93771-2010, Brookhaven National Laboratory; KAERI/TR-4068/2010, Korea Atomic Energy Research Institute.

Nie, J., J.I. Braverman, C.H. Hofmayer, Y.S. Choun, M.K. Kim, and I.K. Choi (2010). *Seismic Fragility Analysis of a Condensate Storage Tank with Age-Related Degradations*, Annual Report for Year 4 Task. BNL Report-95030-2011, Brookhaven National Laboratory; KAERI/TR-4327/2011, Korea Atomic Energy Research Institute.

NRC Inspection Procedure 62002 (1996). *Inspection of Structures, Passive Components, and Civil Features at Nuclear Power Plants*, U.S. Nuclear Regulatory Commission, Washington, D.C.

NRC Inspection Procedure 62706 (2000). *Maintenance Rule*, U.S. Nuclear Regulatory Commission, Washington, D.C.

NRC RG 1.174 (1998). *An Approach for Using Probabilistic Risk Assessment in Risk-Informed Decisions on Plant-Specific Changes to the Licensing Basis*, Nuclear Regulatory Commission, Washington, DC.

NRC RG 1.174 (2002). *An Approach for Using Probabilistic Risk Assessment in Risk-Informed Decisions on Plant-Specific Changes to the Licensing Basis*, Revision 1, Nuclear Regulatory Commission, Washington, DC.

NRC RG 1.174 (2011). *An Approach for Using Probabilistic Risk Assessment in Risk-Informed Decisions on Plant-Specific Changes to the Licensing Basis*, Revision 2, Nuclear Regulatory Commission, Washington, DC.

NRC RG 1.200 (2007). *An Approach for Determining the Technical Adequacy of Probabilistic Risk Assessment Results for Risk-Informed Activities*, Revision 1, Nuclear Regulatory Commission, Washington, DC.

NUMARC 93-01 (1996). *Industry Guideline for Monitoring the Effectiveness of Maintenance at Nuclear Power Plants*, Rev. 2, Nuclear Energy Institute.

NUREG-1800 (2010). *Standard Review Plan for Review of License Renewal Applications for Nuclear Power Plants*, Rev. 2, U.S. Nuclear Regulatory Commission, Washington, D.C.

NUREG-1801 (2010). *Generic Aging Lessons Learned (GALL) Report*, Rev. 2, U.S. Nuclear Regulatory Commission, Washington, D.C.

Oland, C.B., D.J. Naus, and S. Jerath (1993). "A data base for aging of structural materials," *12th International Conference on Structural Mechanics in Reactor Technology*, SMiRT-12, Stuttgart, Germany.

Prassinos, P.G., R.C. Murray, and G.E. Cummings (1987). *Seismic Margin Review of the Maine Yankee Atomic Power Station - Summary Report*, NUREG/CR-4826, UCID-20948, Vol.1, U.S. Nuclear Regulatory Commission, Washington, D.C.

Pratt, W.T., V. Mubayi, T.L. Chu, G. Martinez-Gurid, and J. Lehner (2004). *An Approach for Estimating the Frequencies of Various Containment Failure Modes and Bypass Events*, NUREG/CR-6595, Rev. 1, Nuclear Regulatory Commission, Washington, DC.

R Version 2.12.0: A Language and Environment for Statistical Computing, 2010.

Reed, J.W., R.P. Kennedy, D.R. Buttemer, I.M. Idriss, D.P. Moore, T.Barr, K.D. Wooten, and J.E. Smith (1991). "A methodology for assessment of nuclear power plant seismic margin," EPRI NP-6041-SL, Revision 1, *Department of Energy Workshop on Walkthrough Field Guide and SQUG/EPRI Seismic Evaluation Material*, Vol **7**.

Regulatory Guide 1.60 (1973). *Design Response Spectra for Seismic Design of Nuclear Power Plants*, Revision 1, U.S. Nuclear Regulatory Commission, Washington, D.C.

Saito, K. and J. Kuniya (2001). "Mechanochemical model to predict stress corrosion crack growth of stainless steel in high temperature water." *Corrosion Science*, **43**, 1751-1766.

SECY-97-208 (1997), *Elevation of the Core Damage Frequency Objective to a Fundamental Commission Safety Goal*, September 1997, U.S. Nuclear Regulatory Commission, Washington, D.C.

SRM/SECY 93-087 (1993). *Staff Requirement Memorandum, Subject: SECY-93-087 - Policy, Technical, and Licensing Issues Pertaining to Evolutionary and Advanced Light-Water Reactor (ALWR) Designs*, U.S. Nuclear Regulatory Commission, Washington, D.C.

Stocki, R. (2005). "A method to improve design reliability using optimal Latin hyper-cube sampling," *Computer Assisted Mechanics and Engineering Sciences*, **12**(4), 393-412.

Tada, H., P.C. Paris, and G.R. Irwin (2000). *The Stress Analysis of Cracks Handbook*, 3rd edition, American Society of Mechanical Engineers.

Veletsos, A.S. (1984). "Seismic response and design of liquid storage tanks," Chapter 7, *Guidelines for the Seismic Design of Oil and Gas Pipeline Systems*, American Society of Civil Engineers, Reston, VA.

Zion Probabilistic Safety Study (1981), Commonwealth Edison Company, Chicago, IL.

Appendix A FRAGILITY ANALYSIS OF THE CST WITH DEGRADED STAINLESS TANK SHELL (OPERATIONAL WATER LEVEL)

KAERI Year 5 Task
Fragility Analysis of Condensate Storage Tank
- Case A: Degraded Tank Shell
- using operational water level

Note: the documentation in this calculation sheet has only been changed from the Year 4 sheets slighlty for efficiency.

$year := 65$

$SME_e := 0.09g$

Using deterministic degradation model A:

$abc := \begin{pmatrix} 1 & 0 & 0 \end{pmatrix}^T$

Degradation Case A: Stainless Steel Tank Shell

$scc\_rate := 7.494 \times 10^{-3}\ in$

$tshell\_degraded := \frac{5}{8}in - scc\_rate \cdot year \cdot abc_0 = 0.138 \cdot in$

Degradation Case B: Anchor Bolts

$C := 70.6$

$\alpha := 0.79$

$X(t) := C \cdot t^{\alpha} \cdot \mu m$

$Dbolt\_degraded := 2.5in - 2 \cdot X(year) \cdot abc_1 = 2.5 \cdot in$

Degradation Case C: Anchorage concrete cracking - BNL model

$crack := 0.0078 \cdot year \cdot mm \cdot abc_2 = 0 \cdot in$

H.1 Introduction

KAERI indicated that the seismic DBE in Korea follows the NRC Reg. Guide 1.60 design spectrum shape but with a PGA level scaled down to 0.2 g. An initial HCLPF capacity was assumed to be 1.67 times 0.2 g. However, since the Mathcad sheets in this appendix solve the various equations iteratively by manually setting SME_e to different values, the above SME_e value of 0.032 g represents the converged solution for the degradation level of the combined degradations at 65 years.

Horizontal PGA (SME_e): $A_H := SME_e = 0.09 \cdot g$

Definitions of some useful units:

$kips \equiv 1000 lbf$ $\quad$ $ksi \equiv 1000 psi$

$GPa \equiv 10^9 Pa$ $\quad$ $MPa \equiv 10^6 Pa$

$tonf \equiv 2000 lbf$

H.2 Response Evaluation

The weight W and the center of gravity X (measured as the height above tank base) of various components are calculated as follows:

Head: using a conservative uniform thickness of 5/8" to compensate other attachments. The head configuration is simplified as a spherical cap plus a short cylinder. The spherical cap with a radius a = (25' + 5/16") and a height h= (8.7')*13mm/16mm=7.07' (estimated from drawing). The short cylinder has a radius of (25' + 5/16") and a height of 1.63'. The short cylinder is to be combined with the tank shell in this calculation. The total height of the head above the top of fluid level is 8.7'.

Spherical segment of head (following CRD Standard Mathematical Tables, 20 ed., 1972, page 17):

$a := 25 \cdot ft + \frac{5}{16} \cdot in = 25.026 \cdot ft$

$h := 7.07 ft = 7.07 \cdot ft$

$p := \sqrt{a^2 + h^2} = 26.006 \cdot ft$

R is defined here as the radius of the sphere for the head (to be redefined later as the radius of the tank):

$$R := \frac{p^2}{2 \cdot h} = 47.828 \cdot ft$$

$$t_H := \frac{5}{8} in = 0.625 \cdot in$$

$$\gamma_{steel} := 0.285 \frac{lbf}{in^3} = 492.48 \cdot \frac{lbf}{ft^3}$$

$$W_H := \pi \cdot p^2 \cdot t_H \cdot \gamma_{steel} = 54.497 \cdot kips$$

$$H_S := (37ft + 6in) + 1.63ft = 39.13 \cdot ft$$

$$X_H := \frac{h}{2} + H_S = 42.665 \cdot ft$$

Shell - include the approximated short cylinder (with a height of 0.82ft) from the head.

$$t_S := \frac{5}{8} in = 0.625 \cdot in$$

$$W_S := (2\pi \cdot a \cdot t_S) H_S \cdot \gamma_{steel} = 157.823 \cdot kips$$

$$X_S := H_S \div 2 = 5.963\, m$$

Bottom - assume a thickness of 7 mm as no English unit is available.

$$t_B := 7 \cdot mm = 0.276 \cdot in$$

$$W_B := t_B \cdot \pi \cdot a^2 \cdot \gamma_{steel} = 22.254 \cdot kips$$

$$X_B := t_B \div 2 = 0.138 \cdot in$$

Water - as KAERI explained, T.L. indicates the top of fluid level.

Using the operational water height, per disucssion with KAERI on 10/13/2010:

$H_W := 37ft + 6in = 37.5 \cdot ft$ Maximum design water level used for Year 3 task: 37'-6" (11.43 m)

$H_W := 132ft - (101ft + 9in) = 9.22\, m$ $H_W = 30.25 \cdot ft$

$$\gamma_W := 62.4 \frac{lbf}{ft^3} = 999.552 \cdot \frac{kgf}{m^3}$$

$$W_W := \pi \cdot a^2 \cdot H_W \cdot \gamma_W = 3714.019 \cdot kips$$

$$X_W := H_W \div 2 = 15.125 \cdot ft$$

Hydrostatic fluid pressure function, P_{ST}, as used in Table H-1 (y is pointing downward from TL, with a value of 0ft at TL):

$$P_{ST}(y) := y \cdot \gamma_W \qquad P_{ST}(0ft) = 0 \cdot psi$$

$$P_{ST}(H_W) = 13.108 \cdot psi$$

H.2.1 Horizontal Impulsive Mode Responses:

$$\rho_L := \gamma_W \div g = 999.552 \frac{kg}{m^3}$$

$$\rho_S := \gamma_{steel} \div g = 7.889 \times 10^3 \frac{kg}{m^3}$$

$$\frac{\rho_L}{\rho_S} = 0.127$$

$$E_S := 29000 ksi$$

$$\nu_S := 0.3$$

Redefining R back to the radius of the tank:

$$R := a = 25.026 \cdot ft$$

Also defining H as H_W for compatibility with the equations in the method:

$$H := H_W = 30.25 \cdot ft$$

$$H_W \div R = 1.209$$

$$H_S \div R = 1.564$$

$$H_W \div H_S = 0.773$$

$$t_S \div R = 0.0021$$

The evaluation of horizontal impulsive modal frequency in the original CDFM method by Dr. Kennedy used Table 7.4 of Veletsos 1984, "Guidelines for the Seismic Design of Oil and Gas Pipeline Systems." Using the same table, it is determined that C_{WI}=0.0904 for t_S/R=0.001 and H_W/R=1.209. Using equation 4.18 in BNL 52631(Rev. 10/95):

$$C_{WI} := 0.0904$$

$$C_{LI} := C_{WI} \times \sqrt{\frac{127 t_S \cdot \rho_S}{R \cdot \rho_L}} = 0.131$$

The horizontal impulsive mode natural frequency is estimated to be:

$$f_I := \frac{C_{LI}}{2\pi H_W} \cdot \sqrt{\frac{E_S}{\rho_S}} = 11.346 \cdot Hz$$

As indicated by KAERI, a modified design response spectrum shape as described in Regulatory Guide 1.60 was used in the design and therefore will be used in this calculation to define the SME spectrum shape. The 5% damped acceleration spectrum for a frequency range covering f_I=11.346 Hz from Regulatory Guide 1.60 is used in the following to find the spectral acceleration:

$$Hor\_Freq := \left(0.25 \quad 2.5 \quad 9. \quad 33. \right)^T \cdot Hz$$

$$Hor\_SA\_50 := \left(0.4 \quad 3.13 \quad 2.61 \quad 1 \right)^T \cdot A_H$$

$$S_{AI} := linterp\left(Hor\_Freq, Hor\_SA\_50, f_I\right) = 0.221 \cdot g$$

$$Hor\_amp\_I := S_{AI} \div A_H = 2.453$$

$$H_W \div R = 1.209$$

For the CST with an approximate H/R <1.50, the effective impulsive weight of the contained water (or other fluid) W_I and its effective height above the tank base X_I can be calculated as follows. It is assumed in this calculation that the tank shell is rigid for the effective impulsive weight calculation per ASCE 4-98.

$$W_I := \frac{\tanh\left(\sqrt{3}\cdot\frac{R}{H_W}\right)}{\sqrt{3}\cdot\frac{R}{H_W}}\cdot W_W = 2.313\times 10^3\cdot kips \qquad W_I = 1.029\times 10^4\cdot kN$$

$$X_I := 0.375\cdot H_W = 11.344\cdot ft \qquad X_I = 3.458\,m$$

The impulsive mode base shear V_I and moment M_I at the base of the tank shell:

$$V_I := \frac{S_{AI}}{g}\cdot\left(W_H + W_S + W_I\right) = 557.347\cdot kips$$

$$M_I := \frac{S_{AI}}{g}\cdot\left(W_H\cdot X_H + W_S\cdot X_S + W_I\cdot X_I\right) = 6.986\times 10^3\cdot kips\cdot ft$$

For a depth from the top of the fluid greater than 0.15H (5.625 ft), the impulsive hydrodynamic pressure is estimated as:

$$P_I := \frac{W_I\cdot X_I\cdot S_{AI}}{1.36R\cdot H^2\cdot g} = 1.291\cdot psi \qquad P_I = 8.902\cdot kPa$$

For depths between 0 ft (fluid surface) to 0.15 H, the impulsive pressure varies linearly with height from 0 psi to the value computed above at 0.15H.

H.2.2 Horizontal Convective (Sloshing) Mode Responses:

The fundamental convective mode frequency:

$$f_C := \sqrt{\frac{1.5ft\ \div sec^2}{R}\tanh\left(1.835\frac{H}{R}\right)} = 0.242\cdot Hz$$

This convective mode is very lightly damped and the damping ratio 0.5 percent is used as suggested by the original CDFM method. Using the fundamental convective frequency 0.242 Hz and 0.5% damping on the modified Regulatory Guide 1.60 spectrum, the convective spectral acceleration S_{AC} for the given SME_e can be calculated as follows:

$$Hor\_Freq := \begin{pmatrix} 0.1 & 0.25 & 2.5 & 9. \end{pmatrix}^T\cdot Hz$$

$$Hor\_SA\_05 := \begin{pmatrix} 0.12 & 0.707 & 5.95 & 4.96 \end{pmatrix}^T\cdot A_H$$

$$S_{AC} := linterp\left(Hor\_Freq, Hor\_SA\_05, f_C\right) = 0.061 \cdot g$$

$$Hor\_amp\_C := S_{AC} \div A_H = 0.675$$

It should be noted that f_C is slightly smaller than the corner frequency at point D in Regulatory Guide 1.60 horizontal spectrum, and the spectral acceleration values at point D and at frequency 0.1 Hz are determined by reading the horizontal spectral plot in Regulatory Guide 1.60.

The effective convective mode fluid weight and its effective application height:

$$W_C := W_W \cdot \left(0.46 \frac{R}{H} tanh\left(1.835 \frac{H}{R}\right)\right) = 1.38 \times 10^3 \cdot kips \qquad W_I = 2.313 \times 10^3 \cdot kips$$

$$X_C := H \cdot \left[1.0 - \frac{cosh\left(1.835 \frac{H}{R}\right) - 1.0}{1.835\left(\frac{H}{R}\right) sinh\left(1.835 \frac{H}{R}\right)}\right] = 19.289 \cdot ft \qquad X_I = 11.344 \cdot ft$$

$$V_C := \frac{S_{AC}}{g} \cdot W_C = 83.911 \cdot kips \qquad V_I = 557.347 \cdot kips$$

$$M_C := \frac{S_{AC}}{g} \cdot W_C \cdot X_C = 1.619 \times 10^3 \cdot kips \cdot ft \qquad M_I = 6.986 \times 10^3 \cdot kips \cdot ft$$

The hydrodynamic convective pressure as a function of depth, y (y=0 at fluid surface and its positive direction is pointing downward), is given by:

$$P_C(y) := \frac{0.267 W_W S_{AC}}{R \cdot H \cdot g} \cdot \frac{cosh\left[1.835\left(\frac{H - y}{R}\right)\right]}{cosh\left(1.835 \frac{H}{R}\right)}$$

$$P_C(0 \cdot ft) = 0.553 \cdot psi$$

$$P_C\left(H - X_C\right) = 0.259 \cdot psi$$

$$P_C\left(H - X_I\right) = 0.163 \cdot psi$$

$$P_C(H) = 0.119 \cdot psi$$

Note: $P_C(y)$ is generally smaller at greater depth. The hydrodynamic convective pressures are generally negligible compared to the hydrodynamic impulsive pressure P_I, or the hydrostatic pressure P_{ST}, except at very shallow depths. The fundamental mode fluid slosh height h_s can be estimated to be,

$$h_s := 0.837R \cdot \frac{S_{AC}}{g} = 1.273 \cdot ft \qquad h_s = 0.388\,m$$

Note that this sloshing height is more than half of the height of head. As a possibility, all water weight may be considered as impulsive weight.

H.2.3 Vertical Fluid Mode Response:

The method to compute the natural frequency for the vertical fluid-tank system mode, which was used in the original CDFM method, is not applicable to this CST configuration. The example tank in the CDFM method has a t/R ratio of about 0.001, and the available data in the literature is only applicable to this t/R ratio. Note that the CST has a t/R ratio of 0.0021. As an alternative, also mentioned in the CDFM method, equation C3.5-13 in ASCE 4-98 is used instead in the following:

Water bulk modulus: $K := 2.2 \times 10^9 Pa = 319.083 \cdot ksi$

$$f_V := \frac{1}{4H}\left[\rho_L \cdot \left(\frac{2 \cdot R}{t_S \cdot E_S} + \frac{1}{K}\right)\right]^{-0.5} = 11.824 \cdot Hz$$

The CDFM method recommends 5% of critical damping be used when estimating the vertical spectral acceleration. Using the Reg Guide 1.60 vertical acceleration spectra:

$$Ver\_Freq := \begin{pmatrix} 0.25 & 3.5 & 9.0 & 33. \end{pmatrix}^T \cdot Hz \qquad A_H = 0.09 \cdot g$$

$$Ver\_SA\_50 := \begin{pmatrix} 0.3 & 2.98 & 2.61 & 1 \end{pmatrix}^T \cdot A_H$$

$$S_{AV} := linterp\left(Ver\_Freq, Ver\_SA\_50, f_V\right) = 0.218 \cdot g$$

The hydrodynamic vertical fluid response mode pressure:

$$P_V(y) := 0.8\rho_L \cdot H \cdot S_{AV} \cdot cos\left(\frac{\pi}{2} \cdot \frac{H - y}{H}\right) \qquad P_V(0ft) = 0 \cdot psi$$

$$P_V(H) = 2.285 \cdot psi$$

H.2.4 Combined Responses:

Define a square root of sum of squares (SRSS) function for convenience (v must be a column vector):

$$SRSS(v) := \sqrt{v \cdot v}$$

The combined horizontal seismic responses for the base shear V_{SH}, base moment M_{SH}, and horizontal seismic hydrodynamic pressures P_{SH} can be obtained by the

SRSS of the horizontal impulsive and convective responses.

$$V_{SH} := SRSS\left[\begin{pmatrix} V_I & V_C \end{pmatrix}^T\right] = 563.628 \cdot kips \qquad V_I = 557.347 \cdot kips$$

$$M_{SH} := SRSS\left[\begin{pmatrix} M_I & M_C \end{pmatrix}^T\right] = 7.171 \times 10^3 \cdot kips \cdot ft \qquad M_I = 6.986 \times 10^3 \cdot kips \cdot ft$$

$$P_{SH}(y) := SRSS\left[\begin{pmatrix} P_I & P_C(y) \end{pmatrix}^T\right] \qquad P_{SH}(H) = 1.297 \cdot psi$$

Note that for this CST tank, the combined horizontal seismic responses are essentially equal to the impulsive mode responses and the influence of the convective mode is negligible.

(1): For the purpose of the membrane hoop stress capacity check, the maximum seismic hydrodynamic pressures P_{SM} can be obtained by SRSS of the horizontal seismic pressures P_{SH} and the vertical fluid response hydrodynamic pressure P_V:

$$P_{SM}(y) := SRSS\left[\begin{pmatrix} P_{SH}(y) & P_V(y) \end{pmatrix}^T\right] \qquad P_{SM}(H) = 2.627 \cdot psi$$

(2): For the purpose of estimating the buckling capacity of the tank shell, it is necessary to estimate the expected maximum and minimum of the fluid pressures acting against the tank shell near its base at the location of the maximum axial compression during the time of maximum base moment. The expected maximum and minimum compression zone pressure P_{C+} and P_{C-}, at the time of maximum base moment can be obtained as,

$$P_{C+} := P_{ST}(H) + P_{SH}(H) + 0.4 P_V(H) = 15.319 \cdot psi$$

$$P_{C-} := P_{ST}(H) + P_{SH}(H) - 0.4 P_V(H) = 13.491 \cdot psi$$

Where the factor of 0.4 on P_v is to account for the probable vertical mode hydrodynamic vertical pressure at the time of maximum base moment.

(3): Similarly, for the purpose of estimating the expected minimum fluid hold-down forces in the zone of maximum tank wall axial tension, it is required to estimate the minimum tension zone fluid pressure P_{T-} at the time of maximum moment:

$$P_{T-} := P_{ST}(H) - P_{SH}(H) - 0.4 P_V(H) = 10.898 \cdot psi$$

(4): For the sliding capacity evaluation, the expected minimum average fluid pressure P_a on the base plate, at the time of the maximum base shear, can be

estimated to be:

$$P_a := P_{ST}(H) - 0.4P_V(H) = 8.408 \times 10^4\, Pa$$

(5): The expected minimum total effective weight W_{Te} of the tank shell acting on the base, at the time of maximum moment and base shear, can be estimated by (assuming the vertical stiffness of the tank shell and head system be greater than 33 Hz):

$$W_{Te} := \left(W_H + W_S\right)\cdot\left[1 - 0.4\left(\frac{A_H}{g}\right)\right] = 204.676\cdot kips$$

H.3 Capacity Assessment

The seismic overturning moment capacity of the CST at its base, M_{SC}, depends on the axial compressive buckling capacity of the tank shell C_m, the tensile hold-down capacity of the anchor bolts including their anchorage and attachment to the tank T_{BC}, and the hold-down capacity of the fluid pressure acting on the tank base plate T_e.

Although unlikely for larger radius tanks, the tank SME capacity is sometimes governed by the sliding shear capacity at the tank base, V_{SC}. Even though it does not appear that any butt welded steel tank has ever failed due to seismic induced membrane hoop stresses due to combined hydrostatic and hydrodynamic fluid pressures, the SME capacity of this failure mode, P_{CA}, should also be checked.

Additional assessment of the seismic capacity may include the possibility and consequence of the fluid sloshing against the tank roof, foundation failure for soil sites, and possibility of failure of piping or their attachment to the tank.

H.3.1 Compressive Buckling Capacity of the Tank Shell:

The most likely buckling for tanks is the "elephant-foot" buckling near the base of the tank shell. The "elephant-foot" buckling is a combined effect of hoop tension, axial (vertical) compression, and restriction of radial deformation of the tank shell by the base plate. "Elephant-foot" buckling does not necessarily lead to failure of a tank (e.g., leakage). However, there is no simple capability evaluation method that can predict tank performance after the development of "elephant-foot" buckling. Therefore, for a CDFM SME capacity of tanks, the onset of "elephant-foot" buckling will be judged to represent the limit to the compressive buckling capacity of the tank shell. The onset of "elephant-foot" buckling can be estimated using elastic-plastic collapse theory as presented in the following:

The sidewall thickness near the shell base: $t_s := tshell\_degraded = 0.138\cdot in$

The tank internal pressure near its base: $P := P_{C+} = 1.056 \times 10^5 Pa$

Elastic modulus of the tank: $E_S = 2.9 \times 10^4 \cdot ksi$

The CST shell was made of SA 204-type 304 stainless steel. This material does not have a flat yield plateau and as strain increases its stress can grow to a minimum ultimate stress capacity of 75 ksi. In the CDFM method, an effective yield stress σ_{ye} is set to $2.4S_M$ or 45 ksi, in line with the ASME seismic design limit for primary local membrane plus primary bending [ASME 1983, "ASME Boiler & Pressure Vessel Code"]. The potential uncertainty range for σ_{ye} is reported to be between 30 ksi and 60 ksi, according to the original CDFM method description.

$$\sigma_{ye} := 45ksi$$

$$\frac{R}{t_s} = 2.178 \times 10^3$$

$$S_1 := \frac{R}{t_s} \div 400 = 5.445$$

The "elephant-foot" buckling axial stress of the tank shell can be accurately predicted to be:

$$\sigma_p := \frac{0.6E_S}{R \div t_s} \cdot \left[1 - \left(\frac{P \cdot R}{\sigma_{ye} \cdot t_s}\right)^2\right] \cdot \left(1 - \frac{1}{1.12 + {S_1}^{1.5}}\right) \cdot \left(\frac{S_1 + \frac{\sigma_{ye}}{36ksi}}{S_1 + 1}\right) = 3.467 \cdot ksi$$

The compressive buckling capacity for HCLPF capacity computation utilizes a recommended 0.9 reduction factor of the buckling stress:

$$C_m := 0.9\sigma_p \cdot t_s = 0.43 \cdot \frac{kips}{in}$$

Buckling capacity of the supported cylindrical shells under combined axial bending and internal pressure should also be checked although it is unlikely to govern for overall seismic response of fluid containing tanks. The axial bending induced buckling stress, σ_{CB}, for such a load case can be conservatively estimated (essentially lower bound) as follows.

A parameter $\Delta\gamma$ to be used in the following procedure as an increase factor for internal pressure can be obtained from Figure 6 of "Buckling of Thin-walled Circular Cylinders," [NASA SP-8007]. $\Delta\gamma$ depends on the minimum compression zone pressure at the base of the tank shell, P_{C-}, corresponding to the time of maximum moment.

Considering the potential range on σ_{ye} of 30 to 60 ksi, the resultant range on σ_p is 16.572 ksi to 26.702 ksi. Consequently, C_m has a range of 9.322 kips/in to 15.02 kips/in.

Since $\Delta\gamma$ is to be evaluated based on Figure 6 of NASA SP-8007, this figure is digitized and defined by the following two vectors, in log scale:

$$fig6x := \begin{pmatrix} -1.8197 \\ -1.5124 \\ -1.395 \\ -1.264 \\ -1.1422 \\ -1.0519 \\ -0.94817 \\ -0.81296 \\ -0.67999 \\ -0.52011 \\ -0.40087 \\ -0.28846 \\ -0.18951 \\ -0.09283 \\ -0.00063874 \\ 0.12966 \\ 0.22407 \\ 0.3071 \\ 0.45083 \\ 0.57204 \\ 0.67305 \\ 0.78519 \\ 0.86144 \\ 0.94893 \\ 1.0004 \end{pmatrix} \qquad fig6y := \begin{pmatrix} -1.6448 \\ -1.3884 \\ -1.3056 \\ -1.2088 \\ -1.1297 \\ -1.0676 \\ -1.0058 \\ -0.93763 \\ -0.86938 \\ -0.8017 \\ -0.76514 \\ -0.7391 \\ -0.71278 \\ -0.68996 \\ -0.66704 \\ -0.64849 \\ -0.62918 \\ -0.62739 \\ -0.61269 \\ -0.60816 \\ -0.60321 \\ -0.60915 \\ -0.61434 \\ -0.6162 \\ -0.62796 \end{pmatrix}$$

Figure 6 of NASA SP-8007: Increase in Axial-Compressive Buckling-Stress Coefficient of Cylinders due to Internal Pressure

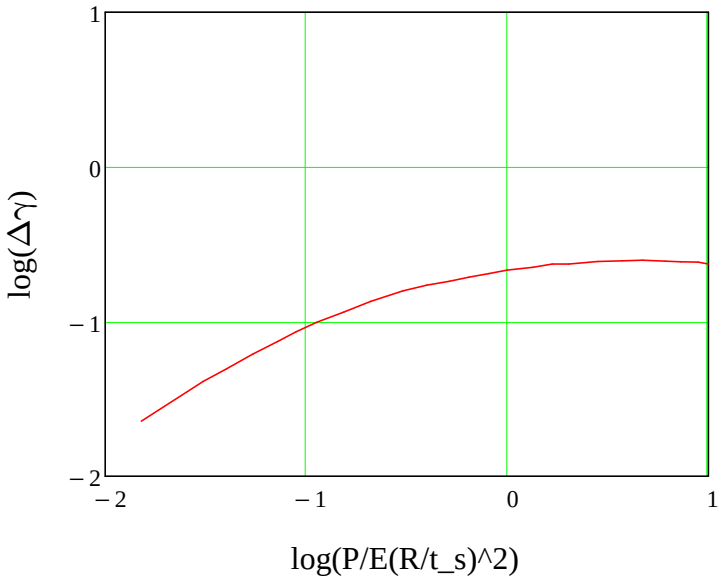

$$10^{linterp(fig6x\ ,fig6y\ ,\log(0.166))} = 0.12004$$

$$ipx := \frac{P_{C\text{-}}}{E_S}\left(\frac{R}{t_s}\right)^2 = 2.207 \qquad \frac{P_{C\text{-}}}{E_S}\left(\frac{R}{t_S}\right)^2 = 0.107$$

$$\Delta\gamma := 10^{linterp(fig6x\ ,fig6y\ ,log(ipx))} = 0.238$$

$$\phi := \frac{1}{16}\cdot\sqrt{\frac{R}{t_s}} = 2.917$$

$$\gamma := 1 - 0.73\left(1 - e^{-\phi}\right) = 0.309$$

Note: there is no experimental data for R/t>1500. $\frac{R}{t_S} = 2.178 \times 10^3$

$$\sigma_{CB} := (0.6\gamma + \Delta\gamma)\frac{E_S}{R \div t_s} = 5.64\cdot ksi$$

$$0.9\sigma_p = 3.12\cdot ksi$$

σ_{CB} exceeds $0.9s_p$, so it does not govern.

H.3.2 Bolt Hold-down Capacity:

The bolt hold-down capacity should be determined as the smallest of the bolt tensile capacity, anchorage of bolt into concrete foundation, capacity of the top plate of bolt chairs to transfer bolt loads to the vertical chair gussets, attachment of the top plate and vertical chair gussets to the tank shell, and the capacity of tank shell to withstand concentrated loads imposed on it by bolt chairs.

Anchor bolt capacity: the anchor bolt has a diameter of 2 1/2" and is made of A36 steel. The tensile capacity can be determined as:

$$d_{bolt} := Dbolt\_degraded = 2.5 \cdot in$$

$$A_{bolt} := \frac{\pi \cdot d_{bolt}^{2}}{4} = 4.909 \cdot in^2$$

Based on the AISC Code [9th edition, 1989] for threaded A36 bolts:

$$T_{BC} := 1.7 A_{bolt} \cdot 19.1 ksi = 159.387 \cdot kips \qquad T_{BC} = 79.693 \cdot tonf$$

Note that T_{BC} is the capacity of one bolt and the capacity of the interacting multi-bolts will be considered later.

Anchor bolt chair capacity check: according to the drawing, the anchor bolt chairs form a circumferentially continuous construction. Based on the continuous chair construction and the sizing of the plates and weld, it is judged that the anchor bolt chair and its attachment to the tank shell is adequate to transfer the bolt capacity load for the CST tank. The tank shell is also considered to be adequate in withstanding the concentrated loads imposed on it by bolt chairs, especially because the "elephant-foot" buckling capacity is also checked.

$$t_{chair} := \left(1 + \frac{3}{8}\right) in = 1.375 \cdot in$$

Weld width is 15 mm (5/8") according to the drawing.

Capacity of bolt anchorage into concrete foundation: the anchorage is constructed using non-shrinking grout. The tensile failure of bolt anchorage mainly consists of bolt failure, plug pull-out, and concrete cone failure, the last two of which typically are a combination of tensile failure of concrete in the upper portion of the anchorage that results in a partial depth cone-shaped spall and bond failure at the grout-concrete interface in the lower portion of the anchorage.

Bolt spacing: $\Delta d := \pi \cdot \left[50 ft + \left(9 + \frac{1}{16} \right) in \right] \div 78 = 2.044 \cdot ft$

Lee, et al [2001] described an experimental and analytical work on the pull-out strength of large-sized anchor bolt, in a SMiRT 16 paper entitled "failure mechanism for large-sized grouted anchor bolt under tensile load." The test specimens were selected based on the real construction of CST in the Yonggwang Nuclear Power Plant of Korea. The anchor bolt is 2-1/2 inches in diameter, and has an embedment length of 2 ft 2-3/8 inches. The anchor bolt material is ASTM A36. Non-shrinking grout was used in the post-installed anchorage construction. These construction variables are basically very similar to those of the subject CST for fragility analysis, except that the subject CST anchors have a slightly shorter embedment length of 2 ft 1 inch. The concrete strength of the subject CST foundation is not available, and is assumed to be the same as in this SMiRT 16 paper, which has a compressive strength of 4500 psi. The circumferential spacing is about 2 ft for both tanks. The test included 5 anchor bolt specimens.

As reported by Lee, et al [2001], the average 7 day and 28 day compressive strength of the concrete were 5419 psi and 7180 psi, respectively. The actual average compressive strength of non-shrinking grout at 7 days and 21 days were 7550 psi and 11100 psi, respectively. The non-shrinking grout has obviously larger compressive strength than the concrete, as expected for normal construction of anchorage. The reported bond strength of the non-shrinking grout (Masterflow 870) was 40 kgf/cm^2 (569 psi). The Young's modulus of A36 is 2.9*10^7 psi and the Poisson's ratio is 0.3.

The test first confirmed a minimum required load of 50 tons (100 kips). Three of the five grouted anchors were tested further until failure. Two specimens was judged to have failed by tensile failure of grout at the lower portion of the grout block, bonding failure between grout and the concrete, and tensile failure of concrete. The other specimen showed abrasion of anchor bolt thread. All specimens achieved at least 100 tons (200kips), after which the load-deformation curve became significantly flatter and the ultimate failure load scatters between 100 tons and 120 tons.

Based on the test, the anchorage capacity should be 200 kips, which is about 26% higher than the estimate based on tensile strength of the anchor bolt. It should be noted that in the test, one specimen had abrasion in its thread, suggesting the anchor bolt capacity should be also close to 200 kips. However, since the embedment in the test was about 1-3/8 inch longer than the subject CST case, the spacing of anchor bolts in the test is twice as long as in the subject CST case, and the lab test condition usually have a higher quality control, the estimate of 159.387 kips will be assumed as the anchorage capacity.

The effective embedment for the anchorage in the subject CST is estimated to be 23", which is determined by subtracting 1" from the total embedment of 2' 1" to account for the nuts.

$h_{eff} := 23 in$

The compressive strength of the concrete is assumed to be 4500 psi, according to the above mentioned paper. It should be pointed out that the measured strength in the test is higher.

$$f'_c := 4500psi$$

Base case of the anchor bolt strength based on concrete based on NUREG/CR-5434 (Figure 5.20):

$$k := 57$$

$$T_{AC} := k \cdot \left(\frac{h_{eff}}{in} \right)^{1.5} \cdot \sqrt{\frac{f'_c}{psi}} \cdot lbf = 421.767 \cdot kips$$

Note that this T_{AC} capacity calculated based on NUREG/CR-5434 is greater than 200 kips as determined in the test as reported in a SMiRT paper by Lee, et al. [2001]. The anchor bolts in the tests reported in NUREG/CR-5434 have a diameter of 3/4" and an embedment of 4", which are much smaller than those used in the CST construction. Therefore, the test data in NUREG/CR-5434 will be used as factors to scale the test data as reported in the paper by Lee, et al. [2001].

$$f_{TAC} := \frac{200kips}{421.767kips} = 0.474$$

Strengths for a crack width of 0mm and 0.3 mm can be assumed to be, based on Figure 5.20 of NUREG/CR-5434:

$$T_{AC\_00} := 200kips$$

$$T_{AC\_03} := 200kips \cdot \frac{15.5}{57} = 54.386 \cdot kips$$

T_{AC} as a function of crack width can be established as:

$$T_{AC}(c) := max\left[T_{AC\_00} + \frac{c}{0.3mm} \cdot \left(T_{AC\_03} - T_{AC\_00} \right), 0kips \right]$$

$$T_{AC}(crack) = 200 \cdot kips$$

$$T_{BC} = 159.387 \cdot kips$$

$$T_{BC} := min\left(T_{BC}, T_{AC}(crack) \right) = 159.387 \cdot kips$$

H.3.3 Fluid Hold-down Forces:

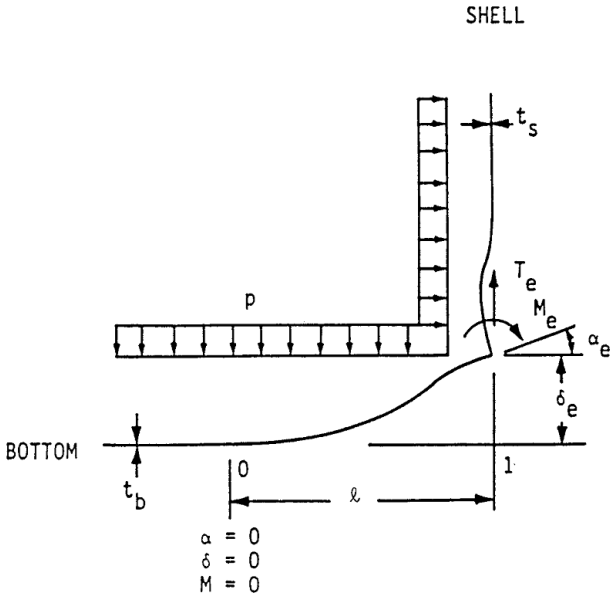

Schematic Illustration of Tank Bottom Behavior Near Tensile Region of Tank Shell [NUREG/CR-5270]

The hold-down force T_e increases with increasing fluid pressure P, which consequently assumes the minimum tension zone fluid press $P_{T\text{-}}$. A number of other related parameters are also defined below.

$P := P_{T\text{-}} = 10.898 \cdot psi$

$\nu := 0.3$

$I_b := \dfrac{t_B^{\,3}}{12\left(1-\nu^2\right)} = 1.917 \times 10^{-3} \cdot in^3$

$K := \dfrac{E_S \cdot t_s^{\,3}}{12\left(1-\nu^2\right)} = 786.672\,J$

$\kappa := \left[\dfrac{R}{t_s}\cdot\sqrt{3\left(1-\nu^2\right)}\right]^{0.5} = 59.988$

$t_S = 0.625 \cdot in$

$t_s = 0.138 \cdot in$

$t_B = 7 \cdot mm$

$R = 25.026 \cdot ft$

$t_s = 3.502 \times 10^{-3}\,m$

$$MFP := \frac{R \cdot t_S}{\sqrt{12\left(1-\nu^2\right)}}\left(1-\frac{R}{H\cdot\kappa}\right) = 7.973\times 10^{-3}\,m^2$$

MFP is a shortcut to M_F / P

$$K_S := \frac{2\cdot K\cdot\kappa}{R} = 1.237\times 10^{4}\,N$$

The uplift height δ_e, the hold down tension T_e, moment M_e, rotation a_e, and maximum positive moment M_+ can then be defined as functions of uplift length *l*:

$$F(l) := 1 + \frac{K_S\cdot l}{2E_S\cdot I_b}$$

$$\delta_e(l) := \left[\frac{l^4}{24} - \frac{1}{F(l)}\left(\frac{K_S\cdot l^5}{72E_S\cdot I_b} + MFP\cdot\frac{l^2}{6}\right)\right]\cdot\left(\frac{P}{E_S\cdot I_b}\right)$$

$$T_e(l) := P\cdot\left[\frac{l}{2} + \frac{1}{F(l)}\cdot\left(\frac{K_S\cdot l^2}{12E_S\cdot I_b} + \frac{MFP}{l}\right)\right]$$

Note: this equation as in the original CDFM method is singular at L= 0 ft. The MFP/L term only has a minor effect on T_e when L is very small. The linear approximation in the original CDFM method can effectively avoid this singularity.

$$M_e(l) := P\cdot\left(\frac{1}{F(l)}\right)\cdot\left(\frac{K_S\cdot l^3}{12E_S\cdot I_b} + MFP\right)$$

$$M_+(l) := P\cdot\left(\frac{l^2}{8} - \frac{M_e(l)}{2P} + \frac{M_e(l)^2}{2P^2\cdot l^2}\right)$$

The singularity in this equation can be similarly avoided by the linear approximation.

$$\alpha_e(l) := \frac{P\cdot l^3}{12E_S\cdot I_b} - \frac{M_e(l)\cdot l}{2E_S\cdot I_b}$$

Given

$$l := 0\ in$$

$$\frac{l^2}{24} - \frac{1}{F(l)}\left(\frac{K_S \cdot l^3}{72 E_S \cdot I_b} + MFP \cdot \frac{1}{6}\right) = 0$$

$$lmin := Find(l) = 6.839 \cdot in$$

Given

$$lmax := 10in$$

$$\delta_e(lmax) = 0.165in$$

$$lmax := Minerr(lmax) = 13.4 \cdot in$$

$$lmax := if(lmax < lmin, 200in, lmax)$$

$$l := lmin, lmin + 0.1in .. lmax$$

Linear Approximation:

$$i := 0 .. \frac{(lmax - lmin)}{0.1in}$$

$$l\_vec_i := lmin + i \cdot 0.1 \cdot in$$

$$\begin{pmatrix} T_{e0} \\ T_{e1} \end{pmatrix} := line\left[\frac{\overrightarrow{\delta_e(l\_vec)}}{in}, \overrightarrow{\left(T_e(l\_vec) \cdot \frac{in}{lbf}\right)}\right] = \begin{pmatrix} 59.732 \\ 187.736 \end{pmatrix}$$

$$T_{e0} := if\left(P_{T\text{-}} > 0psi, T_{e0}, 0\right)\frac{lbf}{in} = 59.732 \cdot \frac{lbf}{in}$$

$$T_{e1} := if\left(P_{T\text{-}} > 0psi, T_{e1}, 0\right) \cdot \frac{lbf}{in^2} = 187.736 \cdot \frac{lbf}{in^2}$$

$$T_{e\_lin}(\delta_e) := T_{e0} + T_{e1} \cdot \delta_e$$

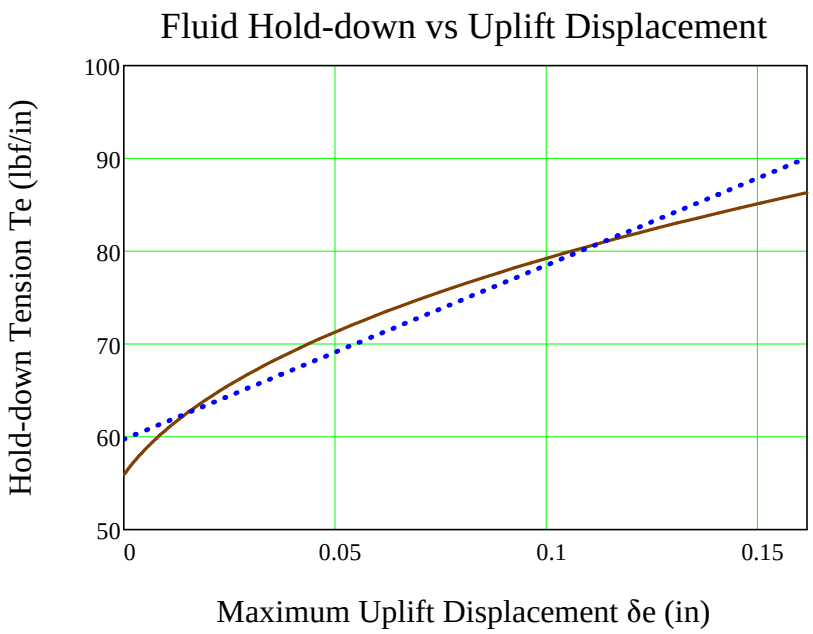

It should be noted that these equations are derived based on small displacement theory, and are applicable to the following conditions:

1. L / R ≤ 0.15. The solution does not consider the stiffening effect of hoop behavior on the base plate and consequently conservatively overpredicts the displacement δ_e , as the ratio of L/R becomes larger.

2. δ_e / t_b ≤ 0.6. As the solution is based on small displacement assumption, which ignores the beneficial influence of the membrane tension in the base plate to reduce δ_e for a given T_e as in large displacement theory. For unanchored tanks, Manos (in "earthquake tank-wall stability of unanchored tanks," *Journal of Structural Engineering*, Vol 112, No. 8, ASCE, 1986) and Haroun and Badawi (in "nonlinear axisymmetric uplift of circular plates," *Dynamics of Structures*, ASCE, 1987) showed that large displacement membrane theory greatly increases the fluid hold-down force T_e and consequently the uplift δ_e . Nevertheless, for anchored tanks like the subject CST, the uplift is not expected to be very large.

3. M_e/M_{pb} ≤ 0.9; M_e/M_{ps} ≤ 0.9; and M_+/M_{pb} ≤ 0.9, where M_{pb} and M_{ps} are the plastic moment capacity of the base plate and shell sidewalls, respectively. These equations are derived from elastic solution, and these conditions prevent the potential unconservatism.

$$0.6t_B = 0.165 \cdot in$$

The second requirement leads to maximum δ_e of 0.165 in, beyond which the small displacement theory becomes increasingly conservative. The original CDFM solved the problem by making a linear approximation of the δ_e-T_e curve in a range of δ_e=0 to $0.6t_B$, and then use the linear equation to extrapolate beyond the $0.6t_B$ to partially account for membrane tension effects. This approach will also be used in this study.

$$T_e := T_{e\_lin}$$

Assessment of the upper limit on the fluid hold-down force: based on a yield stress σ_y of 30 ksi, and an ultimate stress of 75 ksi, the fully plastic moment capacity M_{pb} of the 7 mm base plate is estimated to be 0.949 kips-inch/inch when the outer fiber reaches 75 ksi. It is also assumed that the effective hoop compressive yield stress σ_{ye} is equal to 45 ksi. The upper limit of the horizontal component of the membrane tension F_H can be found to be:

$$\sigma_{ye} = 45 \cdot ksi$$

$$M_{pb} := \frac{t_B^{\,3}}{12} \div \left(\frac{t_B}{2}\right) \cdot 75ksi = 0.949 \cdot \frac{kips \cdot in}{in} \qquad t_B = 7 \cdot mm$$

$$F_H := \frac{\sigma_{ye} \cdot t_s}{2\kappa} + \frac{M_{pb} \cdot \kappa}{R} = 0.241 \cdot \frac{kips}{in}$$

$$\left(4 M_{pb} P_{T\text{-}}\right)^{0.5} = 203.432 \cdot \frac{lbf}{in}$$

$$\frac{F_H}{2M_{pb}} = 0.127 \cdot \frac{1}{in}$$

Thus, the upper limit of the fluid hold-down force is estimated to be:

$$T_m\left(\delta_e\right) := 168.841 \frac{lbf}{in}\left(1 + \frac{0.31 \cdot \delta_e}{in}\right)^{0.5}$$

The maximum δ_e can be found by equating T_e and T_m:

Given

$$\delta_{ee} := 0.15in$$

$$T_e\left(\delta_{ee}\right) = T_m\left(\delta_{ee}\right)$$

$$\delta_{ee} := Minerr\left(\delta_{ee}\right) = 0.67 \cdot in$$

$\delta_{ee} := max\left(\delta_{ee}, 0in\right) = 0.67 \cdot in$

Therefore, the linearized equation for T_e should not be extrapolated beyond δ_{ee}.

Note that linearization is necessary later when developing overturning moment capacity.

H.3.4 Overturning Moment Capacity:

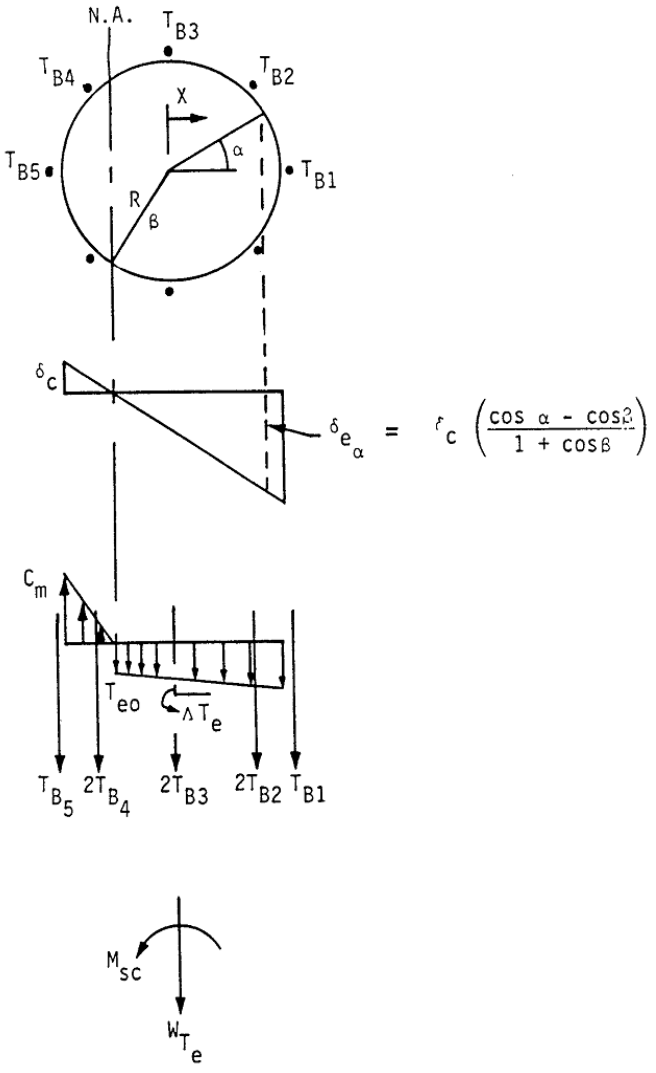

Vertical Loading on Tank Shell at Base [NUREG/CR-5270]

The overturning moment capacity M_{SC} can be estimated using the compressive

buckling capacity of the tank shell (C_B), the anchor bolt hold-down capacity (T_{BC}), and the relationship between fluid hold-down force and uplift displacement. The estimation approach in the CDFM method requires several conservative but reasonable assumptions as noted below:

1. The bottom of the tank shell is assumed to rotate rigidly about the neutral axis (plane sections remain plane).

2. The cross-section of the tank at the top of the top plate of the bolt chairs (h_c above the base) is assumed to remain horizontal so that all vertical tank distortions needed to result in base uplift and mobilization of the anchor bolts must be accommodated over the height h_c.

3. The compressive stress varies linearly from zero at the neutral axis (α=β as in the figure above) to its maximum value C_m at α=180°, as given by $C_m = E_s t_s \delta_c / h_c \leq C_B$ (by converting eq. H-39), where δ_c is the maximum compressive shortening.

Summary of parameters:

$C_m = 0.43 \cdot \frac{kips}{in}$ $T_{BC} = 159.387 \cdot kips$

$T_{e0} = 0.06 \cdot \frac{kips}{in}$ $T_{e1} = 0.188 \cdot \frac{kips}{in^2}$

$W_{Te} = 204.676 \cdot kips$ $A_B := A_{bolt}$ $A_B = 4.909 \cdot in^2$

$E_B := 29 \times 10^3 ksi$

$R = 25.026 \cdot ft$

$t_s = 0.138 \cdot in$ $E_s := E_S = 29 \times 10^3 \cdot ksi$

$h_c := 207mm = 8.15 \cdot in$

$h_a := 2ft + 1in = 25 \cdot in$

Using the approach outlined in NUREG/CR-5270 instead of the EPRI NP-6041-SL appendix H in the following:

$$\delta_c := \frac{C_m \cdot h_c}{E_s \cdot t_s} = 8.769 \times 10^{-4} \cdot in$$

$$K_B := \frac{\delta_c \cdot A_B \cdot E_B}{h_a + h_c} = 3.766 \cdot kips$$

$$\Delta T_e := T_{e1} \cdot \delta_c = 1.646 \times 10^{-4} \cdot \frac{kips}{in}$$

$$\delta_{ea}(a, b) := \delta_c \cdot \left(\frac{\cos(a) - \cos(b)}{1 + \cos(b)} \right)$$

Because the bolt pretension T_{BP} is unreliable after a number of years in service, it is conservatively assumed to be 0.

$$T_{BP} := 0 kips$$

The neutral axis angle β can be determined iteratively using the following procedure.

Bolt locations: $i := 0 .. 77$

$$\alpha_i := \frac{2\pi}{78} i$$

$$Tfunc(\alpha, \beta) := \left| \begin{array}{l} c \leftarrow T_{BP} + K_B \cdot \dfrac{\cos(\alpha) - \cos(\beta)}{1 + \cos(\beta)} \\ c \leftarrow T_{BC} \quad if \quad c > T_{BC} \\ c \leftarrow 0 \quad if \quad c < 0 \end{array} \right.$$

$$C_1(\beta) := \frac{1 + \cos(\beta)}{\sin(\beta) + (\pi - \beta)\cos(\beta)}$$

$$C_2(\beta) := \frac{\sin(\beta)\cos(\beta) + \pi - \beta}{1 + \cos(\beta)}$$

$$C_3(\beta) := \frac{\sin(\beta) - \beta \cdot \cos(\beta)}{\sin(\beta) + (\pi - \beta)\cos(\beta)}$$

$$C_4(\beta) := \frac{\beta - \sin(\beta)\cos(\beta)}{1 + \cos(\beta)}$$

$$T_B(\alpha, \beta) := \overrightarrow{Tfunc(\alpha, \beta)}$$

$$Cf'_m(\alpha, \beta) := \left(\frac{W_{Te} + \sum T_B(\alpha, \beta)}{2R} + T_{e0} \cdot \beta \right) \cdot C_1(\beta) + \Delta T_e \cdot C_3(\beta)$$

Equating Cf'_m and C_m to determine β:

$$func(\alpha,\beta) := Cf'_m(\alpha,\beta) - C_m$$

$$\beta := root(func(\alpha,\beta),\beta,0,3.14159)$$

$$\beta = 1.3004 \qquad \beta\cdot\frac{180}{\pi} = 74.507$$

$$C'_m := Cf'_m(\alpha,\beta) = 0.43\cdot\frac{kips}{in} \qquad C_m = 0.43\cdot\frac{kips}{in}$$

Use C'_m and β to find the overturning moment capacity M_{SC}:

$$M_{SC} := C'_m\cdot C_2(\beta)\cdot R^2 + \sum\overrightarrow{\left(T_B(\alpha,\beta)\cdot R\cdot cos(\alpha)\right)} + T_{e0}\cdot R^2\cdot 2\cdot sin(\beta) + \Delta T_e\cdot C_4(\beta)\cdot R^2$$

$$M_{SC} = 7184.719\cdot kips\cdot ft$$

$$\sum T_B(\alpha,\beta) = 45.463\cdot kips$$

The largest bolt elongation (at α=0) should be checked to ensure that the anchorage has the capability:

$$\delta_{e0} := \delta_{ea}(\alpha_0,\beta) = 5.072\times 10^{-4}\cdot in$$

Elongation ratio: $$\frac{\delta_{e0}}{h_a + h_c} = 1.53\times 10^{-3}\cdot\%$$

The maximum elongation ratio is much smaller than 1%, which is recommended in the original CDFM method for the A307 bolt. One percent is also considered to be an appropriate percentage value for the A36 anchor bolt used in the subject CST construction.

The maximum tank shell uplift distortion δ_{e0} = 0.026 in, which is much less than the limit of 0.165 in for the small displacement theory to be applicable in developing the fluid hold-down capacity.

Because there are 78 anchor bolts (the example tank in the original CDFM method had only 8), the case where α=0 lies midway between bolts need not be checked.

The uncertainty in HCLPF buckling capacity of the tank shell due to the uncertain σ_{ye} can lead to an M_{SC} as low as 119133.414 kips-ft or as high as 192156.702 kips-ft. It should be noted that unlike in the original CDFM method, M_{SC} is sensitive to the estimate of C_m.

Inelastic energy absorption reduction factor k can be applied to linearly computed seismic response to obtain the actual overturning moment capacity. The combined

bolt yielding and tank shell buckling failure mode for overturning moment is not brittle so that k can be less than unity. However, as stated in the original CDFM method, it is difficult to make an appropriate estimate of k for this failure mode. Therefore, it is conservatively assumed to be unity.

$k := 1.0$

$$SME_M := \frac{M_{SC}}{k \cdot M_{SH}} \cdot SME_e \qquad SME_M = 0.09 \cdot g$$

Since SME_M is substantially different from SME_e, the above procedure should be iterated to obtain the appropriate SME estiamte. The resultant SME_e is found to be 0.97g.

H.3.5 Sliding Capacity:

The base plate of the CST has a slight cone (with a slope of 1 to 96) so that the fluid will always drain away from the center of the tank. This cone is generally created by variable thickness of the oiled sand cushion between the tank bottom plate and its foundation. Therefore, the coefficient of friction between the tank base and its foundation is reasonably assumed to have a conservative value of 0.55:

$COF := 0.55$

The sliding shear capacity can then be calculated as,

$$V_{SC} := COF \cdot \left(W_{Te} + P_a \cdot \pi \cdot R^2 + \sum T_B(\alpha, \beta) \right) = 2.038 \times 10^3 \cdot kips$$

The shear capacity of the bolts should not be considered because (a) there is a large space between the concrete foundation and the anchor bolt chair, and (b) there is a 1/4" diametric clearance in the hole in the anchor bolt chair.

The sliding capacity with a unit inelastic absorption factor as suggested by the original CDFM method:

$$SME_V := \frac{V_{SC}}{k \cdot V_{SH}} \cdot SME_e \qquad SME_V = 0.325 \cdot g$$

By varying SME_e, the HCLPF shear capacity is found to be 0.549g.

Unlike the example tank in the original CDFM method, the capacity of the CST appears to be governed by the sliding capacity. The sliding capacity considers only the friction between the bottom plate and the foundation.

H.3.6 Fluid Pressure Capacity:

Summary of SME capacities:

$year = 65$ $t_s = 0.138 \cdot in$ $d_{bolt} = 2.500 \cdot in$ $crack = 0.000 \cdot mm$

$$SME_e = 0.09 \cdot g$$

$$SME_{cr} := min\left(SME_M, SME_V, SME_p\right) = 0.09 \cdot g$$

$SME_M = 0.090 \cdot g$ $SME_V = 0.325 \cdot g$ $SME_p = 0.176 \cdot g$

$$if\left[SME_{cr} = SME_M, \text{"Moment"}, \left(if\left(SME_{cr} = SME_V, \text{"Shear"}, \text{"Fluid Pressure"}\right)\right)\right] = \text{"Moment"}$$

Summary of results:

Years:	0	5	10	15	20	25	30	35	40
ts (in):	0.625	0.588	0.550	0.513	0.475	0.438	0.400	0.363	0.325
dbolt(in):									
cr(mm):									
SME:	0.549	0.526	0.503	0.480	0.456	0.433	0.410	0.387	0.364
SMEM:	1.969	1.812	1.655	1.496	1.336	1.177	1.018	0.860	0.704
SMEV:	0.549	0.526	0.503	0.480	0.456	0.433	0.410	0.387	0.364
SMEP:	2.781	2.581	2.380	2.180	1.979	1.779	1.579	1.378	1.178
Mode:	Shear	Shear	Shear	Shear	Shear	Shear	Shear	Shear	Shear

Years:	45	50	55	60	65	70	75	80
ts (in):	0.288	0.250	0.213	0.175	0.138			
dbolt(in):								
cr(mm):								
SME:	0.342	0.321	0.275	0.178	0.090	NA		
SMEM:	0.552	0.404	0.275	0.178	0.090			
SMEV:	0.342	0.321	0.310	0.317	0.325			
SMEP:	0.978	0.777	0.577	0.376	0.176			
Mode:	Shear	Shear	Moment	Moment	Moment			

H.3.7 Consideration of Other Capacities:

(1) Slosh height for roof damage: note that even with a SME_e = 0.334 g (the initial guess), the slosh height is about 4.8 ft. With the HCLPF shear capacity of SME_e=0.555 g, the sloshing height can be about 7.9 ft, which is close to the total height of the head (8.7', as approximated in the beginning part of this calculation).

$h_s = 1.273 \cdot ft$ $SME_e = 0.09 \cdot g$

The increase of sloshing height is not significant as SMEe increases from 0.334 g to 0.555 g. In addition, as pointed out in the original CDFM method, even if roof damage might be expected, such damage usually does not impair the ability of the tank to contain fluid.

(2) The CST is assumed to sit on rock/very stiff soil; therefore, soil-tank

foundation interaction is not considered.

(3) Piping failure or failure of nozzles may lead to loss of fluid in the tank, and more importantly, may impair the normal function of the condensation system. As reported in the original CDFM method, a significant fraction of the cases of seismic induced loss of tank contents have been due to piping/nozzle failures because of poor detailing. The CDFM method also stated that a SME evaluation of piping/nozzle failure is only necessary when poor seismic detailing is found in the involved piping attached to the tank. This analysis assumes that the subject CST is appropriately detailed, i.e. the piping and nozzle directly attached to the tank are properly designed and constructed so that sufficient piping flexibility can be achieved to accommodate large relative seismic anchor movements.

(4) The influence of the building in between the two CSTs on the SME are assessed in the following. The gap between the auxiliary building and the CSTs at the roof level is filled with elastomeric sealant.

The maximum tank shell uplift distortion is found to be 0.026 in, which corresponds to a neutral axis angle β of 2.29161 rad. Since the horizontal plane at the anchor bolt chair is assumed to remain plane and all distortion is assumed to occur below this level, the rotation angle around the neutral axis can be estimated to be:

$$Rotation := \frac{\delta_{e0}}{R\cdot(1-cos(\beta))} = 2.304\times 10^{-6}$$

$$\beta = 1.3 \qquad cos(\beta) = 0.267$$

The maximum horizontal displacement at the roof of the auxiliary building, which is at an elevation of 114' 9" (Parapet elevation, compared to the tank floor elevation of 101' 9"), can be estimated to be:

$$Rotation\cdot 13ft = 3.595\times 10^{-4}\cdot in$$

This horizontal displacement is much less than the width of the seismic separation joint at the roof elevation, which is 3 in. Therefore, the influence of the auxiliary building to the two CSTs is considered minimal.

The Fragility of the CST

$$SME_{HCLPF} := (\ 0.549 \quad 0.526 \quad 0.503 \quad 0.480 \quad 0.456 \quad 0.433 \quad 0.410 \quad 0.387 \quad 0.364 \quad 0.342 \quad 0.3$$

$SME_{HCLPF\_DWL} := (\ 0.426 \quad 0.409 \quad 0.393 \quad 0.376 \quad 0.360 \quad 0.343 \quad 0.326 \quad 0.310 \quad 0.294 \quad 0.27$

It should be emphasized that the HCLPF SME capacity assumes the Regulatory Guide 1.60 spectra anchored to the HCLPF SME PGA.

To determine the seismic fragility of the CST tank, one needs to convert the HCLPF SME PGA to median SME PGA. This conversion requires the estimate of both aleatory and epistemic uncertainties (β_R and β_U). The Fragility Method, also presented along with the original CDFM method, estimates the aleatory and epistemic uncertainties to be 0.2 and 0.27, respectively. These uncertainties are nearly identical to those reported by Choun, et al [2008]. The SME median SME_m can then be estimated as well.

$i := 0, 1 .. 13$

$\beta_R := 0.2$

$\beta_U := 0.27$

$\beta_C := \sqrt{\beta_R^{\,2} + \beta_U^{\,2}} = 0.336$

$Hm := exp\left[1.645\left(\beta_R + \beta_U\right)\right] = 2.167$

$SME_{m_i} := SME_{HCLPF_i} \cdot Hm$

$$F(Q, a) := cnorm\left(\frac{ln\left(\frac{a \cdot g}{SME_m}\right) + \beta_U \cdot qnorm(Q, 0, 1)}{\beta_R}\right)$$

$$F_{mean}(a) := cnorm\left(\frac{ln\left(\frac{a \cdot g}{SME_m}\right)}{\beta_C}\right)$$

$sa := 0.05, 0.1 .. 3$

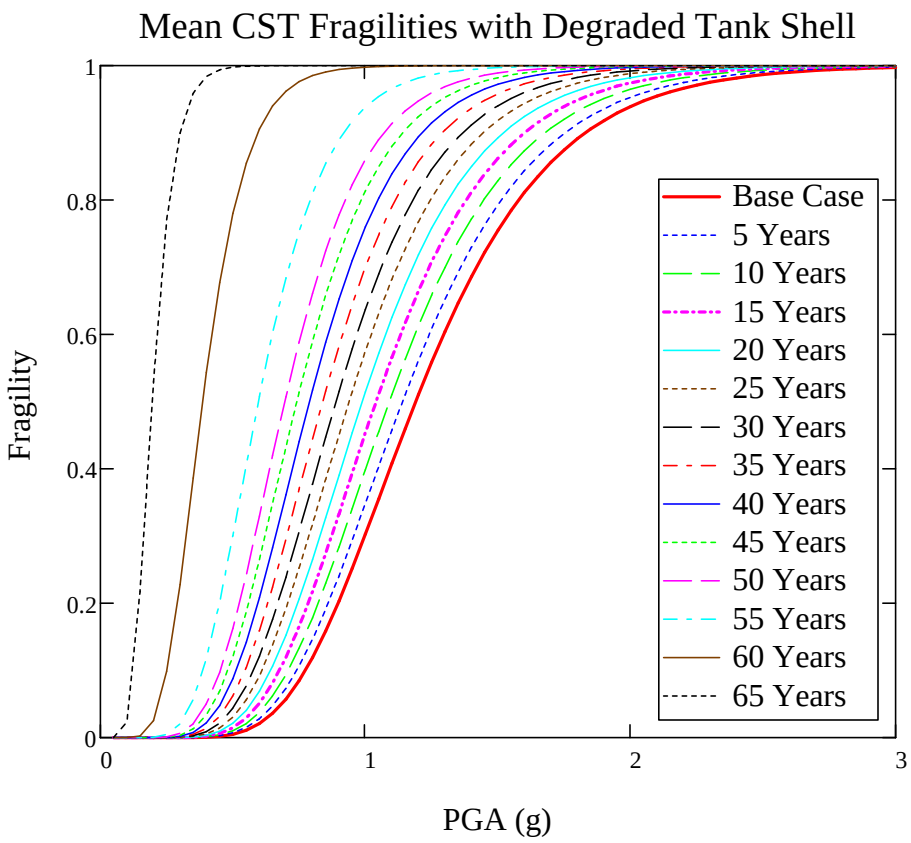

$year_i := i \cdot 5$

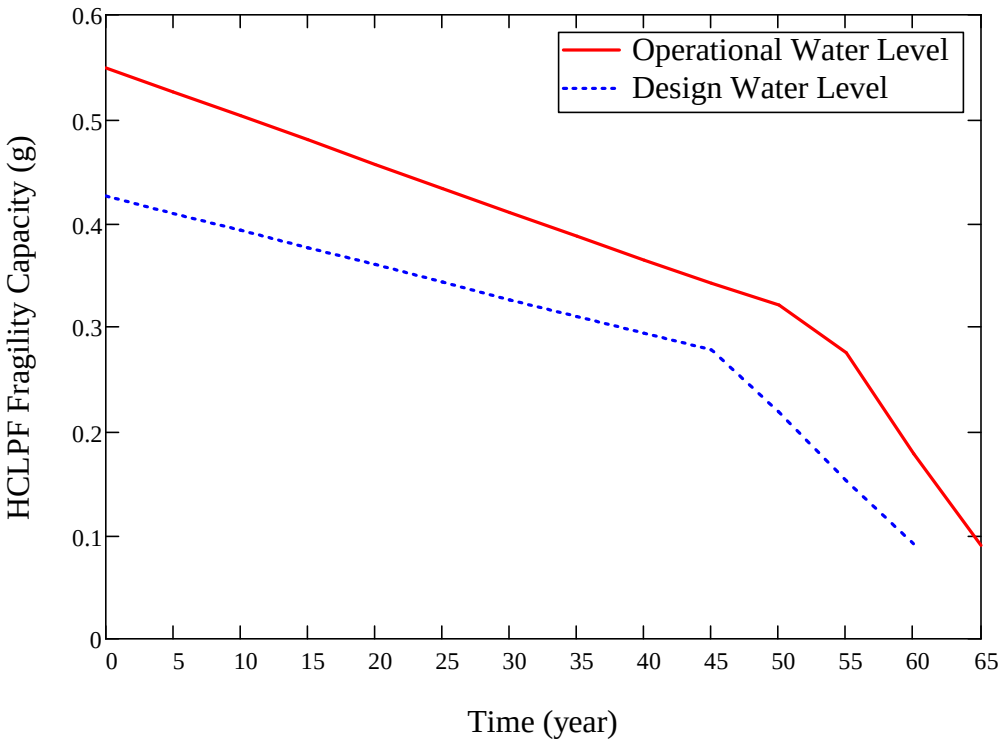
Operational Water Level
Design Water Level
HCLPF Fragility Capacity (g)
Time (year)
0
0.1
0.2
0.3
0.4
0.5
0.6
0
5
10
15
20
25
30
35
40
45
50
55
60
65

THESE DATA ARE THE CONTINUATION OF PAGE A-28.

$321 \quad 0.275 \quad 0.178 \quad 0.090 \big)^T \cdot g$

$\} \ 0.218 \ \ 0.152 \ \ 0.091 \big)^T \cdot g$

THESE DATA ARE THE CONTINUATION OF PAGE A-29.

Appendix B FRAGILITY ANALYSIS OF THE CST WITH DEGRADED ANCHOR BOLTS (OPERATIONAL WATER LEVEL)

KAERI Year 5 Task
Fragility Analysis of Condensate Storage Tank
- Case B: Degraded Anchor Bolts
- using operational water level

This appendix shows only a portion of the calculation sheet that differs from Appendix A. Appendix A shows more details in the developement of the calculation sheet.

$year := 80$

$SME_e := 0.538g$

Using deterministic degradation model B:

$abc := \begin{pmatrix} 0 & 1 & 0 \end{pmatrix}^T$

Degradation Case A: Stainless Steel Tank Shell

$scc\_rate := 7.494 \times 10^{-3}\ in$

$tshell\_degraded := \frac{5}{8}in - scc\_rate \cdot year \cdot abc_0 = 0.625 \cdot in$

Degradation Case B: Anchor Bolts

$C := 70.6$

$\alpha := 0.79$

$X(t) := C \cdot t^{\alpha} \cdot \mu m$

$Dbolt\_degraded := 2.5in - 2 \cdot X(year) \cdot abc_1 = 2.32281 \cdot in$

Degradation Case C: Anchorage concrete cracking - BNL model

$crack := 0.0078 \cdot year \cdot mm \cdot abc_2 = 0 \cdot in$

Summary of SME capacities:

$year = 80$ $t_s = 0.625 \cdot in$ $d_{bolt} = 2.323 \cdot in$ $crack = 0.000 \cdot mm$

$$SME_e = 0.538 \cdot g$$

$$SME_{cr} := min\left(SME_M, SME_V, SME_p\right) = 0.538 \cdot g$$

$$SME_M = 1.890 \cdot g \quad SME_V = 0.538 \cdot g \quad SME_p = 2.781 \cdot g$$

$$if\left[SME_{cr} = SME_M, \text{"Moment"}, \left(if\left(SME_{cr} = SME_V, \text{"Shear"}, \text{"Fluid Pressure"}\right)\right)\right] = \text{"Shear"}$$

Summary of results:

Years:	0	5	10	15	20	25	30	35	40
ts (in):									
dbolt(in):	2.500	2.480	2.466	2.453	2.441	2.429	2.418	2.408	2.398
cr(mm):									
SME:	0.549	0.548	0.547	0.546	0.546	0.545	0.544	0.543	0.543
SMEM:	1.969	1.960	1.954	1.948	1.943	1.938	1.933	1.928	1.924
SMEV:	0.549	0.548	0.547	0.546	0.546	0.545	0.544	0.543	0.543
SMEP:	2.781	2.781	2.781	2.781	2.781	2.781	2.781	2.781	2.781
Mode:	Shear	Shear	Shear	Shear	Shear	Shear	Shear	Shear	Shear

Years:	45	50	55	60	65	70	75	80
ts (in):								
dbolt(in):	2.388	2.378	2.368	2.359	2.350	2.341	2.332	2.323
cr(mm):								
SME:	0.542	0.542	0.541	0.541	0.540	0.539	0.539	0.538
SMEM:	1.919	1.915	1.911	1.907	1.907	1.898	1.894	1.890
SMEV:	0.542	0.542	0.541	0.541	0.541	0.539	0.539	0.538
SMEP:	2.781	2.781	2.781	2.781	2.781	2.781	2.781	2.781
Mode:	Shear	Shear	Shear	Shear	Shear	Shear	Shear	Shear

Summary of results:

Years:	0	100	200	300	400	500	600	700	800
ts (in):									
dbolt(in):	2.500	2.289	2.135	1.997	1.868	1.746	1.630	1.517	1.407
cr(mm):									
SME:	0.549	0.536	0.526	0.516	0.505	0.493	0.478	0.463	0.447
SMEM:	1.969	1.875	1.802	1.735	1.653	1.546	1.427	1.300	1.169
SMEV:	0.549	0.536	0.526	0.516	0.505	0.493	0.478	0.463	0.447
SMEP:	2.781	2.781	2.781	2.781	2.781	2.781	2.781	2.781	2.781
Mode:	Shear	Shear	Shear	Shear	Shear	Shear	Shear	Shear	Shear

Years:	900	1000	1100	1200	1300	1400	1500	1600	1700	1800
ts (in):										
dbolt(in):	1.301	1.197	1.095	0.995	0.897	0.800	0.705	0.611	0.518	0.427

cr(mm):										
SME:	0.430	0.414	0.396	0.379	0.363	0.347	0.332	0.319	0.307	0.292
SMEM:	1.040	0.914	0.795	0.684	0.584	0.497	0.424	0.365	0.321	0.292
SMEV:	0.430	0.414	0.396	0.379	0.363	0.347	0.332	0.319	0.307	0.297
SMEP:	2.781	2.781	2.781	2.781	2.781	2.781	2.781	2.781	2.781	2.781
Mode:	Shear	Shear	Shear	Shear	Shear	Shear	Shear	Shear	Shear	Moment

The Fragility of The CST

$SME_{HCLPF} := (\ 0.549 \quad 0.548 \quad 0.547 \quad 0.546 \quad 0.546 \quad 0.545 \quad 0.544 \quad 0.543 \quad 0.543 \quad 0.542 \quad 0.5$

$SME_{HCLPF\_DWL} := (\ 0.426 \quad 0.425 \quad 0.424 \quad 0.423 \quad 0.423 \quad 0.422 \quad 0.422 \quad 0.422 \quad 0.421 \quad 0.4$

It should be emphasized that the HCLPF SME capacity assumes the Regulatory Guide 1.60 spectra anchored to the HCLPF SME PGA.

To determine the seismic fragility of the CST tank, one needs to convert the HCLPF SME PGA to median SME PGA. This conversion requires the estimate of both aleatory and epistemic uncertainties (β_R and β_U). The Fragility Method, also presented along with the original CDFM method, estimates the aleatory and epistemic uncertainties to be 0.2 and 0.27, respectively. These uncertainties are nearly identical to those reported by Choun, et al [2008]. The SME median SME_m can then be estimated as well.

$i := 0, 1 .. 16$

$\beta_R := 0.2$

$\beta_U := 0.27$

$\beta_C := \sqrt{\beta_R^{\,2} + \beta_U^{\,2}} = 0.336$

$Hm := exp\left[1.645\left(\beta_R + \beta_U\right)\right] = 2.167$

$SME_{m_i} := SME_{HCLPF_i} \cdot Hm$

$$F(Q, a) := cnorm\left(\frac{ln\left(\frac{a \cdot g}{SME_m}\right) + \beta_U \cdot qnorm(Q, 0, 1)}{\beta_R}\right)$$

$$F_{mean}(a) := \overrightarrow{cnorm\left(\frac{ln\left(\frac{a \cdot g}{SME_m}\right)}{\beta_C}\right)}$$

$sa := 0.05, 0.1 .. 3$

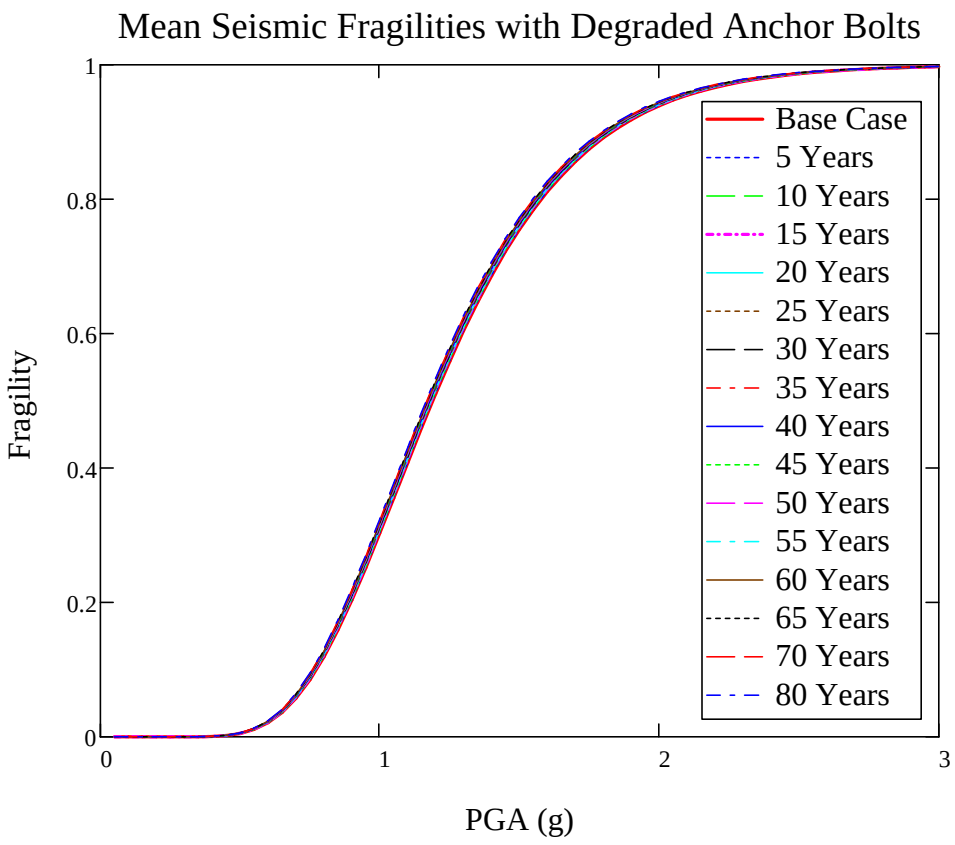

$year_i := i \cdot 5$

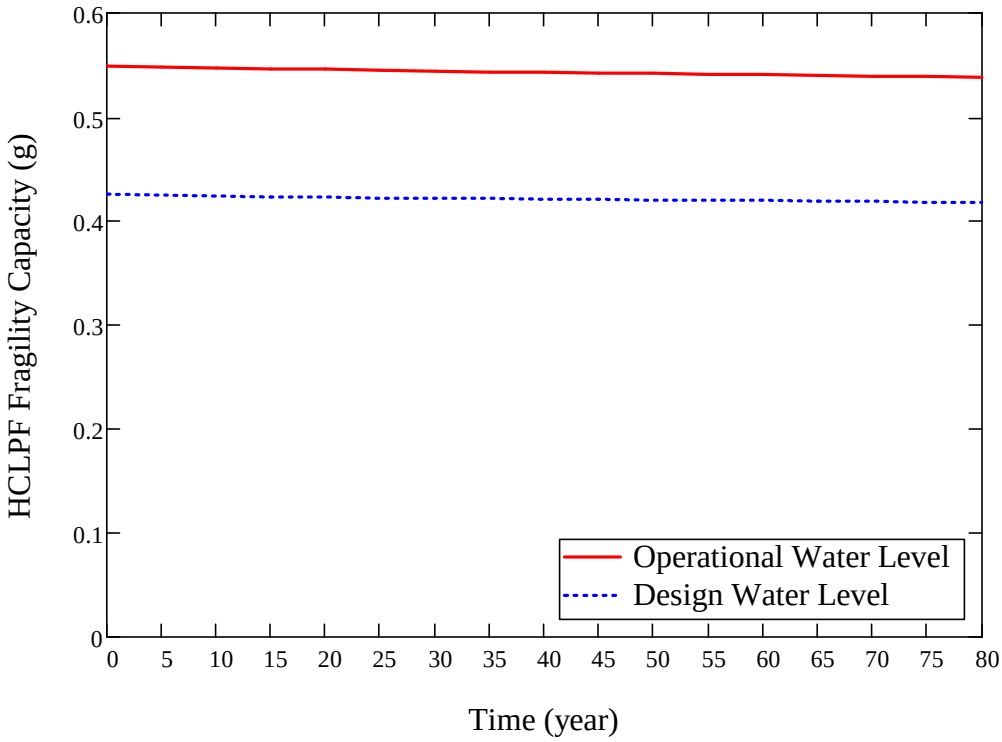

$542 \quad 0.541 \quad 0.541 \quad 0.540 \quad 0.539 \quad 0.539 \quad 0.538)^T \cdot g$

$21 \quad 0.42 \quad 0.420 \quad 0.42 \quad 0.419 \quad 0.419 \quad 0.418 \quad 0.418)^T \cdot g$

THESE DATA ARE THE CONTINUATION OF PAGE B-3.

Appendix C FRAGILITY ANALYSIS OF THE CST WITH FOUNDATION CONCRETE CRACKING – APPLICATION OF MODEL C-2 (OPERATIONAL WATER LEVEL)

KAERI Year 5 Task
Fragility Analysis of Condensate Storage Tank
- Case C: Reinforced Concrete Cracking
- using operational water level

This appendix shows only a portion of the calculation sheet that differs from Appendix A. Apendix A shows more details in the development of the calculation sheet.

$year := 80$

$SME_e := 0.255g$

Using deterministic degradation model C-2:

$abc := \begin{pmatrix} 0 & 0 & 1 \end{pmatrix}^T$

Degradation Case A: Stainless Steel Tank Shell

$scc\_rate := 7.494 \times 10^{-3}\ in$

$tshell\_degraded := \frac{5}{8}in - scc\_rate \cdot year \cdot abc_0 = 0.625 \cdot in$

Degradation Case B: Anchor Bolts

$C := 70.6$

$\alpha := 0.79$

$X(t) := C \cdot t^{\alpha} \cdot \mu m$

$Dbolt\_degraded := 2.5in - 2 \cdot X(year) \cdot abc_1 = 2.5 \cdot in$

Degradation Case C: Anchorage concrete cracking - BNL model

$crack := 0.0078 \cdot year \cdot mm \cdot abc_2 = 0.025 \cdot in$

Summary of SME capacities:

$year = 80$ $t_s = 0.625 \cdot in$ $d_{bolt} = 2.500 \cdot in$ $crack = 0.624 \cdot mm$

$$SME_e = 0.255 \cdot g$$

$$SME_{cr} := min\left(SME_M, SME_V, SME_p\right) = 0.255 \cdot g$$

$$SME_M = 0.255 \cdot g \quad SME_V = 0.278 \cdot g \quad SME_p = 2.781 \cdot g$$

$$if\left[SME_{cr} = SME_M, \text{"Moment"}, \left(if\left(SME_{cr} = SME_V, \text{"Shear"}, \text{"Fluid Pressure"}\right)\right)\right] = \text{"Moment"}$$

Summary of results:

Years:	0	5	10	15	20	25	30	35	40
ts (in):									
dbolt(in):									
cr(mm):	0.000	0.039	0.078	0.117	0.156	0.195	0.234	0.273	0.312
SME:	0.549	0.549	0.549	0.549	0.549	0.547	0.533	0.507	0.466
SMEM:	1.969	1.969	1.969	1.969	1.969	1.932	1.776	1.521	1.182
SMEV:	0.549	0.549	0.549	0.549	0.549	0.547	0.533	0.507	0.466
SMEP:	2.781	2.781	2.781	2.781	2.781	2.781	2.781	2.781	2.781
Mode:	Shear	Shear	Shear	Shear	Shear	Shear	Shear	Shear	Shear

Years:	45	50	55	60	65	70	75	80
ts (in):								
dbolt(in):								
cr(mm):	0.351	0.390	0.429	0.468	0.507	0.546	0.585	0.624
ME:	0.407	0.327	0.255	0.255	0.255	0.255	0.255	0.255
SMEM:	0.785	0.383	0.255	0.255	0.255	0.255	0.255	0.255
SMEV:	0.407	0.327	0.278	0.278	0.278	0.278	0.278	0.278
SMEP:	2.781	2.781	2.781	2.781	2.781	2.781	2.781	2.781
Mode:	Shear	Shear	Moment	Moment	Moment	Moment	Moment	Moment

The Fragility of The CST

$$SME_{HCLPF} := (0.549 \quad 0.549 \quad 0.549 \quad 0.549 \quad 0.549 \quad 0.547 \quad 0.533 \quad 0.507 \quad 0.466 \quad 0.407 \quad 0.3$$

$$SME_{HCLPF\_DWL} := (0.426 \quad 0.426 \quad 0.426 \quad 0.426 \quad 0.426 \quad 0.424 \quad 0.416 \quad 0.399 \quad 0.371 \quad 0.33$$

It should be emphasized that the HCLPF SME capacity assumes the Regulatory Guide 1.60 spectra anchored to the HCLPF SME PGA.

To determine the seismic fragility of the CST tank, one needs to convert the HCLPF SME PGA to median SME PGA. This conversion requires the estimate of both aleatory and epistemic uncertainties (β_R and β_U). The Fragility Method, also presented along with the original CDFM method, estimates the aleatory and epistemic uncertainties to be 0.2 and 0.27, respectively. These uncertainties are nearly identical to those reported by Choun, et al [2008]. The SME median SME_m can then be estimated as well.

$i := 0, 1 .. 16$

$\beta_R := 0.2$

$\beta_U := 0.27$

$\beta_C := \sqrt{\beta_R^2 + \beta_U^2} = 0.336$

$Hm := exp\left[1.645\left(\beta_R + \beta_U\right)\right] = 2.167$

$SME_{m_i} := SME_{HCLPF_i} \cdot Hm$

$$F(Q, a) := cnorm\left(\frac{ln\left(\frac{a \cdot g}{SME_m}\right) + \beta_U \cdot qnorm(Q, 0, 1)}{\beta_R}\right)$$

$$F_{mean}(a) := cnorm\left(\frac{ln\left(\frac{a \cdot g}{SME_m}\right)}{\beta_C}\right)$$

$sa := 0.05, 0.1 .. 3$

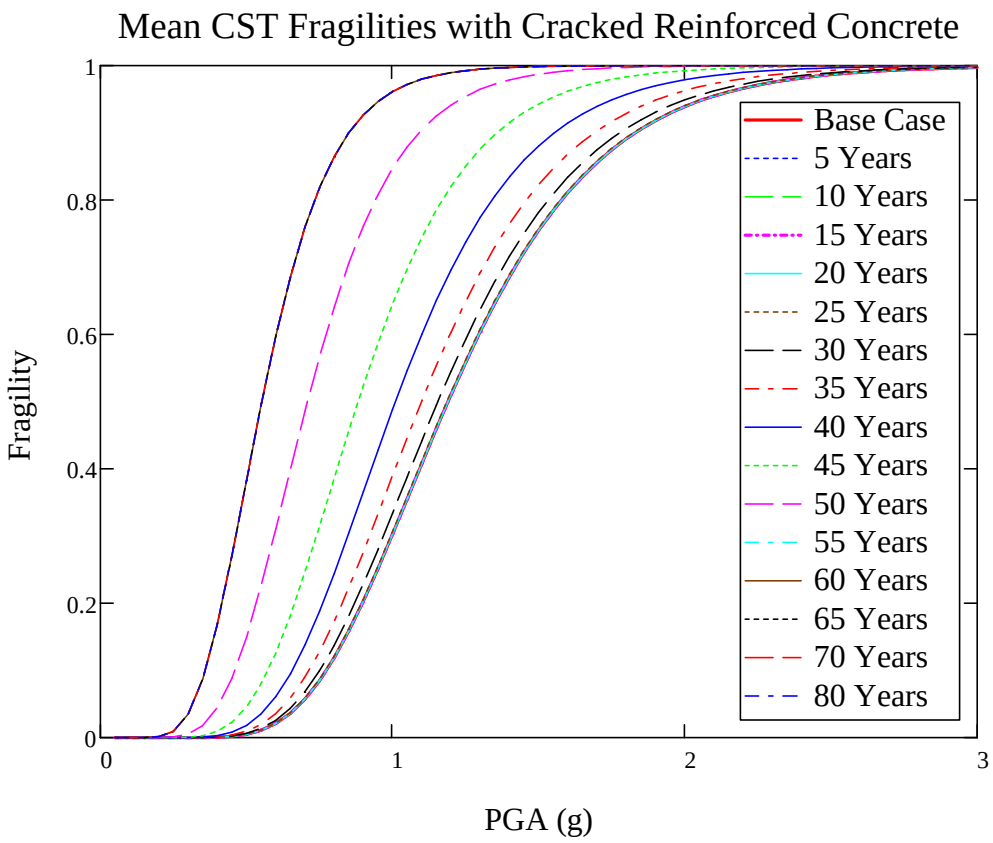

$year_i := i \cdot 5$

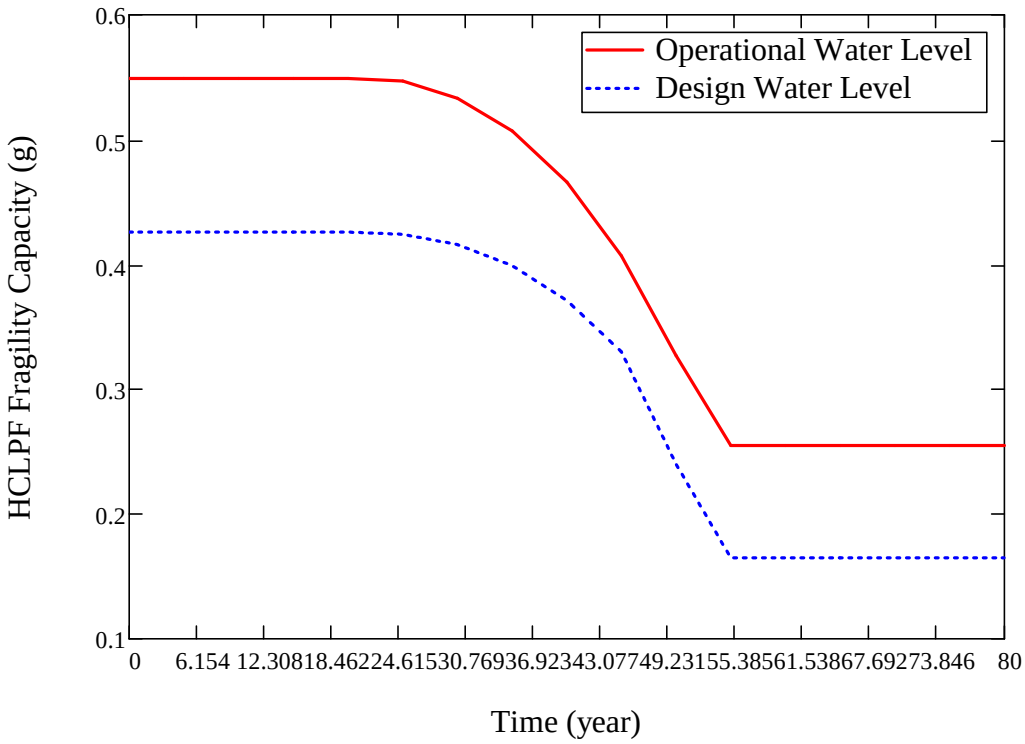
Operational Water Level
Design Water Level
HCLPF Fragility Capacity (g)
0.6
0.5
0.4
0.3
0.2
0.1
0
6.154
12.308
18.462
24.615
30.769
36.923
43.077
49.231
55.385
61.538
67.692
73.846
80
Time (year)

$327 \quad 0.255 \quad 0.255 \quad 0.255 \quad 0.255 \quad 0.255 \quad 0.255)^T \cdot g$

$30 \quad 0.240 \quad 0.165 \quad 0.165 \quad 0.165 \quad 0.165 \quad 0.165 \quad 0.165)^T \cdot g$

THESE DATA ARE THE CONTINUATION OF PAGE C-2.